Thesis, FRANZEN Rachelle

Auteur : Simonts, Ilona
Promoteur(s) : Laguesse, Sophie
Faculté : Faculté de Médecine
Diplôme : Master en sciences biomédicales, à finalité approfondie
Année académique : 2025-2026
URI/URL : http://hdl.handle.net/2268.2/25970

LIÈGE université
GIGA institute

CONSEQUENCES OF ALCOHOL DURING ADOLESCENCE

HOW DOES BINGE-DRINKING DISRUPT PREFRONTAL CORTEX

MASTER THESIS

PRESENTED BY ILONA SIMONTS

LABORATORY OF MOLECULAR REGULATION OF NEUROGENESIS,
GIGA INSTITUTE, UNIVERSITY OF LIEGE

PROMOTER

Dr. S. Laguesse

Acknowledgements

First of all, I would like to sincerely thank Sophie Laguesse for welcoming me into the laboratory and for her invaluable guidance, support, and constant presence throughout my master's thesis. Your trust and encouragement, especially during challenging moments, allowed me to grow both as a scientist and personally. I am deeply grateful for your support regarding my aspiration to pursue a PhD, and I truly hope to continue this journey within the laboratory.

I would also like to sincerely thank Manon Charlet-Briart and Léa Oskera for their daily support and presence from the very beginning. Manon, thank you for your guidance, patience, and constant encouragement throughout this project. Léa, thank you for your kindness, support, listening and advice. To both of you, thank you for your support through both the challenging moments and the small victories such as finally obtaining a successful Western Blot. Thank you for your scientific expertise, insightful advice, and willingness to answer my countless questions. You always took the time to help me overcome obstacles and grow more confident in my work. I truly hope that we will continue this adventure together.

I would also like to thank Sylvia Tielens and Coralie Reyskens for their help, advice, support, and constant good mood throughout this experience. I would also like to express my gratitude to all the members of the Nguyen team for their kindness, attentiveness, and willingness to help whenever needed.

I would also like to sincerely thank my mother, Anett, my stepfather, Benoît, my father Jerry, thank you for their daily support, encouragement, advice and for reassuring me during moments of doubt. Thank you to all my family and especially to my little brother, Viktor, who was my number one supporter and has always been there to make me smile and encourage me throughout this journey.

I would like to thank my boyfriend, Manuel, for his daily support, patience, and help, even when I was not always easy to deal with. Your presence and encouragement mean a lot to me. Thank you for believing in me every day.

I would also like to sincerely thank Odile Van Hoye and Charlotte Tonelli for sharing this journey with me. Thank you for being there every day. Without you, these past years would not have been the same. I am deeply grateful for your support, friendship, and the many moments we have shared together. I look forward to many more great adventures to come with you.

Abstract

Alcohol use disorder (AUD) is a chronic and multifactorial psychiatric condition characterized by compulsive alcohol consumption, loss of control over intake, and negative emotional states during abstinence. Although AUD is typically diagnosed in adulthood, increasing evidence indicates that its vulnerability has strong developmental origins, suggesting that early-life alcohol exposure contributes to the emergence of later compulsive drinking behaviors. In this context, adolescent alcohol exposure (AAE) may disrupt ongoing brain maturation processes and thereby increase the risk of developing AUD in adulthood. The central hypothesis of this work is that AAE alters the normal developmental trajectory of the PFC, leading to persistent molecular, cellular, and structural changes that contribute to long-term behavioral dysfunction. This hypothesis is supported by the prolonged maturation of the PFC during adolescence, a brain region essential for executive functions, decision-making, and emotional regulation. During this period, the PFC undergoes extensive synaptic remodeling and circuit refinement, making it particularly sensitive to environmental insults such as binge-drinking. Clinical and preclinical studies consistently show that AAE does not necessarily induce immediate behavioral deficits but leads to long-term consequences in adulthood, including increased anxiety- and depressive-like behaviors, impaired cognitive flexibility, and enhanced alcohol consumption. Based on this framework, this master's thesis investigates how AAE affects PFC development at multiple levels. At the cellular level, we focused on layer II/III projection neurons and interneurons, which are essential for cortical connectivity and the regulation of excitatory-inhibitory balance. At the molecular levels, we examined activity-dependent translational control mechanisms, with a particular focus on the eukaryotic elongation factor 2 (eEF2) pathway, a key regulator of synaptic protein synthesis. Although only a limited number of studies have implicated eEF2 signaling in addiction-related processes, dysregulation of the eEF2/eEF2K pathway has been associated with altered synaptic plasticity and prefrontal cortex dysfunction. Finally, we sought to link these molecular alterations to structural changes in neuronal architecture, including dendritic complexity and spine morphology in layer II/III projection neurons, as well as a potential changes in interneuron populations. Together, this work seeks to provide an integrated understanding of how AAE disrupts PFC maturation and contributes to long-term vulnerability to behavioral alterations.

Résumé

L'addiction à l'alcool est une pathologie psychiatrique chronique et multifactorielle caractérisée par une consommation compulsive d'alcool, une perte de contrôle de la consommation et des états émotionnels négatifs lors de l'abstinence. Bien que l'addiction à l'alcool soit généralement diagnostiquée à l'âge adulte, un nombre croissant de données indique que sa vulnérabilité possède des origines développementales, suggérant que l'exposition précoce à l'alcool contribue à l'émergence ultérieure de comportements de consommation compulsive. Dans ce contexte, l'exposition à l'alcool durant l'adolescence pourrait perturber les processus de maturation cérébrale en cours et augmenter le risque de développer une addiction à l'alcool à l'âge adulte. L'hypothèse centrale de ce travail est que l'exposition à l'alcool durant l'adolescence altère la trajectoire développementale normale du cortex préfrontal, entrainant des modifications durables aux niveaux moléculaire, cellulaire et structurel susceptibles de contribuer à des troubles comportementaux à long terme. Cette hypothèse est soutenue par la maturation prolongée du cortex préfrontal durant l'adolescence, une région cérébrale essentielle aux fonctions exécutives, à la prise de décision et à la régulation émotionnelle. Au cours de cette période, le cortex préfrontal subit un remodelage synaptique important, ce qui le rend particulièrement sensible aux agressions environnementales telles que la consommation excessive d'alcool. Les études cliniques et précliniques montrent de manière consistante que l'exposition à l'alcool durant l'adolescence n'induit pas nécessairement de déficits comportementaux immédiats, mais entraine des conséquences durables à l'âge adulte, notamment une augmentation des comportements anxieux et dépressifs, une altération de la flexibilité cognitive et une consommation accrue d'alcool. Ce mémoire s'intéresse à la manière dont la consommation d'alcool durant l'adolescence affecte le développement du cortex préfrontal à différents niveaux. Au niveau cellulaire, nous nous sommes concentrés sur les neurones de projection de la couche II/III ainsi que sur les interneurones, essentiels à la connectivité corticale et à la régulation de l'équilibre excitation-inhibition. Au niveau moléculaire, nous avons analysé les mécanismes de contrôle de la traduction avec un intérêt particulier pour le facteur d'élongation eucaryotique 2 (eEF2), un régulateur clé dans la synthèse protéique. Bien que peu d'études aient impliqué la signalisation eEF2 dans les processus liés à l'addiction, une dérégulation de la voie eEF2/eEF2K a été associée à des altérations de la plasticité synaptique et à des dysfonctionnements du cortex préfrontal. Enfin, nous avons cherché à relier ces altérations moléculaires à des changements dans l'architecture neuronale, notamment dans la complexité dendritique et la morphologie des épines des neurones de projection de la couche II/III, ainsi qu'à d'éventuelles modifications des populations d'interneurones. Dans son ensemble, ce travail vise à mieux comprendre

comment l’exposition à l’alcool durant l’adolescence perturbe la maturation du cortex préfrontal et contribue à une vulnérabilité accrue aux troubles comportementaux à l’âge adulte.

Abbreviations & acronyms

4E-BP	4E-binding protein
5-HT	Serotonin
AAE	Adolescent alcohol exposure
ACC	Anterior cingulate cortex
AUD	Alcohol use disorders
BAC	Blood alcohol concentration
CCK	Cholecystokinin
CNS	Central nervous system
CT	Corticothalamic
CR	Calretinin
DA	Dopamine
DID	Drinking in the dark
eEFs	Eukaryotic elongation factors
eIFs	Eukaryotic initiation factors
GABA	Gamma-aminobutyric acid
IL	Infralimbic
INs	Interneurons
IPCs	Intermediate progenitor cell
IT	Intratelencephalic
LPFC	Lateral prefrontal cortex
LTD	Long-term depression
LTP	Long-term potentiation
MZ	Marginal zone
mPFC	Medial prefrontal cortex
NAc	Nucleus accumbens
NSCs	Neural stem cells
NMDA	N-methyl-D-aspartate
oFC	Orbitofrontal cortex
PV	Parvalbumin
PBS	Phosphate Buffered Saline
PFC	Prefrontal cortex
PL	Prelimbic
PNs	Projection neurons
PT	Pyramidal tract
PV	Parvalbumin
RBPs	RNA-binding proteins
RGCs	Radial glial cells
S6K	S6 kinase
SP	Subplate
SST	Somatostatin
VIP	Vasoactive intestinal peptide
VTA	Ventral tegmental area

Table of contents

Introduction

1.1. Alcohol use and AUD

1.1.1. Alcohol consumption and health burden

Alcohol consumption has been present throughout human history across many cultures, but it is associated with substantial health risks and societal harm. In 2019, alcohol consumption was responsible for an estimated 2.6 million deaths worldwide, including 2 million men and 0.6 million women. Across countries, men consume more alcohol than women (Our World in Data, 2024; World Health Organization, 2024). However, recent research shows that the gender gap in consumption is narrowing, particularly among younger adults. In some age groups, women's rates of binge drinking have approached or even exceeded those of men, reflecting changing societal norms and drinking patterns (White, 2020). Younger adults are particularly affected by alcohol-related harm. Among individuals aged 20-39 years, alcohol consumption accounts for the highest proportion of alcohol-attributable deaths (13%). Globally, approximately 400 million people aged 15 years and older are affected by disorders linked to alcohol consumption, with about half living with alcohol dependence. Alcohol use is associated with more than 200 diseases and injury conditions, including liver disease, cardiovascular disease, and several cancers, as well as mental health conditions such as depression, anxiety, and alcohol use disorders (AUD) (Jeanblanc, 2015; Steinberg, 2008a; Yang et al., 2022). Beyond its direct effects, alcohol can also indirectly harm others through road traffic accidents, violence, and injuries. In the long term, harmful alcohol consumption can negatively affect social functioning, leading to family conflict, occupational difficulties, financial strain and in severe cases, unemployment (Steinberg, 2008). The level of risk associated with alcohol use depends on multiple factors, including the amount and frequency of consumption, individual health status, age, and sex. Societal determinants play an important role in shaping patterns of alcohol consumption, such as cultural norms, alcohol availability, and socio-economic conditions (İlhan & Yapar, 2020; World Health Organization, 2024).

1.1.2. AUD and neuroadaptations

Addiction is defined as a chronic relapsing brain disorder. It is initiated by repeated exposure to drugs or alcohol in vulnerable individuals and is influenced by genetic factors as well as developmental and adverse social experiences (Volkow et al., 2019; Yang et al., 2022). AUD is a psychiatric and multifactorial disorder. It is characterized by a loss of control over alcohol intake, compulsive alcohol use and a negative emotional state when not drinking, often following a chronic relapsing course. Approximately, 10-15% of the populations develops difficulties controlling alcohol consumption during their lifetime (Yang et al., 2022).

It is characterized by a strong desire to drink and inability to control consumption, despite negative consequences. One of the core features of AUD is the transition from occasional alcohol use to drinking behaviors that become consolidated into harmful habits (Ghin et al., 2022). As mentioned previously, in average, men consume more alcohol than women and are more likely to develop alcohol addiction. However, the genetic risk of developing AUD appears to be comparable between men and women, suggesting that the unequal prevalence of alcohol dependence is largely influenced by social and cultural factors. Among environmental factors, social stress is a prominent risk factor for the development of AUD. Other factors, such as dysfunctional familial structures, and difficult or traumatic life events, also contribute to the risk of developing AUD. At the genetic level, multiple mechanisms are involved in addiction vulnerability, including genetic variants, epigenetic regulation, alternative splicing, and changes in protein expression (Yang et al., 2022). Certain gene polymorphisms are associated with reduced sensitivity to the physiological effects of alcohol, which can lead to increased alcohol consumption. Repeated acute or chronic exposure induces neuroadaptations that alter the activity of specific brain regions and cell types. These neuroadaptive mechanisms contributed to the development of alcohol tolerance and can promote behaviors such as excessive alcohol consumption (Ghin et al., 2022; Koob & Volkow, 2016). AUD is particularly difficult to treat because individuals often present comorbid psychiatric conditions such as depression, anxiety, or personality disorders. Psychosocial interventions are among the most effective treatments for AUD and rank among the top ten evidence-based interventions. In addition, several medications are available including disulfiram (an aldehyde dehydrogenase inhibitor), naltrexone (an opioid receptor antagonist), nalmefene (an opioid system modulator), and acamprosate (glutamatergic and GABAergic modulators). These treatments have different indications and are used depending on the clinical context. Despite the availability of these therapeutic options AUD remains one of the psychiatric disorders with the lowest treatment engagement and adherence rates, partly due to the limited efficacy of current pharmacological treatments but also because only about 10% of individuals with alcohol use disorder engage in treatment seeking behaviours (Ghin et al., 2022).

1.1.3. Neurobiological actions of alcohol

Ethanol has a very simple chemical structure, which allows it to readily diffuse across the lipid membranes of cells. Once in the brain, ethanol can directly interact with components of the cell membrane, such as receptors and transporters, as well as with intracellular structures and molecules. Through these interactions, alcohol affects multiple cellular processes and functions. In particular, ethanol strongly influences synaptic function by modulating several neurotransmitters systems, including serotonin (5-HT), dopamine (DA), gamma-aminobutyric acid (GABA), glutamate and acetylcholine (Yang et al., 2022).

Both acute and chronic alcohol consumption interfere with the balance between glutamatergic and GABAergic transmissions. Glutamate is the main excitatory neurotransmitter in the central nervous system (CNS) and plays a critical role in synaptic plasticity, learning and memory (Gilpin, 2008). In contrast, GABA is the primary inhibitory neurotransmitter in the brain and is essential for inhibitory control and learning processes. Under physiological conditions, these two neurotransmitter systems are tightly balanced; however, alcohol exposure disrupts this equilibrium (Yang et al., 2022).

Acute alcohol intoxication reduces the activity of N-methyl-D-aspartate (NMDA) glutamate receptors, thereby impairing glutamatergic transmission. At the same time, alcohol enhances GABAergic signaling by acting as a positive modulator of $GABA_A$ receptors and increasing GABA release, leading to enhanced neural inhibition. These transient neurochemical changes explain the common behavioral responses to acute alcohol intoxication, such as reduced anxiety, sedation and impairment in learning, memory, and cognitive control. With chronic alcohol consumption, the brain adapts to these repeated effects through neuroadaptive mechanisms. These include an upregulation of NMDAR activity and a downregulation of $GABA_A$ receptors. Together, these adaptations result in a state of hyperexcitability which can manifest behaviorally as agitation, dysphoria, anxiety, and increased stress reactivity, particularly during withdrawal (Yang et al., 2022).

Alcohol also affects the dopaminergic system, which plays a central role in reward processing and addiction. Dopamine is a key neurotransmitter within the mesolimbic system (Gilpin, 2008), which is critically involved in the development and reinforcement of alcohol addiction (Kalsi et al., 2009). Dopaminergic neurons originating in the ventral tegmental area (VTA) project to several brain regions, including the nucleus accumbens (NAc), the PFC and the amygdala. Repeated alcohol intake increases dopamine release in regions such as PFC and amygdala, facilitating the learning and reinforcement of behaviors associated with alcohol dependence (Alasmari et al., 2018).

1.1.4. Alcohol and adolescence

Adolescence is a transitional period between childhood and adulthood (Spear, 2000) characterized by profound neural, psychological, cognitive, and behavioral changes associated with puberty and ongoing brain maturation. Adolescence is also a period during which individuals are more likely to experiment with new behaviours, including alcohol and drug use (Lee & Lee, 2023; Marshall, 2014). During adolescence, peer approval becomes increasingly important, often outweighing family influences, and social acceptance by peers represents a powerful reward for adolescents (Marshall, 2014; Pascale et al., 2022; Steinberg, 2008). Increased sensation seeking and behavioral disinhibition during this period are

associated with a higher risk of substance use and the development of substance use disorders (Koob & Volkow, 2016; Marshall, 2014). Compared to adults, adolescents tend to consume alcohol in larger quantities over shorter periods of time, rather than drinking smaller amounts more frequently. This pattern of consumption is known as “binge-drinking” and is defined as the consumption of five (for men) or four (for women) or more alcoholic drinks within a two-hour period (Hasselgård-Rowe et al., 2022; Lee & Lee, 2023). Adolescent binge-drinking has been associated with cognitive deficits, poorer academic performance, and impairment in attention and visual working memory (Alfonso-Loeches & Guerri, 2011; Lees et al., 2020). Importantly, brain maturation continues throughout adolescence, with the PFC being one of the last brain regions to fully develop. PFC maturation is typically completed around the age of 25, making this region particularly vulnerable to external influences such as alcohol exposure during adolescence (Sicher et al., 2023). Together, these behavioural and neurodevelopment characteristics make adolescence a critical window of vulnerability during which alcohol exposure can have lasting effects on brain and mental health.

1.2. Cerebral cortex development

1.2.1. In utero cerebral cortex development

Human brain development begins during the third gestational week. This process depends on the interaction between genetic and environmental factors, both of which are essential for normal brain development. Alterations in either genetic programs or environmental conditions during critical developmental periods may lead to abnormalities in brain structure and function. The first step of brain development is the differentiation of neural progenitor cells. During the third week of gestation, the neural tube begins to form; this structure represents the earliest precursor of the central nervous system. This process is known as neurulation. Once the neural tube is fully formed, neural stem cells (NSCs) organize into a single layer of rapidly proliferating cells lining the ventricular zone, which later gives rise to radial glial cells (RGCs). Following neurulation, the primitive nervous system continues to undergo extensive morphological and cellular changes. At this stage, the initial pool of neural progenitor cells is insufficient to support the large-scale production of neurons required for brain formation. Consequently, progenitor cells first expand their pool through symmetrical divisions. From the end of gastrulation until approximately embryonic day 42 (E42), neural progenitors predominantly undergo symmetrical divisions, producing two identical neural progenitor cells. Beginning around E42, neural progenitor divisions progressively shift from symmetrical to asymmetrical divisions. Asymmetrical divisions result in the production of one self-renewing RGC and one intermediate progenitor cell (IPC), thereby maintaining the stem cell pool while amplifying neuronal output through an additional proliferative step.

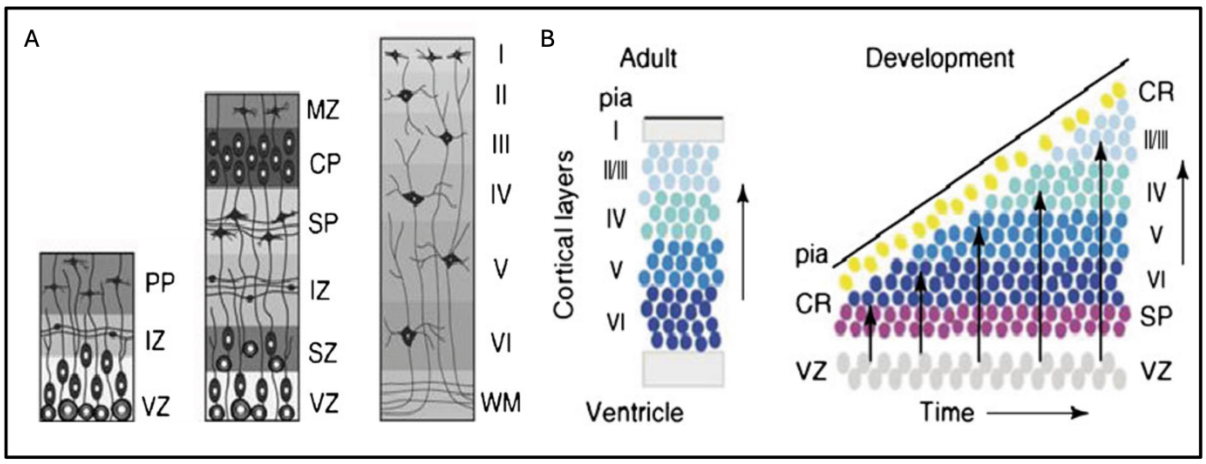

Figure 1: A. In the first panel, the earliest neurons move outward from the ventricular zone (VZ) to create the preplate (PP). In the second panel, newly generated neurons migrate in and divide the PP into two temporary structures: the marginal zone (MZ) and the subplate (SP). In the mature cortex shown in the third panel, these embryonic layers (MZ, SP, VZ) are no longer present, and the cortex has developed six distinct layers (I-VI). The intermediate zone (IZ) has differentiated into the adult white matter (WM). **B.** The first neurons to be generated move into the deepest cortical layers (dark blue). Neurons produced later then migrate past them to form superficial layers (light blue), resulting in an inside-out pattern of cortical layering (From Stiles & Jernigan, 2010).

IPCs constitute a transit-amplifying population, allowing for the expansion of neural output through additional rounds of cell division while preserving the neural stem cell pool. IPCs typically migrate to the subventricular zone, where they undergo one or more rounds of division, often symmetric, before differentiating into neurons (Lodato & Arlotta, 2015; Stiles & Jernigan, 2010).

1.2.2. Neuronal network development: Projection neurons and interneurons

Shortly after their generation, newly born neurons begin to migrate toward their final position in the developing brain (Stiles & Jernigan, 2010). Cortical networks are mainly composed of two major neuronal classes: excitatory projection neurons (also called pyramidal neurons) (PNs) and inhibitory interneurons (INs). These two populations differ in terms of developmental origin, migration mode and functional role within cortical circuits.

Projection neurons are generated from the radial glial progenitors in the ventricular zone of the dorsal telencephalon. After becoming postmitotic, they migrate radially toward the cortical plate along radial glial fibers. In contrast, cortical interneurons are generated from progenitor zones in the ganglionic eminence of the ventral telencephalon and migrate tangentially over long distances before entering the cortex, where they subsequently switch to radial migration to reach their final laminar position (Liu et al., 2016; Nishimura et al., 2012).

Early in corticogenesis, the first wave of migrating neurons form a transient structure called the preplate. Subsequent waves of neurons split the preplate into two compartments: the marginal zone (MZ) and the subplate (SP), while newly arriving neurons form the cortical plate between them. Although the MZ and SP are transient layers that largely disappear later in development, they play a critical role in cortical organization (Stiles & Jernigan, 2010).

The marginal zone contains Cajal-Retzius cells, which secrete Reelin, an extracellular signaling protein essential to proper laminar positioning of cortical neurons. Reelin contributes to migration termination and layer specification, although it acts together with multiple additional molecular guidance mechanisms (Nishimura et al., 2012; Stiles & Jernigan, 2010). Cortical layers are established through an inside-out pattern, in which early-born neurons populate deep layers and later-born neurons settle in progressively more superficial layers (**Figure 1**) (Stiles & Jernigan, 2010). As the brain grows, neurons must migrate over increasing distances and adjust their migratory behavior accordingly. After reaching their appropriate layer, neurons extend axons and dendrites and form synaptic connections to integrate into functional neural circuits. Disruption of these coordinated processes can lead to neurodevelopmental disorders (Nishimura et al., 2012).

1.2.3. Brain maturation: from infancy to adolescence

Adolescence is a critical developmental period in which certain brain areas undergo important structural and functional remodeling, particularly in synaptic plasticity and neural connectivity. Brain maturation continues into early adulthood, extending roughly to the mid-twenties. Association cortices, including the PFC, are among the last regions to reach full structural and functional maturity. Hormonal changes occurring during puberty contribute to the reorganization of brain connectivity and are associated with characteristic adolescent behavioral profiles. Two major neurobiological processes are particularly prominent during this period: continued axon myelination and synaptic pruning (Blakemore, 2012).

Across development, grey matter and white matter follow complementary trajectories reflecting progressive network specialization. Grey matter, composed of neuronal cell bodies, dendrites and synapses, expands rapidly after birth due to intense synaptogenesis and dendritic growth. Synaptic density rises sharply during early postnatal life, reaching levels two to three times higher than in adulthood in many cortical regions (Jadhav & Boutrel, 2019), with a peak typically occurring between two and five years depending on the region. Sensory and motor areas mature earlier, whereas the PFC, which is involved in executive functions and cognitive control, develops more gradually and reaches maturity later. From childhood and particularly during adolescence, synaptic pruning progressively eliminates less-used connections, leading to an apparent reduction in grey matter volume (Blakemore, 2012; Mills et al., 2016; Vijayakumar et al., 2018).

In parallel, white matter increases continuously from the prenatal period through early adulthood, reflecting progressive axonal myelination. Myelination, driven by oligodendrocytes, begins in sensory and motor pathways before extending to associative and frontal regions, thereby improving the speed and efficiency of long-range communication between brain areas (J. H. Gilmore et al., 2018). Importantly, oligodendrocyte progenitor cells receive neuronal input and adjust myelin formation in an activity-dependent manner, contributing to circuit refinement and functional optimization (Sancho et al., 2021).

Beyond neurons and oligodendrocytes, glial cells play an essential role in sculpting adolescent brain circuits. Microglia actively participate in synaptic pruning by eliminating weak or unnecessary synapses, while astrocytes regulate synapse formation, stabilization, and elimination through direct synaptic interactions and the release of synaptogenic factors such as thrombospondins, glypicans, and Hevin. These processes are strongly activity-dependent, promoting the maintenance of functional synapses while facilitating the removal of weaker connections (Farhy-Tselnicker & Allen, 2018). Together, microglia and astrocytes contribute to the fine-tuning of neural networks during adolescence.

Synaptic pruning also contributes to the maturation of the excitation-inhibition balance within cortical circuits, which is essential to efficient cognitive and executive functions. Disruption of this balance has been linked to several neuropsychiatric conditions (Selemon, 2013). Developmental studies indicate that adolescence is associated with the strengthening of inhibitory signaling and maturation of GABAergic interneuron function (Caballero et al., 2021). For example, increased expression of parvalbumin (PV) interneuron marker and decreased expression of calretinin (CR) interneuron marker have been reported in the PFC during adolescent maturation (Caballero et al., 2021). In addition to synaptic and inhibitory circuit maturation, adolescence is characterized by continued refinement of neuromodulatory systems, including dopaminergic projections, which play important roles in motivation, reward processing and executive control (Jadhav & Boutrel, 2019).

1.3. Prefrontal cortex

1.3.1. Structure of prefrontal cortex

The PFC occupies the anterior part of the frontal lobes, located rostral to the motor cortex. It is not a single homogeneous structure but a group of interconnected subregions with distinct connectivity and functional specialization (Jadhav & Boutrel, 2019; Kolk & Rakic, 2022). In humans, the PFC is commonly subdivided into medial (mPFC), lateral (lPFC) and orbitofrontal (oFC) regions (**Figure 2**). Broadly, the lateral PFC is strongly involved in executive and language-related processing, whereas medial and orbitofrontal regions contribute to emotional regulation, valuation, and decision-making (Klein-Flügge et al., 2022).

In rodents, the PFC is more limited in size and organization. It includes medial, orbitofrontal, and cingulate areas, but lacks a clear dorsolateral PFC homologue as defined in primates (Kolk & Rakic, 2022). The rodent mPFC is commonly subdivided into the infralimbic (IL), prelimbic (PL), and anterior cingulate cortex (ACC), each associated with partially distinct behavioral functions, including stress regulation and cognitive control (McKlveen et al., 2015). Like the rest of the neocortex, the PFC is organized into six cortical layers, from the superficial layer I to the deep layer VI (E. C. Gilmore & Herrup, 1997; Le Merre et al., 2021). These layers differ in neuronal composition, connectivity, and thickness. Rodent frontal cortex is often described as agranular because layer IV is poorly defined or absent compared with primate cortex (Le Merre et al., 2021).

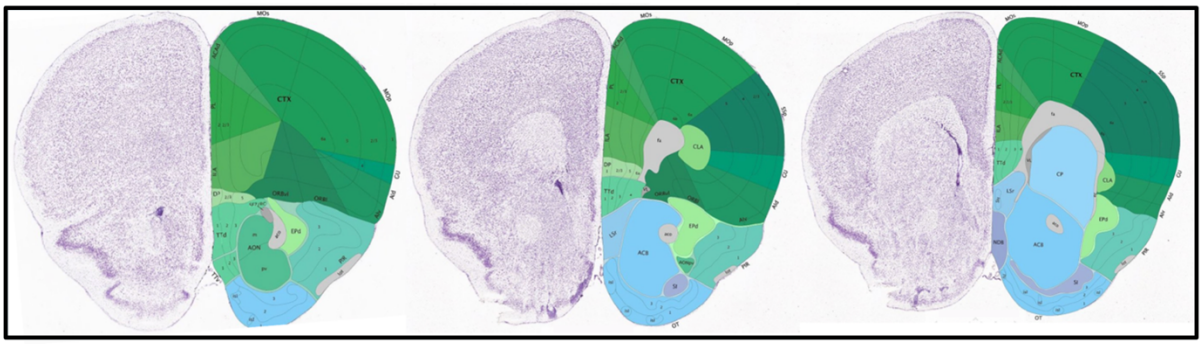

Figure 2: Prefrontal cortex coronal slices in P56 mouse. (A) Rostral slice. (B) Medial slice. (C) Caudal slice (From Allen Brain Atlas).

1.3.2. Neuronal population of the PFC

1.3.2.1. Projection neurons

Pyramidal neurons represent approximately 75-80% of cortical neurons and form glutamatergic excitatory synapses (Kamigaki, 2019). They can be subdivided into major classes based on their long-range axonal projection targets.

Intratelencephalic (IT) neurons are mainly found in layer II/III, V and VI. IT neurons express the neuronal marker SatB2 and project locally to various cortical regions and also make axonal connections bilaterally to the striatum.

Corticothalamic (CT) neurons are located mainly in layer VI. CT neurons express TBR1 and project to the thalamus.

Pyramidal tract (PT) neurons, enriched in layer Vb, express both CTIP2 and FEZF2 and send their axons to numerous cortical and subcortical regions, the striatum and the thalamus.

Molecular markers and transcription factors, SATB2 (IT), TBR1 (CT), and CTIP2/FEZF2 (PT), contribute to projection neuron subtype specification and projection identity (Kamigaki, 2019). Among these populations, superficial layer II/III IT neurons are of particular interest in the present study because they undergo extensive maturation during adolescence and play a key role in cortico-cortical communication.

1.3.2.1. Interneurons

PFC interneurons form a highly diverse population characterized by varied morphology, electrophysiological properties, and connectivity patterns (Kamigaki, 2019; Rudy et al., 2011). Despite this diversity, most interneurons can be grouped into three major molecular classes: parvalbumin (PV), somatostatin (SST), and 5HT3a receptor (5HT3aR) interneurons (**Figure 3**) (Kamalova et al., 2024).

PV interneurons include basket cells and chandelier cells. Basket cells mainly target the soma and proximal dendrites of pyramidal neurons, whereas chandelier cells specifically target the axon initial segment and exert strong control over spike initiation.

SST interneurons primarily target distal dendrites of pyramidal neurons and regulate dendritic integration. The most common SST subtype is the Martinotti cell, which often projects toward superficial layers. SST interneurons can inhibit both pyramidal neurons and other interneurons but show limited mutual inhibition within their own class.

5HT3aR interneurons include VIP (vasoactive intestinal peptide) and non-VIP subtypes. VIP interneurons preferentially inhibit other interneurons – especially SST and PV cells – thereby producing disinhibition of pyramidal neurons. Some VIP interneurons can also directly inhibit pyramidal neurons. Many VIP interneurons display bipolar morphology and co-express calretinin, whereas a smaller subset is multipolar and may co-express cholecystokinin (CCK). These cells are enriched in superficial cortical layers but are also present in deeper layers (Kamigaki, 2019; Rudy et al., 2011).

Together, projection neurons and interneurons establish balanced excitatory-inhibitory networks that are essential to normal cortical processing.

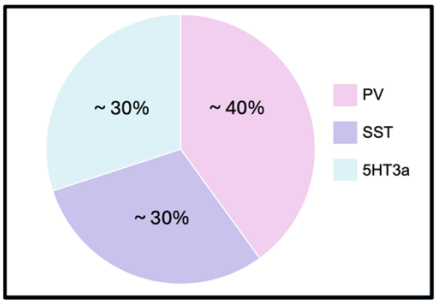

Figure 3: Distribution of major interneuron subclasses in somatosensory cortex (Adapted from Rudy et al., 2011).

1.3.3. Function and vulnerability of executive control: Why does late maturation lead to vulnerability?

Neural changes begin primarily in posterior regions and progress to more anterior regions, with the PFC being among the last brain regions to reach full functional maturity (Kolk & Rakic, 2022; Squeglia & Gray, 2016). Its protracted development parallels the gradual emergence of higher cognitive abilities involved in behavioral control and coordination. Cortical development results from continuous interaction between genetic programs and environmental factors (Jadhav & Boutrel, 2019). At the structural level, this maturation is characterized by a

significant decrease in grey matter volume, which is driven by synaptic pruning, and a concurrent linear increase in myelinated white matter tracts, which optimizes information processing (Squeglia & Gray, 2016). Functionally, the PFC plays a central role in executive control, attention, working memory, decision-making, emotional regulation, motivation and social behaviors (Carlén, 2017).

Crucially, this neurodevelopmental trajectory is non-linear, creating a temporary maturational imbalance: subcortical mesolimbic and reward systems mature much faster than the prefrontal executive control areas. This neurobiological “mismatch” creates a critical window of adolescent vulnerability, characterized by heightened sensation-seeking behaviors and increased propensity for risk-taking, such as substance use, before top-down cognitive control is fully operating (Squeglia & Gray, 2016). Because of its prolonged maturation, the PFC is particularly vulnerable to environmental insults, including exposure to psychoactive substances, and is implicated in multiple neuropsychiatric disorders (Yan & Rein, 2022). Indeed, prospective studies demonstrate a bidirectional risk, while pre-existing frontal structural and functional aberrations predispose youth to substance initiation, early exposure to toxic insults conversely disrupts normal prefrontal development, significantly altering neurocognitive trajectories (Squeglia & Gray, 2016).

1.4. Effects of adolescent binge-drinking on prefrontal cortex and behavior

1.4.1. Structural and behavioral consequences on human

Importantly, clinical and preclinical studies indicate that AAE does not necessarily induce immediate behavioral deficits, but may alter developmental trajectories, leading to behavioral abnormalities that emerge later in adulthood (Van Hees et al., 2022).

Numerous neuroimaging studies have reported that heavy alcohol consumption during adolescence is associated with reduced cortical thickness and smaller regional brain volume, including in frontal cortical areas. Decreases in both gray and white matter volume have been described in heavy drinkers compared with low or non-drinking peers. Some studies also report reduced brain stem volume in individuals with a history of heavy alcohol use (Cservenka & Brumback, 2017; Spear, 2016).

Functional imaging studies show altered brain activation patterns during cognitive tasks in adolescents with a history of heavy drinking. Individuals at earlier stages of alcohol use often display increased task-related activation, which is interpreted as compensatory recruitments to maintain performance. In contrast, longer drinking histories are associated with reduced activation and poorer cognitive performance. Heavy drinking during adolescence is also linked

with impairments in language, learning and visuospatial processing, attention, memory, and executive functions (Spear, 2016).

1.4.2. Structural and behavioral consequences in rodents

Rodent models of adolescent binge-like alcohol exposure also reveal persistent behavioral and neural alterations. Short-term effects on behavior during adolescence are often limited, but long-term consequences become evident in adulthood. These include increased anxiety-like behaviors and cognitive flexibility deficit, such as impaired reversal learning and reduced inhibitory control (Hiller-Sturmhöfel & Spear, 2018; Spear, 2016; Van Hees et al., 2022). Increased risk-taking and behavioral disinhibition have also been reported. In contrast, social behaviors appear relatively preserved depending on the paradigm used (Van Hees et al., 2022). Importantly, AAE has been reported to increase adult alcohol consumption and vulnerability to develop addiction-like behaviors.

At the neural level, AAE affects both brain structure and function. Experimental studies report reduced hippocampal neurogenesis and evidence of neuronal damage in selected brain regions, along with altered synaptic connectivity (Spear, 2016; Vetreno & Crews, 2015). Alcohol exposure during adolescence is also associated with persistent changes in gene expression, including increased neuroinflammatory signaling and epigenetic modifications that can durably alter transcriptional regulation (Hiller-Sturmhöfel & Spear, 2018, Spear, 2016).

Alcohol interacts with major neurotransmitter systems, including GABAergic and glutamatergic signaling, thereby altering excitatory-inhibitory balance. In the PFC, AAE has been associated with altered NMDA receptor expression and function, as well as changes in deep-layer pyramidal neuron excitability. Such alterations are thought to contribute to impaired executive control, increased impulsivity and reduced regulation of alcohol intake (Hiller-Sturmhöfel & Spear, 2018).

The mechanisms through which AAE disrupts PFC maturation remain incompletely understood. Since adolescence is characterized by extensive refinement of synaptic connectivity, alcohol-induced interference with synaptic plasticity may represent a key mechanism linking early exposure to later behavioral dysfunction. Structural features such as dendritic arborization and dendritic spine morphology are closely related to synaptic integration and connectivity, and therefore provide relevant cellular readouts of altered cortical maturation. In parallel, maturation of inhibitory interneuron populations contributes to the establishment of excitation-inhibition balance in the PFC, another process that may be vulnerable to alcohol exposure.

1.5. Synaptic plasticity

Synaptic plasticity refers to activity-dependent changes in synaptic strength that modify neuronal network function and is widely considered a cellular basis of learning and memory. These changes include long-term potentiation (LTP), which strengthens synaptic transmission, and long-term depression (LTD), which weakens it (Buffington et al., 2014).

Crucially, these functional alterations are intrinsically linked to structural remodeling at the level of dendritic spines, which serve as the primary specialized structures for neuronal connectivity and signaling. Dendritic spines are highly dynamic, capable of rapidly altering their morphology, number, density, and motility in response to environmental inputs. During synaptic plasticity, the physical architecture of these spines is remodeled to sustain new neuronal connections, while synaptic strengthening and LTP are associated with increases in spine density and/or spine enlargement, whereas synaptic weakening induced by LTD typically causes spines shrinkage and retraction (Gipson & Olive, 2017a). However, this structural dynamism requires tight homeostatic regulation, as synaptic overstimulation can conversely prompt spine shrinkage to prevent excitotoxic damage from excess calcium influx (Paulin et al., 2016).

This interplay between functional and structural plasticity represents a core mechanism driving the post-natal maturation of the PFC. This process is particularly prominent during adolescence, a critical developmental window where the PFC undergoes extensive synaptic pruning and circuit refinement heavily shaped by experience and environmental inputs. The dynamic formation, stabilization, or elimination of these prefrontal spines depend on long-lasting forms of plasticity, which require *de novo* protein synthesis at or near synapses (Buffington et al., 2014; Laguesse & Ron, 2020). Proper circuit function thus depends on tight spatial and temporal control of synaptic protein composition to support spine dynamics (Oliveira & Klann, 2021). Consequently, dysregulation of this translational control and the resulting aberrant spine morphology have been associated with multiple neurodevelopmental and psychiatric disorders characterized by prefrontal dysfunction (Laguesse & Ron, 2020).

1.6. mRNA translation in neurons

1.6.1. Global translation: Core mechanisms

Protein synthesis is essential for normal cellular and synaptic function. Translation occurs in three main stages: initiation, elongation and termination. Initiation is the most regulated step and involves assembly of the translation initiation complex at the start codon of the mRNA. This process requires multiple eukaryotic initiation factors (eIFs) that recruit the initiator methionyl-tRNA (Met-tRNAi) and assemble the active 80S ribosome at the

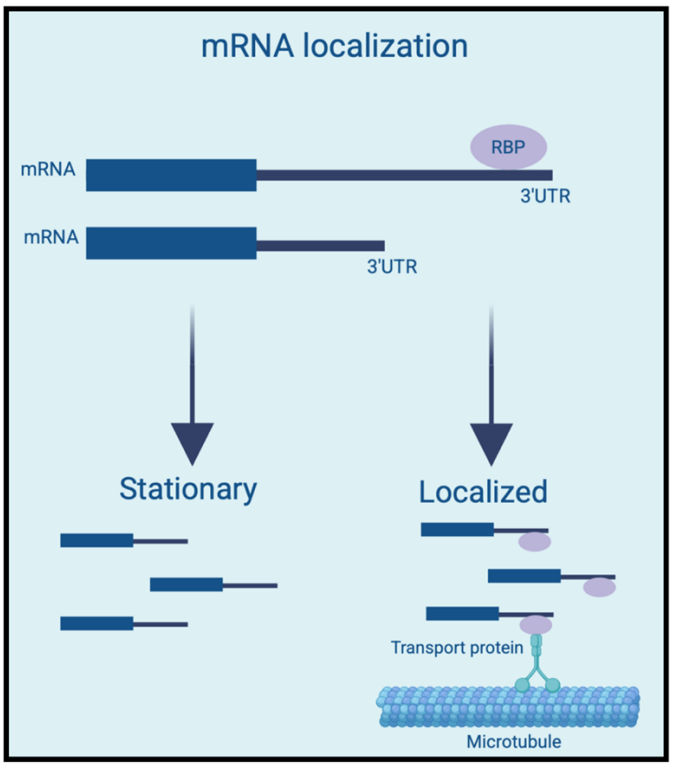

Figure 4: mRNAs transported into dendrites can display a “scanning” behaviors, remaining near previously activated synapses where they become locally translated (Adapted from Glock et al., 2017).

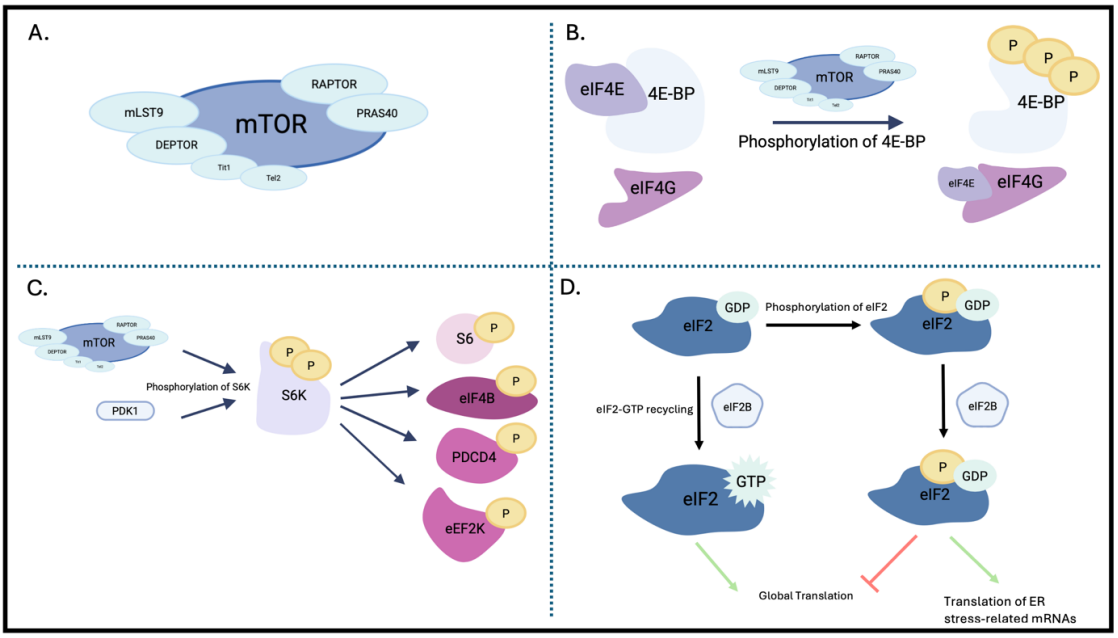

Figure 5:(A) Composition of mTORC1 complex. **(B)** mTORC1 induces 4E-BP phosphorylation. **(C)** mTORC1 induces S6K phosphorylation. **(D)**Conversion of inactive eIF2-GDP into active eIF2-GTP (Adapted from Laguesse & Ron, 2020; by Biorender)

AUG start codon. During elongation, elongation factors guide codon-dependent addition of amino acids to the growing polypeptide chain. Termination occurs when a stop codon (UAA, UGA, or UAG) is recognized, leading to release of the completed polypeptide and ribosome recycling (Buffington et al., 2014; Laguesse & Ron, 2020).

1.6.2. Local mRNA translation in neurons

Because neurons possess highly polarized and extended morphologies, they rely on local mRNA translation to rapidly adjust protein levels at synapses in response to activity (Glock et al., 2021; Holt et al., 2019). Local translation enables fast, spatially restricted protein synthesis without requiring long-distance protein transport from the soma.

Transporting mRNA rather than fully synthesized proteins is also energetically efficient, as a single transcript can generate multiple protein copies (Van Driesche & Martin, 2018). mRNA localization is directed by cis-regulatory elements, typically located in the 3' untranslated region (3'UTR). These elements are recognized by RNA-binding proteins (RBPs), which mediate mRNA packaging into transport granules and their association with motor proteins for subcellular targeting (**Figure 4**) (Glock et al., 2017).

Transport granules typically contain translational repressors that maintain mRNAs in a silent state during transport, together with components of the translational machinery that allow rapid on-site protein synthesis upon synaptic stimulation (Van Driesche & Martin, 2018).

1.6.3. Regulation of mRNA translation

Synaptic plasticity requires *de novo* protein synthesis at or near synapses (Buffington et al., 2014; Laguesse & Ron, 2020). Local translation is tightly regulated by multiple signaling pathways that control different steps of the translation process. Although translation initiation is generally rate-limiting and the most tightly regulated, elongation and termination are also subject to important control mechanisms. Major regulatory pathways include mTORC1 signaling, eIF2α and eEF2 phosphorylation, elongation factor control, and RBP- and miRNA-mediated regulation (Glock et al., 2021; Laguesse & Ron, 2020). Alcohol has been shown to dysregulate these translation control pathways, particularly mTORC1 signaling, thereby promoting persistent neuroadaptations.

1.6.3.1. mTORC1 and its downstream effectors

mTORC1 is a central regulator of cellular metabolism and protein synthesis. mTORC1 is required for PFC development, connectivity, and executive behaviors (Niu et al., 2018). mTORC1 is a multi-protein complex composed of the serine/threonine kinase mTOR, the regulatory-associated protein RAPTOR and mLST8, along with inhibitory subunits including PRAS40 and DEPTOR (**Figure 5A**). mTORC1 promotes translation primarily through

phosphorylation of two major targets: 4E-binding proteins (4E-BPs) and S6 kinase (S6K) (Laguesse & Ron, 2020).

In the basal state, 4E-BP binds eIF4E and prevents assembly of the eIF4F initiation complex. mTORC1-dependent phosphorylation of 4E-BP releases eIF4E, allowing recruitment of eIF4G and activation of cap-dependent translation initiation (**Figure 5B**). S6K is activated by phosphorylation via mTORC1 and PDK1 and phosphorylates several translation-related targets, including the ribosomal protein S6 and eIF4B, thereby enhancing translational efficiency. S6K also inhibits eEF2 kinase, indirectly promoting elongation (**Figure 5C**) (Laguesse & Ron, 2020).

As is well known, mTORC1 signaling is required for activity-dependent local translation and contributes to synaptic plasticity, learning, and memory. Disruption of this pathway can result in neurodevelopmental, neurodegenerative, and psychiatric disorders, including addiction (Laguesse & Ron, 2020). Importantly, binge-drinking has been shown to activate mTORC1 signaling in the adult Nac and orbitofrontal cortex (OFC), two brain regions critically involved in reward processing and alcohol-related behaviours (Laguesse et al., 2017)

1.6.3.2. eIF2α pathway

Regulation of eIF2α phosphorylation provides another major mechanism controlling translation initiation. Conversion of eIF2-GDP to active eIF2-GTP requires the exchange factor eIF2B. When eIF2α is phosphorylated, eIF2 inhibits eIF2B, reducing global protein synthesis. At the same time, this pathway selectively enhances translation of specific stress-response mRNAs, particularly those involved in endoplasmic reticulum stress signaling (**Figure 5D**) (Laguesse & Ron, 2020). Phosphorylation of eIF2a plays a key role in long-term synaptic plasticity that underlies learning, memory, and addiction, including memory reconsolidation of drug-paired memory (Chesnokova et al., 2017; Trinh & Klann, 2013).

1.6.3.3. eEF2 pathway

Elongation phase of mRNA translation is regulated by eEF2 and its kinase eEF2K, which together modulate ribosomal translocation speed. Although only a limited number of studies have implicated eEF2 in addiction-related neuroadaptations, the eEF2/eEF2K pathway has emerged as a potential regulator of activity-dependent mRNA translation in alcohol use disorder (David et al., 2020; Laguesse & Ron, 2020). Furthermore, dysregulated eEF2 activity has been associated with PFC dysfunction and resulting behavioral impairments (Laguesse & Ron, 2020a; W. Li et al., 2021).

Among translational control mechanisms, the eEF2/eEF2K pathway is particularly relevant because it directly regulates the elongation phase of protein synthesis.

eEF2 promotes ribosomal translocation along mRNA, whereas phosphorylation of eEF2 by eEF2 kinase inhibits its activity by preventing it from binding to the ribosome and it leads to slower elongation (Taha et al., 2013). While eEF2 phosphorylation generally reduces global protein synthesis in neurons, it is also associated with increased expression of selected proteins in the vicinity of the synapses (Heise et al., 2016). Through its ability to regulate both overall protein synthesis rates and the expression of specific synaptic proteins, the eEF2/eEF2K pathway may influence dendritic spine remodeling, synaptic plasticity and behavioral adaptations. Consequently, dysregulation of this pathway during adolescence could interfere with normal PFC maturation. However, whether AAE modifies eEF2 signaling in the developing PFC remains poorly understood.

Interestingly, eEF2K is itself regulated by upstream translational control pathways. In particular, eEF2K is a substrate of S6K, a major downstream effector of mTORC1 signaling. Phosphorylation of eEF2K by S6K inhibits its activation under basal Ca^{2+} concentrations. As a result, eEF2 remains dephosphorylated and active, thereby promoting translation elongation (Taha et al., 2013).

In addition to elongation factors, RBPs further regulate translation by controlling mRNA localization, stability, and translation efficiency. Furthermore, several microRNAs (miRNAs) are enriched in dendrites and contribute to local translation repression and synaptic plasticity, although mechanisms controlling their local regulation remain incompletely understood (Laguesse & Ron, 2020).

1.7. Translational control pathways in alcohol-related neuro-adaptions

mTORC1 signaling is one of the best-characterized translational control pathways involved in alcohol-induced neuroadaptations (Ron & Barak, 2016). Excessive alcohol consumption can activates mTORC1 signaling in reward-related regions, including the nucleus accumbens and orbitofrontal cortex leading to increased phosphorylation of downstream targets such as 4E-BP, S6K, and S6. This activation promotes the synthesis of synaptic proteins involved in structural and functional plasticity, including ARC, PSD-95, GLUA1, HOMER, CRMP2, and Prosapip1. While mTORC1 has emerged as a major translational regulator in alcohol-related neuroadaptations, considerably less is known about the contribution of other translational control pathways. Moreover, the impact of AAE on translational regulation during PFC maturation remains poorly understood. In particular, whether eEF2 signaling is altered by AAE has not been extensively investigated (Laguesse & Ron, 2020).

Objectives and strategy

We employed the voluntary adolescent binge-drinking model previously described by Van Hees *et al.* (2022). Alcohol intake was monitored throughout the drinking sessions and compared between male and female mice. This model was used to assess the impact of AAE on the PFC maturation.

Based on this framework, this Master's thesis aims to determine whether AAE alters molecular and cellular mechanisms involved in PFC maturation. More specifically we investigated whether AAE affects translational control pathways, with a particular focus on eEF2 signaling, and whether these molecular alterations are associated with changes in dendritic arborization, dendritic spine morphology, and interneuron populations. To address these questions, we combined biochemical analyses of translation-related signaling pathways with morphological characterization of layer II/III projection neurons and immunohistochemical assessment of interneuron populations in the PFC. Together, these complementary approaches were designed to provide an integrated view of how AAE may disrupt PFC maturation and contribute to long-term vulnerability to behavioral dysfunction.

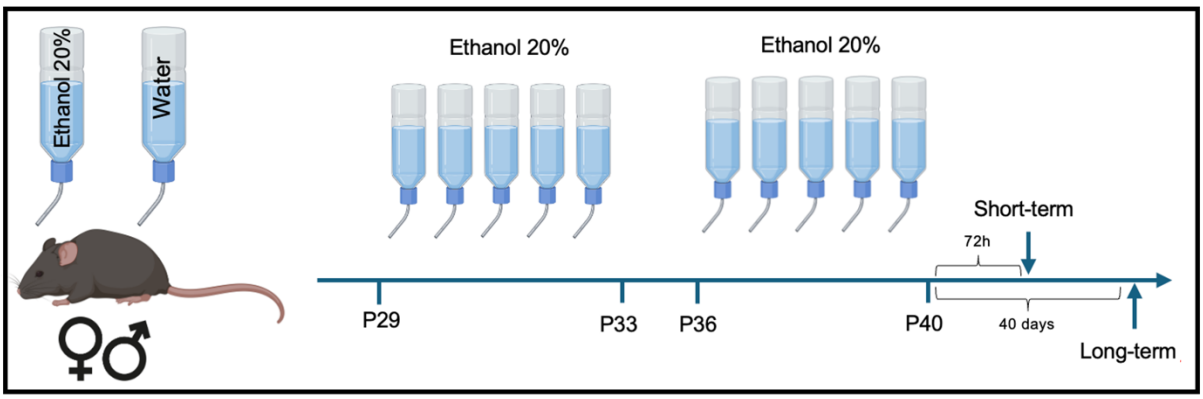

Figure 6: Adolescent alcohol exposure model and timeline of subsequent analysis (Adapted from Laguesse & Ron, 2020; by Biorender)

Material & Methods

3.1. Experimental model

3.1.1. Animals

C57BL/6J male and female mice (Janvier Labs, Saint Berthevin, France) were treated according to the guidelines of the Belgian Ministry of Agriculture in agreement with the European Community Laboratory Animal Care and Use Regulations (86/609/EEC) for care and use of laboratory animals under the supervision of authorized investigators (ethical file 23-2562). Experimental animals were bred in-house and maintained with *ad libitum* access to food and constant temperature (19–22°C) and humidity (40–50%) under a reversed light/dark cycle (lights on at 22:00, off at 10:00) (Van Hees et al., 2022).

3.1.2. Adolescent Alcohol exposure

Male and female adolescent mice were exposed to a modified Drinking in the dark (DID) paradigm (Van Hees et al., 2022) from P29 to P33 and from P36 to P40 (**Figure 6**). The age for AAE was chosen during early/mid adolescence. All mice were group-housed to prevent the emergence of social isolation stress, except for the 4 hours alcohol drinking sessions. At 9:30, mice were weighed and transferred to single cages with food and water *ad libitum*. At 12:00, water was replaced by ethanol (20% in tap water). At 16:00, alcohol was removed, and mice were group-housed until the next day. Animals that drank less than 4g/kg/4h for more than three sessions were excluded (Van Hees et al., 2022), resulting in the exclusion of 26 animals out of 92 AAE mice. The threshold of 4g/kg/4h represents the amount of alcohol ingested leading to the minimal binge-drinking BAC value (Thiele & Navarro, 2014a). This model has previously been validated in the lab by showing that adolescent mice voluntarily consumed high amount of alcohol and reached BAC values ranging between 100 and 200 mg/dl, which correspond to binge-drinking values observed in humans (Van Hees et al., 2022). Control mice received only water and alternated between single- and group-housing accordingly. Mice samples were collected 72 hours after the last drinking session (P43, middle adolescence) or following 40 days of abstinence (P80, adulthood) for molecular and morphological analysis (**Figure 6**). Individual drinking data can be found in **Table 1** in the annexes.

3.2. Morphological analysis: methods details

3.2.1. Collection of brain samples

72 hours or 40 days following the last drinking session (see Adolescent alcohol exposure section), mice were sacrificed, and brains were collected. Brain coronal slices were prepared in an ice-cold solution (in mM: 87 NaCl, 25 NaHCO3, 10 D-glucose, 75 sucrose, 2.5 KCl, 1.25 NaH2PO4, 0.5 CaCl2 and 7 MgCl2, equilibrated with 95% O2 / 5% CO2 (320-330 mOsm). Three hundred µm coronal slices containing the PFC were cut using a vibratome (Leica VT-1200, Nussloch, Germany).

3.2.2. Biocytin filling of PFC layer II/III projection neurons (L. Oskera)

Pipettes were filled with intracellular solution containing 120 mM K-gluconate, 20 mM KCl, 2 mM MgCl2, 4 mM Na2ATP, 0.5 mM Na2GTP, 5 mM Na1Phosphocreatine, 0.1 mM EGTA, 10 mM HEPES, and 0.2% biocytin (Sigma-Aldrich, #576-19-2) (~ 300 mOsm, pH 7.3). Neurons were maintained at a holding potential of -70 mV. Under infrared differential interference contrast, whole-cell patch-clamp recordings were obtained layer II/III projection neurons of the PL PFC. Biocytin diffused into the neurons from the recording pipette and the recording time was ~ 15 min to allow homogeneous distribution of biocytin in distal dendritic and axonal processes. Patch-clamp recordings and biocytin filling were performed by Léa Oskera.

3.2.3. Immunohistochemistry

Following biocytin processing, brain slices were fixed in freshly 4% paraformaldehyde (PFA) (PFA (40 g/L), Na2HPO4 (14.2 g/L), KH2PO4 (0.75 g/L), NaCl (9 g/L), NaOH (12 drops/L) for 24 hours and transferred in Phosphate Buffered Saline (PBS) for storage before immunostaining. For immunolabelling, brain slices were washed 3 times in PBS followed by 4 hours blocking and permeabilization step in 10% donkey serum (DS) in PBS-Triton 0,1% (PBST) buffer at 4°C. Brain slices were then incubated with primary antibodies (rat anti-Ctip 2, 1/500, Abcam, #ab18465; mouse anti-Satb2, 1/500, Abcam, #ab51502; rabbit anti-Cux1, 1/500, Merck Millipore, #ABE217) in PBST-DS 5% over two nights at 4°C. Three five-minute washes were carried out with PBS before incubating the brain slices with secondary antibodies (anti-rat 647, 1/500, Jackson ImmunoResearch Laboratories #712-605-153; anti-mouse 555, 1/500, Invitrogen # A31570; anti-rabbit 750, 1/500, ABCAM, # Ab175731) and Fluorescein Avidin DCS (Vector Laboratories, # A-2001-5) which binds to biocytin in order to reveal the whole structure of injected neurons. Three five-minute washes were again carried out with PBS, including one containing DAPI (1/5000, Sigma-Aldrich Ca, # D9542-10M6). Sections were finally mounted on microscope slides cut frosted (Epredia #AA00000112E01MNZ10) with Fluorescence Mounting Medium (DAKO, #S3023). Slides were dried and stored at 4°C.

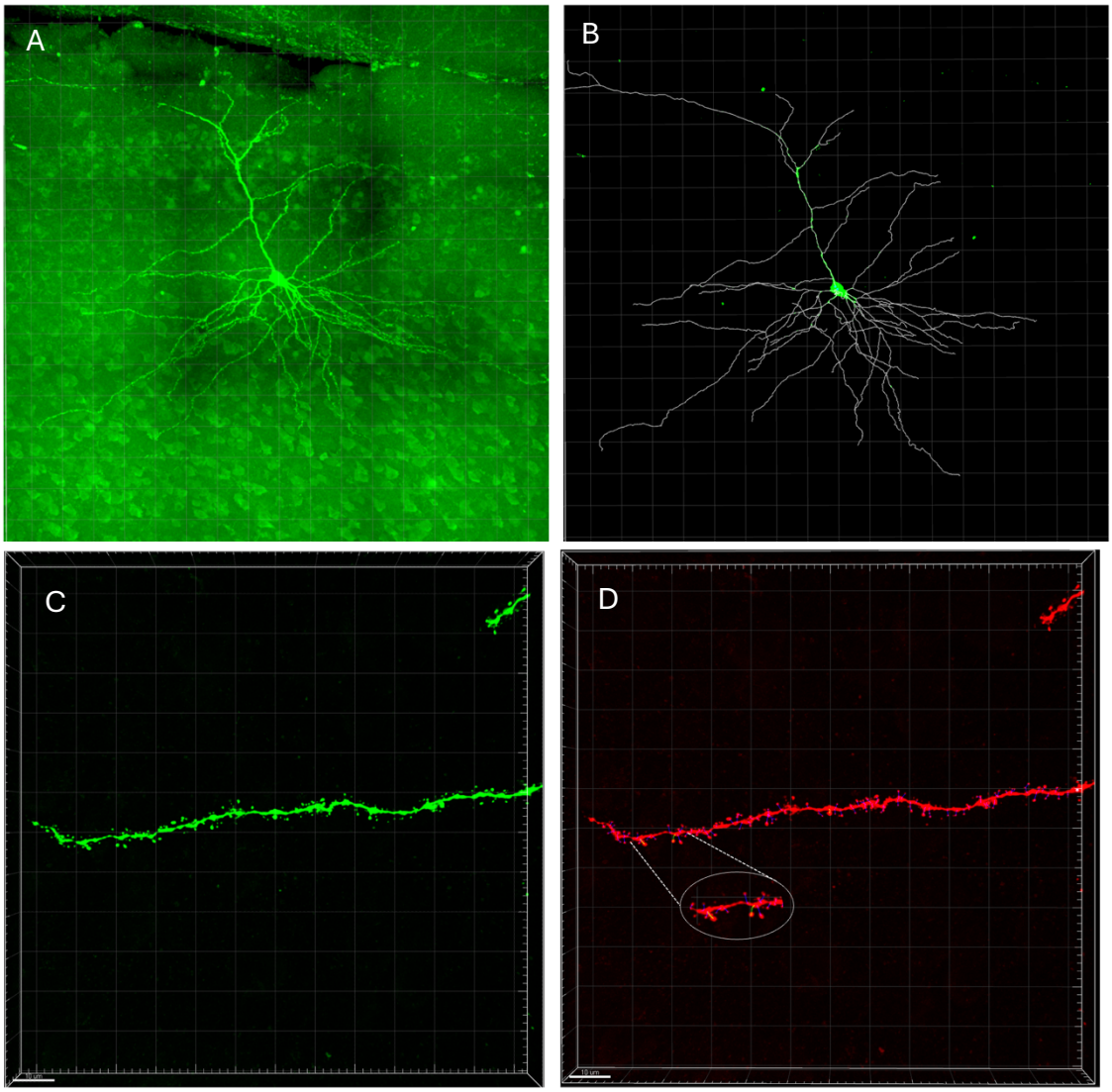

Figure 7: Morphological analysis of dendritic arborizations and spines from PFC layer II/III projection neurons. (A-B) Representative picture of a layer II/III biocytin-filled projection neurons in the PFC. Dendritic arborization analysis was performed using Imaris software. (C-D) Representative picture of a dendrite from a layer II/III biocytin-filled projection neuron in the PFC. Dendritic spine morphometric measurements were performed using Imaris software (D) Dendritic spine classification using Imaris Spines Classifier. Blue=long thin-type, green=mushroom-type, red=stubby-type (see Figure 8). Images were acquired with A1 Nikon confocal, and neurons (A-B) and dendrites (C-D) were reconstructed with Imaris software. Scale bar = 30 µm (A-B); scale bar = 10 µm (C-D).

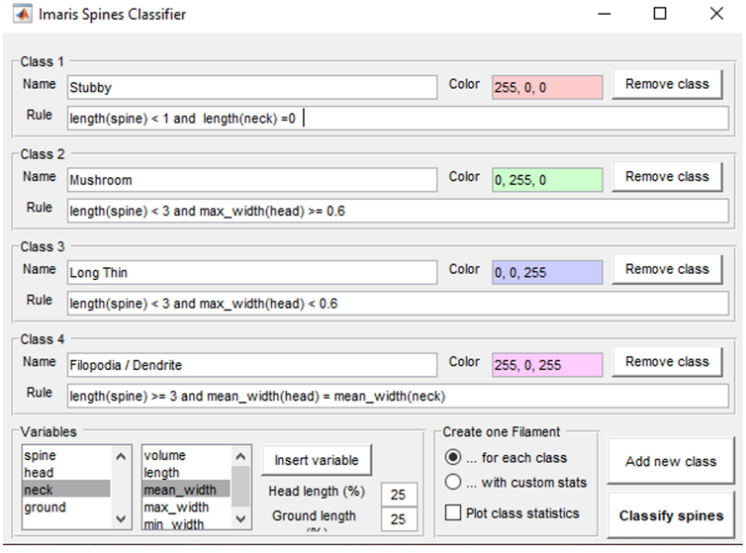

Figure 8: Classification of dendritic spine subtypes (Mushroom-, Long thin-, stubby- and Filopodia-type) using Imaris

3.2.4. Dendrites analyses

Images capturing the full dendritic arborization and soma of biocytin-filled layer II/III projection neurons in the prelimbic PFC were acquired using the Nikon A1R with a 40x objective with a z interval of 1.5 µm (30-35 images per cell). Images were reconstructed in 3D, and biocytin-filled neurons were traced using Imaris software (**Figure 7**). Dendritic complexity was assessed by Sholl analysis, with concentric spheres centered on the soma. The analysis extended from a starting radius of ten µm to a maximum radius of 600 µm, using ten µm increments. In addition, the number of branching points and terminal endpoints were quantified using Imaris software. Four water-exposed and four AAE mice were used and a total of 13 neurons were analyzed. All analyses were performed blind to experimental conditions.

3.2.5. Dendritic spine analysis

Images were acquired with confocal microscopy using a 100x oil immersion lens. Individual neurons were chosen for spine analysis based on the following criteria: (i) There was minimal or no overlap with other labelled cells, (ii) At least three primary dendrites needed to be visible for the cell to be used for analysis, (iii) Only distal dendrites (3^{rd} or 4^{th} order) were analyzed (Laguesse et al., 2017). A first image z stack of between four and six images was taken at a z separation of one µm for each biocytin-injected neuron using a 40x oil immersion lens to establish whether neurons expressed Cux1, SatB2, and/or Ctip2. As part of this master thesis project, analyses were performed on Cux1- and SatB2-positive neurons. Then, dendrites and their protrusions were visualized by acquiring image z stacks of approximatively 30 images at a z separation of 0.225 µm using the 100x objective with 2x zoom. (**Figure 7C**). Three to four dendritic segments were imaged per neuron. After confocal imaging, spine density and morphometric measurements were analyzed by using IMARIS software. (**Figure 7D**). Spine density was defined as spine number on dendritic segment length per ten µm, and the mean of spine morphological parameters (spines length, spines volume, head volume and head max diameter) was measured per dendrite. In parallel, dendritic spines were classified into four types based on their length and neck and head morphology (Risher et al., 2014).

Filopodia were defined as long filamentous protrusions >= 3 µm in length that lacked a discernible head (head mean width equal to neck mean width). Stubby protuberances were defined as protrusions < 1 µm in length, which did not appear to have neck. Thin spines were defined as protrusions < 3 µm in length and characterized by a small head (head max width < 0.6 µm). Mushroom-shaped spines were defined as dendritic protrusions < 3 µm in length and characterized by a large head (head max width >= 0.6 µm) (**Figure 8**). For each of the animal examined in each group, one to five neurons were analyzed, with at least 3 dendrites analyzed per neuron. Four water-exposed mice and five AAE mice were used and a total of 18 neurons were analyzed.

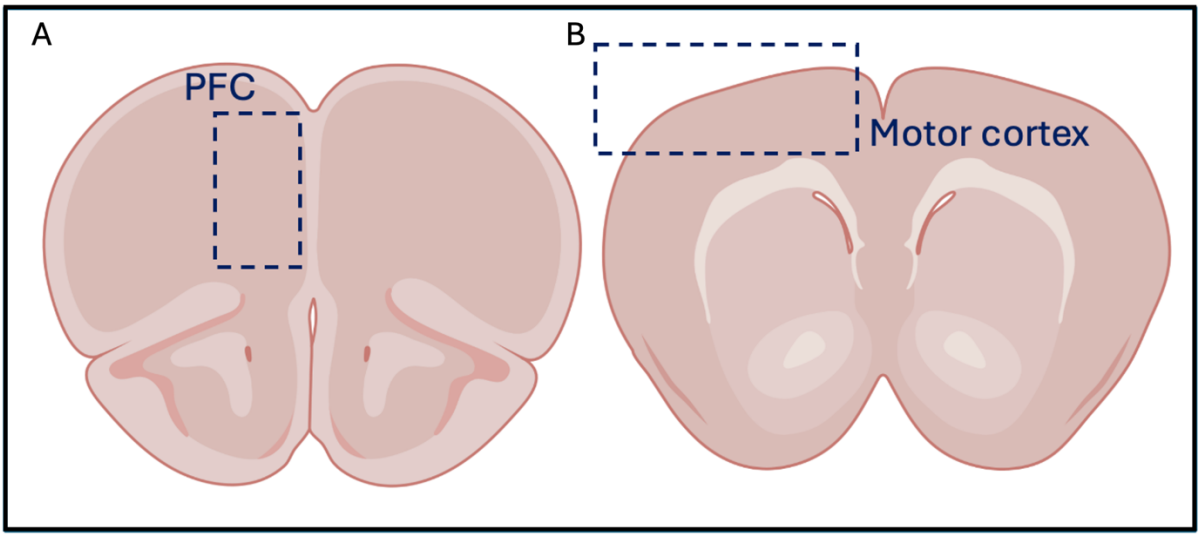

Figure 9: Schematic representation of the region of interest (A, prefrontal cortex) and the control region (B, motor cortex) (Created from Biorender).

3.3. Local and global translation analysis: methods details

3.3.1. Collection of brain sample

Mice exposed to the DID paradigm were sacrificed by cervical dislocation 72 hours or 40 days after the final drinking session. Afterward, brains were quickly removed, the PFC and the motor cortex (as a control region) were dissected on an ice-cold platform by using a punch and a slicer for molecular analysis (**Figure 9**). Brains were directly snap-frozen in liquid nitrogen and stored at -80°C.

3.3.2. Purification of synaptic fraction

This protocol allows the isolation of total (H), cytoplasmic (S2) and synaptic (P2) protein fractions. The tissue fragment was removed from -80°C and placed on ice in 400 µl of Hepes buffer (Hepes (10mM), EGTA (1mM), saccharose (0,32M), protease (1 tablet/ 10mL) and phosphatase inhibitors). The tissue was homogenized with a two mL dounce. 100 µl of the mix were collected in a new tube and 100 µl of RIPA buffer (Tris-HCl (50 nM, EDTA (5 mM), NaCl (120mM), NP-40 (1%), Deoxycholate (0,1%), SDS (0,5%), with proteases and phosphatases inhibitors) were added. A centrifugation (10.000 g) during ten minutes at 4°C was done. The supernatant was collected and constitutes the total protein homogenate (H). The remaining 300 µl in the starting tube underwent a centrifugation (1.000 g) ten minutes at 4°C. Then, the pellet was discarded, and the supernatant (S1) underwent a second centrifugation (12.000 g) for 15 minutes at 4°C. The supernatant was then isolated and corresponded to the cytoplasmic fraction (S2). The pellet was washed with 300 µL of HEPES-EGTA-Saccharose buffer and centrifuged (12.000 g) for ten minutes at 4°C. Supernatant was discarded and the pellet was resuspended in 100 µl of RIPA buffer and constituted the synaptic fraction (P2) (**Figure 10**).

3.3.3. Protein dosage

The protein concentration of each fraction (H, S2 and P2) was determined by using the Pierce BCA Protein Assay Kit" (Thermo Fisher, Rockford, USA; REF:23225). Briefly, by using a bovine serum albumin standard curve (between 0 and 2000 µg/ml), protein dosage is realized by the Biuret reaction. Ten µl of each BSA standard and protein samples are placed in a 96 well-plate (in duplicate). The two reagents were mixed by the ratio 50:1 and 200 µl of this mix was added to each well. The plate was then placed at 37°C for 30 minutes. An absorbance measurement was performed at 562 nm by the Multiskan Ascent (Thermo Labsystems). A standard curve was realized to determine the concentration in µg/µl of each sample.

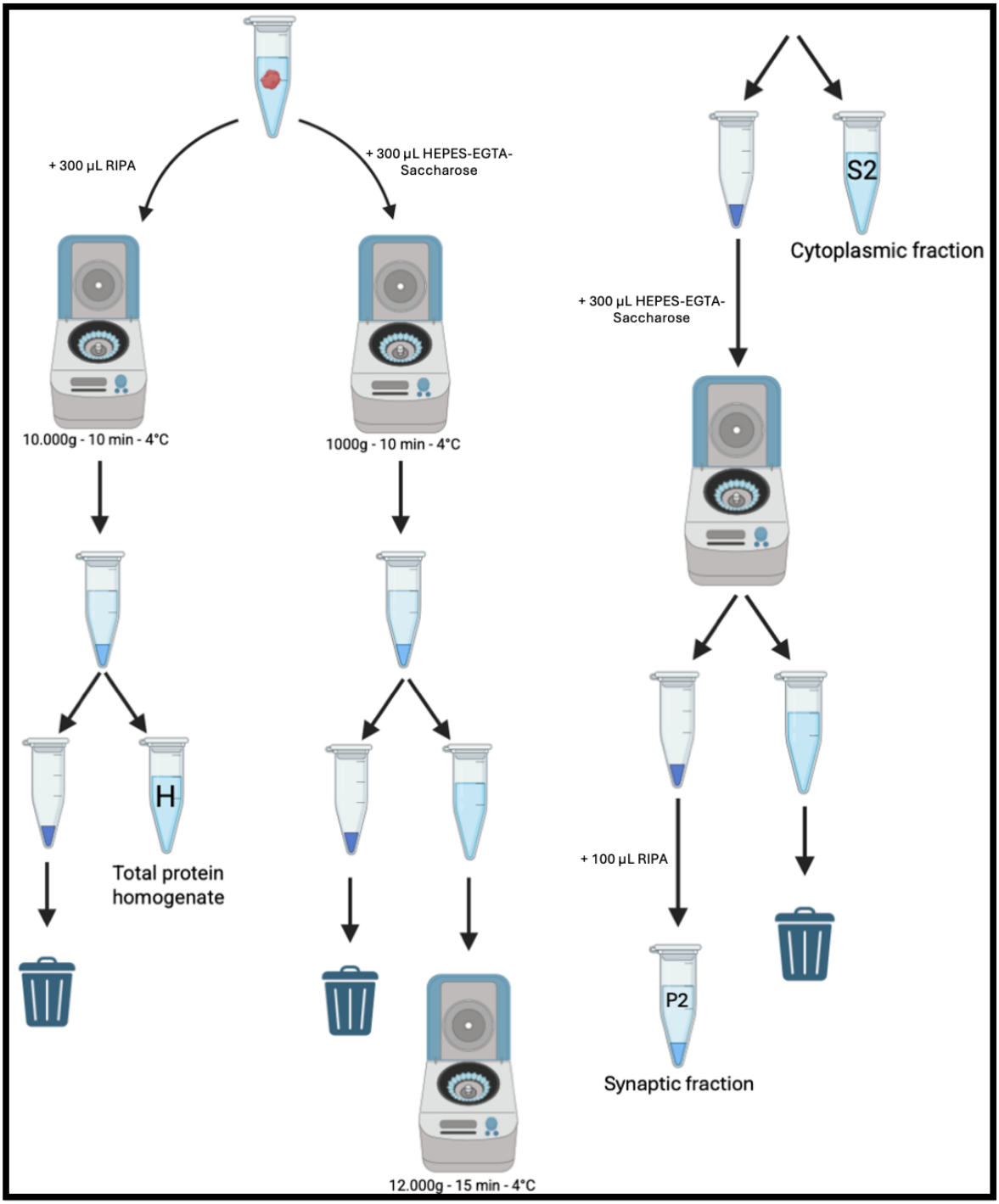

Figure 10: Protocol of total, cytoplasmic and synaptic fraction isolation (by Biorender).

3.3.4. Sample preparations for Western Blot

Samples were diluted in RIPA buffer at the same concentration. 25% of loading buffer [SDS (2%), glycerol (10%), Tris (60 mM, pH 6,8), bromophenol blue (0,02%), β-mercaptoethanol (140 mM)] were added to each tube and samples were heated at 95°C for five minutes to denature proteins. Samples can be used directly in the Western Blot (WB) or stored at -20°C.

3.3.5. Western Blotting

3.3.5.1. Principle

WB analysis allows the detection of specific proteins in tissue samples and the assessment of their relative expression compared to a control condition. Proteins are separated according to their molecular weight by migration through an SDS-PAGE gel, then transferred on a nitrocellulose membrane. The presence and relative abundance of the protein of interest are revealed using specific antibodies.

3.3.5.2. Methods

Migration:

For migration, a separating gel of bis-acrylamide (8%) and a concentrating gel (4%) were prepared (**Table 2**). Samples were loaded in addition to 6 µl of a molecular weight marker « PageRuler Plus Prestained Protein Ladder » (ThermoFisher Scientific Inc., MA, USA, #26619). Proteins were separated by electrophoresis in a running buffer (Tris (25 mM), Glycine (192 mM), SDS (0,1%)), first 30-45 min at 80V and then for two hours at 120V.

Transfer:

Proteins were transferred from the gel onto a nitrocellulose membrane (Amersham). Protein transfer was performed at 300 mA for two hours in transfer buffer (Tris (25mM), glycine (192 mM), and methanol (20%), pH 8.3).

Blocking:

The membrane was incubated for 30 minutes in 5% BSA prepared in TBST buffer (Tris (20mM), NaCl (150mM), Tween 20 (0.1%), pH 7.6) to block non-specific binding sites and prevent non-specific antibody interactions.

For 2 gels	Separating gel (8%)	Stacking gel (5%)
H2O	9,3 mL	6,8 mL
Acrylamide	5,34 mL	1,68 mL
Tris	(pH 8.8; 1.5 M) 5 mL	1,25 mL
20% SDS	100 µL	50 µL
TEMED	8 µL	10 µL
APS 10%	200 µL	100µL

Table 2: Composition of SDS-PAGE gels for Western Blot

Detected protein	Antibody type	Source	Dilution	Company	Reference number
eEF2	Polyclonal	Rabbit	1/250	Cell Signaling	2332
peEF2	Polyclonal	Rabbit	1/250	Cell Signaling	2331
S6	Monoclonal	Rabbit	1/250	Cell Signaling	2217
pS6	Monoclonal	Rabbit	1/250	Cell Signaling	4858
β-actin HRP coupled	Monoclonal	Mouse	1/2000	Sigma	A3854

Table 3: Primary antibodies used for Western Blot.

Antibodies incubation:

The membrane was incubated with the primary antibodies (**Table 3**) for one or two nights at 4°C. After three ten-minute washes in TBST, membranes were incubated for one hour at room temperature with the secondary antibody (1/1000, goat anti-rabbit IgG conjugated to horseradish peroxidase, Invitrogen, CA, USA).

Detection:

Detection was performed using the Pierce™ ECL Western Blotting Substrate Kit (Thermo Scientic, Rockford, USA), which contains two reagents: horseradish peroxidase (HRP) pro-substrates and luminol. The HRP pro-substrates react with the HRP conjugated to the secondary antibodies, generating a component that interacts with luminol, causing its excitation. When luminol returns to its ground state, it emits light, which is captured using the Amersham ImageQuant 800 imaging system (Cytiva). Signal intensity was quantified using FIJI software (NIH, USA).

3.4. Interneuron analysis

3.4.1. Collection of brain slices

Mice exposed to the DID paradigm were perfused at P43 and P80, following anesthesia with euthasol administered by intraperitoneal injection. After opening the rib cage, a saline solution containing 0.9% NaCl and 0.1% heparin was injected into the heart, followed by paraformaldehyde (PFA) fixation solution (PFA (40 g/L), Na2HPO4 (14.2 g/L), KH2PO4 (0.75 g/L), NaCl (9 g/L), NaOH (12 drops/L)). The PFA perfusion enables fixation of tissues via the circulatory system, which helps avoid autofluorescence from blood vessels. The animals were then decapitated and the brains removed.

The brains were post-fixed overnight at 4°C in 4% PFA and subsequently transferred to a cryoprotective solution of 30% sucrose in PBS (Phosphate Buffered saline: NaCl 137 mM, phosphate 10 mM, KCL 2.7 mM, pH 7.4) for 48 hours. Brain sections (40 µm thick) were prepared using a cryostat (Microm NX70, Thermo Fisher Scientific), collected in PBS, and stored at 4°C.

3.4.2. Immunohistochemistry

Brain slices underwent a four hours blocking step at 4°C and permeabilization step in 10% donkey serum (DS) in PBST buffer at 4°C. Brain slices were then incubated with primary antibodies (**Table 4**) in PBST-DS 5% overnight at 4°C. Sections were washed three times in PBS before incubating the brain slices with secondary antibodies (anti-Mouse Ig2B 647, Invitrogen, #A21242; 1/500; anti-rabbit 750, 1/500, ABCAM, # Ab175731; anti-Guinea Pig 488, Invitrogen, #A11073). Three five-minute washes were again carried out with PBS, including one containing DAPI (1/5000, Sigma-Aldrich Ca, # D9542-10M6). Sections were finally mounted on microscope slides cut frosted (Epredia #AA00000112E01MNZ10) with Fluorescence Mounting Medium (DAKO, #S3023). Slides were dried and stored at 4°C.

Interneuron quantification was performed using the software QuPath. For each section, interneurons were counted manually and normalized to the total number of DAPI-positive cells. Results were expressed as the percentage of interneurons relative to the total cell population (interneuron count/$DAPI^+$ cells) x100. The different subregions of the PFC, including the prelimbic, infralimbic, and anterior cingulate cortex, were analyzed separately. Quantification was performed on 1-2 sections per animal.

Detected protein	Antibody type	Source	Dilution	Company	Reference number
Somatostatin	Monoclonal	Mouse	1/250	Santa Cruz Biotechnology	sc-55565
Calbindin	Polyclonal	Rabbit	1/250	Abcam	ab108404
Parvalbumin	Polyclonal	Guinea Pig	1/500	Synaptic system	195004
Calretinin	Monoclonal	Mouse	1/250	Santa Cruz Biotechnology	sc-365956

Table 4: Primary antibodies used for immunohistochemistry.

3.5. Statistical analysis

All data were analyzed using GraphPad Prism 10 (GraphPad Software, USA), with a two-tailed unpaired Welch's t-test, except for drinking and Sholl data, which were analyzed using two-way analysis of variance (ANOVA). Data are presented as mean ± SEM, and statistical significance was set at $p < 0.05$.

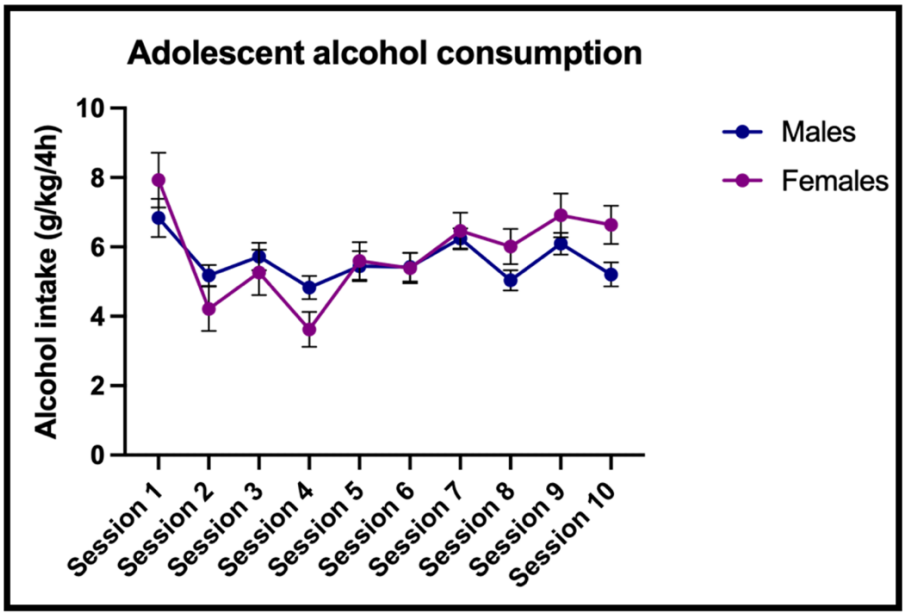

Figure 11: Alcohol consumption of adolescent mice. Mice consumed alcohol between P29 (session 1) and P40 (session 10). Two-ways ANOVA showed a significant main effect of sessions on alcohol intake ($p < 0.0001$, $F_{(4.856, 437.1)} = 9.631$) and a significant sessions-by-sex interaction ($p = 0.0434$, $F_{(4.856, 437.1)} = 2.330$). No main effect of sex on alcohol intake was observed ($p = 0.5892$, $F_{(1, 90)} = 0.2937$). N=44 males, n=22 females.

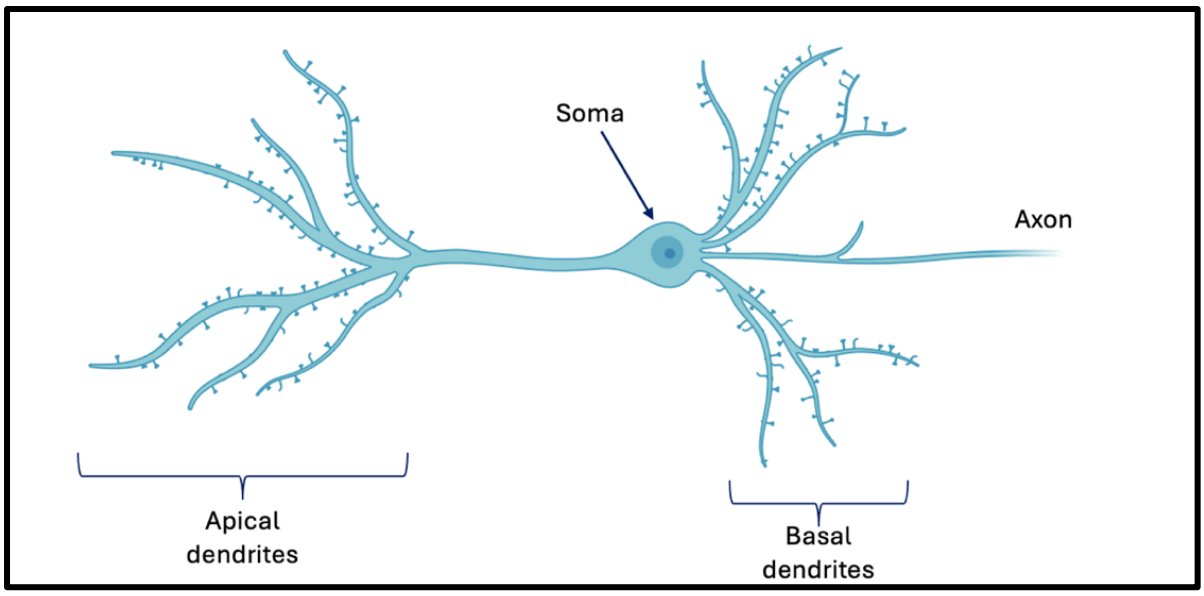

Figure 12: Schematic representation of a neuron and its apical and basal dendritic arborizations (By Biorender).

Results

4.1. Mouse model of adolescent alcohol binge-drinking

Mice were exposed to a slightly modified version of the Drinking in the Dark paradigm across ten sessions from P29 to P40. Alcohol intake (g/kg/4h) was recorded during each session and analyzed as a function of sex and drinking sessions for all adolescent mice included in the study (**Figure 11**) (see **Table 1 in annexes** for detailed consumption data).

Two-way repeated-measures ANOVA revealed a significant effect of sessions on alcohol consumption ($p < 0.0001$), indicating that alcohol intake varied across the exposure period. A significant session-by-sex interaction was also observed ($p = 0.0434$), whereas no overall effect of sex was detected ($p = 0.5892$).

Alcohol consumption was highest during the first drinking session in both sexes and subsequently decreased during sessions 2-4. Intake progressively increased thereafter and stabilized between 5 and 7 g/kg/4h during the final sessions. The significant interaction between sex and session was mainly driven by a higher alcohol intake in females during the last drinking sessions (sessions 8-10). However, when averaged across all sessions, alcohol consumption did not differ between sexes, with females consuming 5.80 ± 0.4039 g/kg/4 h and males consuming 5.60 ± 0.1975 g/kg/4 h.

Overall, alcohol intake levels were consistent with those previously shown to produce binge-like blood alcohol concentrations in this model (Thiele & Navarro, 2014; Van Hees et al., 2022). These results confirm successful implementation of the AAE model and indicate that both male and female mice voluntarily consumed pharmacologically relevant amount of alcohol throughout adolescence.

4.2. Structural analysis of AAE-induced alterations in dendritic and spine morphology in layer II/III prelimbic projection neurons

Previous studies from our laboratory have shown that AAE induces delayed behavioral alterations and transient changes in dendritic spine maturation in layer V prelimbic projection neurons. We therefore investigated whether similar structural alterations could also be detected in superficial layer II/III projection neurons of the prelimbic PFC. Morphological analyses were performed at P43 and P80 following AAE to investigate the short- and long-term effects of AAE on layer II/III PL projection neurons.

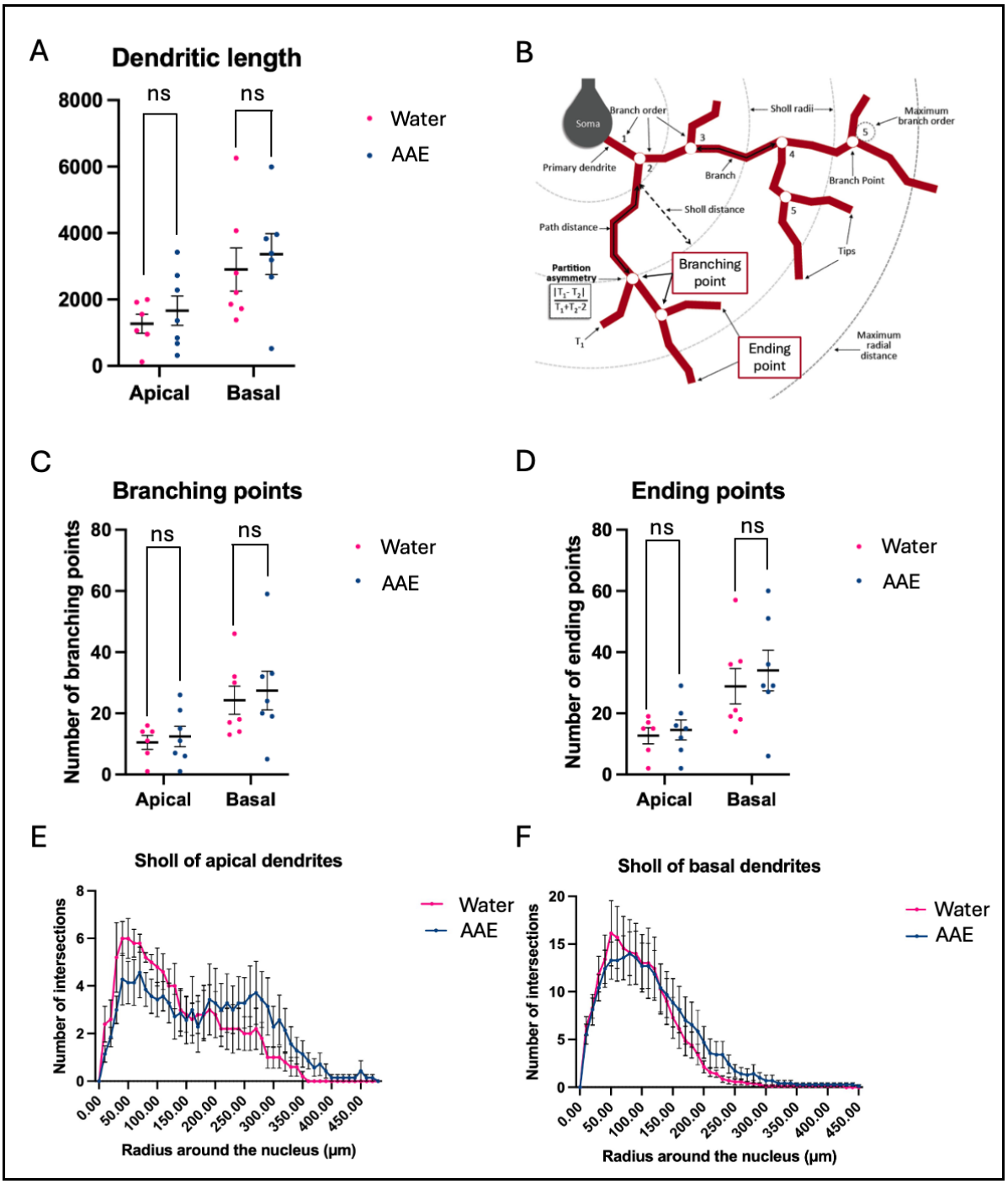

Figure 13: Morphometric analysis of apical and basal dendrites in layer II/III projection neurons of the prelimbic PFC at P43 in water- and alcohol-exposed mice. (A) Total length of apical (left) and basal (right) dendritic arborization evaluated by Welch's t test. **(B)** Schematic representation of Sholl analysis illustrating dendritic morphometric parameters. The number of dendritic intersections is measured at successive radial distances from the soma, with branching points and terminal endings represented (adapted from *Rietveld et al.*, 2015). **(C-D)**. **(E-F)** Sholl analysis of apical (**E**) and basal (**F**) dendrites analyzed by two-way ANOVA to evaluate the main effects of distance from the soma, AAE exposure, and their interaction. Preliminary data are presented as mean **±** SEM: for apical dendrites: n=5 water neurons, n=6 AAE neurons; for basal dendrites: n=5 water neurons, n=5 AAE neurons: n=2 water mice, n=3 AAE mice: *p<0.05, **p<0.01,***p<0.001.

4.2.1. P43 mice

4.2.1.1. Dendrite analysis

To determine whether AAE induces short-term changes in dendritic morphology and complexity, we separately analyzed morphometric parameters of apical and basal dendritic arborizations in layer II/III projection neurons of the prelimbic PFC at P43. Apical dendrites correspond to the most distal processes extending along the ascending neuronal trunk, whereas basal dendrites originate directly from the soma (**Figure 12**). Dendritic morphology was assessed using measurements of total dendritic length, as well as the number of branching points and terminal endpoints. Additionally, Sholl analysis was performed to quantify the number of dendritic intersections at increasing radial distances from the soma (**Figure 13B**). All analysis were conducted in male mice. Statistical analyses were performed at the neuron level and should therefore considered preliminary due to the limited number of animals. Between one and three neurons were analyzed per animal. A total of two water and three AAE mice were included in these analyses.

At P43, no difference was observed in total dendritic length between water- and AAE-exposed groups, neither for apical ($p = 0.8267$) or basal ($p = 0.2052$) dendritic arborizations (**Figure 13A**). Similarly, the number of branching ($p_{apical} = 0.2611$, $p_{basal} = 0.7573$) and terminal points ($p_{apical} = 0.2147$, $p_{basal} = 0.9726$) did not differ between groups in either dendritic compartment (**Figures 13C-D**). Sholl analyses further revealed a significant effect of the distance from the soma on the number of dendritic intersections in both apical ($p < 0.0001$) and basal ($p < 0.0001$) trees, reflecting the expected variation in dendritic complexity across radial distances. No main effect of AAE was detected for either apical ($p_{apical} = 0.5713$) or basal ($p_{basal} = 0.0750$) dendrites. However, a significant distance-AAE interaction was observed for both apical and basal dendritic arborization ($p_{apical} = 0.0234$, $p_{basal} < 0.0001$) **(Figure 13E-F**), suggesting that AAE may alter the spatial distribution of dendritic branches without affecting overall dendritic morphology. Overall, these preliminary data suggest that AAE does not induce major changes in global dendritic morphology or complexity.

4.2.1.2. Dendritic spine analysis

We next evaluated whether AAE leads to short-term alterations in dendritic spine density and morphology in layer II/III projection neurons of the prelimbic PFC at P43. Statistical analyses were performed at the neuron level, with each data point representing a single neuron. Consequently, these analyses should be considered preliminary given the limited number of animals included in the study. For each neuron, at least three dendritic segments were analyzed independently. Spine density was quantified as the number of spines per ten µm of dendrite. At P43, no differences were observed in spine density ($p=0.2390$), length ($p=0.2214$),

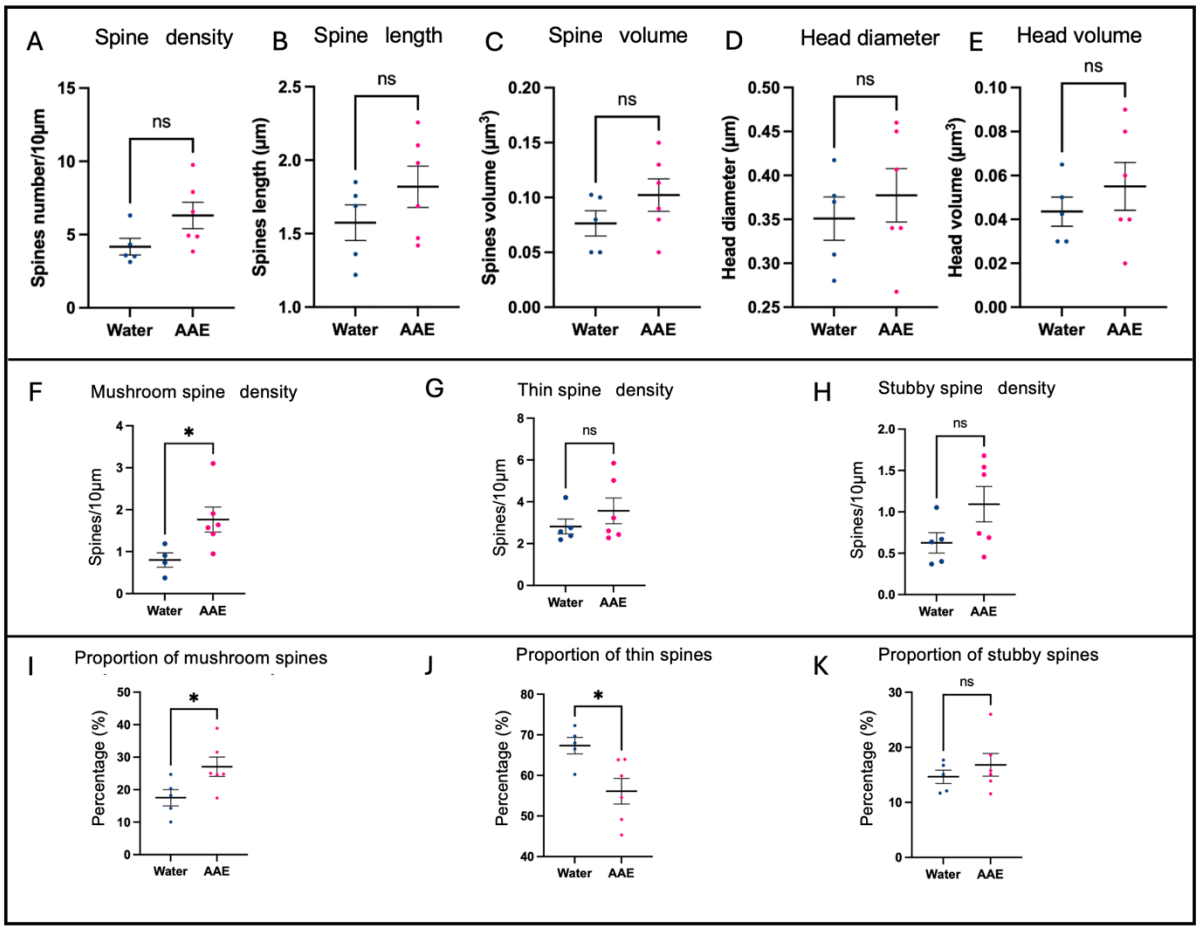

Figure 14: Dendritic spine analysis of layer II/III projection neurons of the prelimbic PFC at P43 in water- and AAE-exposed mice. (A) Spine density defined as the number of spines per 10 µm of dendrite. **(B-E)** Average spine length, spine volume, head maximum diameter and head volume. **(F-H)** Density of mushroom-, thin-, and stubby-type spines. **(I-K)** Proportion of mushroom-, thin- and stubby-type spines. The proportion correspond to the number of spines of a given subtype divided by the total number of spines per dendrite*100. Statistical analyses were performed using Welch's t-test. Preliminary data are presented as mean ± SEM; n=5 water neurons, n=6 AAE neurons; n=2 water mice, n=4 AAE mice: *p < 0.05, **p < 0.01, ***p < 0.001.

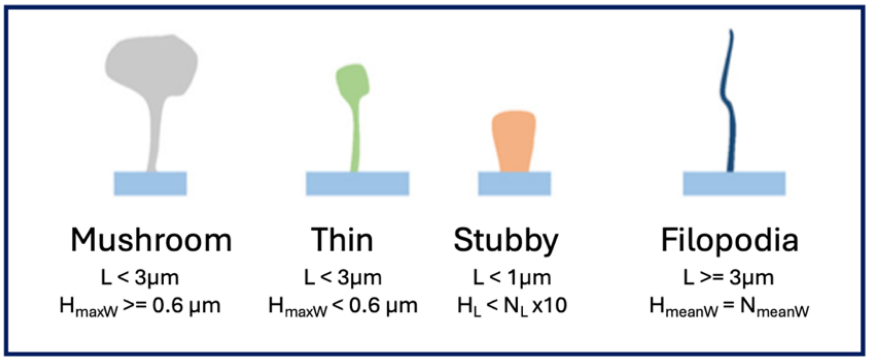

Figure 15: Classification of dendritic spine subtypes. Head, length and neck dimensions used for analysis are indicated. L=spine length; H_L=head length; H_{maxW}= head max width; H_{meanW}=head mean width; N_L=neck length; N_{meanW}=neck mean width (adapted from Pchitskaya & Bezprovanny, 2020).

spine volume (p=0.2033), head diameter (0.5156), or head volume (0.3924) between AAE and water mice (**Figure 14A-E**).

To further investigate whether AAE affects dendritic spine maturation, spines were classified into mushroom-, thin-, stubby- and filopodia-type subtypes according to established morphological criteria (**Figure 15**). Briefly, mushroom spines are characterized by a large head and narrow neck and are generally considered more stable structures, whereas thin spines display a smaller head and are thought to represent a more dynamic population. Stubby spines lack a clearly identifiable neck, while filopodia are long protrusions without a defined head and are typically associated with immature neuronal circuits (**Figure 15**) (Gipson & Olive, 2017b; Pchitskaya & Bezprozvanny, 2020).

Analysis of spine subtype density revealed a significant increase in mushroom spine density in AAE mice compared to water controls (p=0.0241), whereas thin (p=0.3209) and stubby (p=0.0957) spine densities remained unchanged (**Figure 14F-H**).

We next examined the relative proportion of each spine subtype. Preliminary results revealed a significant increase in the proportion of mushroom spines (p=0.0371) at the expense of thin (p=0.0171) spines in AAE mice compared to water controls. The abundance of stubby (p=0.3917) spines remained unchanged, and no filopodia were detected in either group (**Figure 14I-K**).

Together, these preliminary findings indicate that AAE does not affect overall dendritic spine density or morphology at P43 but is associated with changes in dendritic spine subtype distribution.

4.2.2. P80 mice

4.2.2.1. Dendrite analysis

Because only one AAE mouse was available at P80 (n = two reconstructed neurons), no statistical analyses could be performed. Consequently, all observations presented below are descriptive and should be interpreted with caution. Nevertheless, examination of the data suggested potential differences between water- and AAE-exposed animals (**Figure 16**).

Apical dendritic length appeared lower in AAE-exposed neurons compared with water controls, while basal dendritic length also appeared reduced in the AAE group (**Figure 16A**). The number of branching points in apical dendrites appeared higher and more variable in AAE-exposed neurons, whereas basal dendrites displayed similar values between groups (**Figure 16B**). Similarly, the number of apical dendritic ending points appeared higher in the AAE group, while only minor differences were observed in basal dendrites (**Figure 16C**).

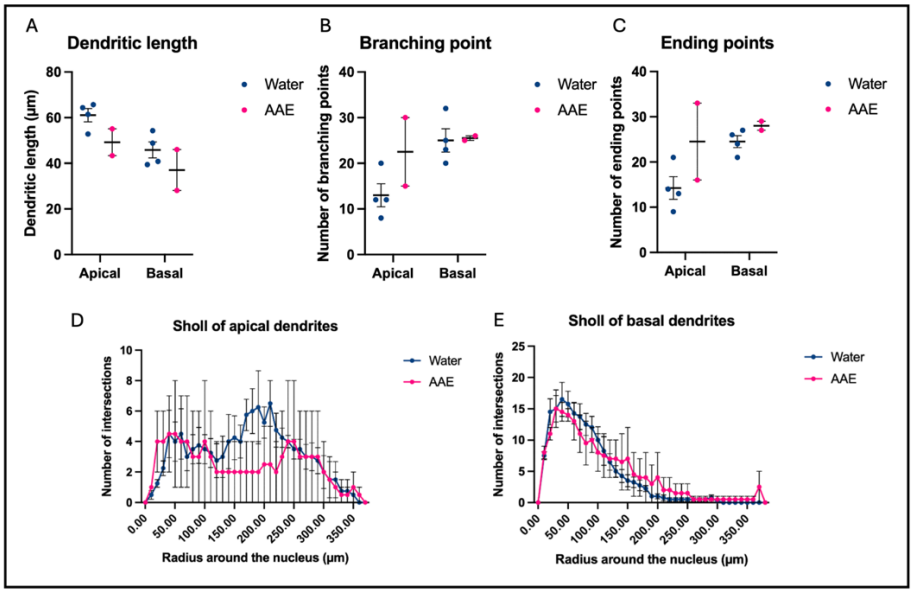

Figure 16: Morphometric analysis of apical and basal dendrites in prelimbic PFC layer II/III projection neurons at P80. (A) Total length of apical (left) and basal (right) dendritic arborizations, expressed in µm. **(B-C)** Number of branching and ending points in apical (left) and basal (right) dendritic arborization. **(D-E)** Sholl analysis of apical **(D)** and basal **(E)** dendrites. *Preliminary data are presented as mean ± SEM; for apical dendrites: n=4 water neurons, n=2 AAE neurons; for basal dendrites: n=4 water neurons, n=2 AAE neurons; n=2 water mice, n=1 AAE mouse *p < 0.05, **p < 0.01, ***p < 0.001. No statistical analyses were performed due to the limited sample size in the AAE group.*

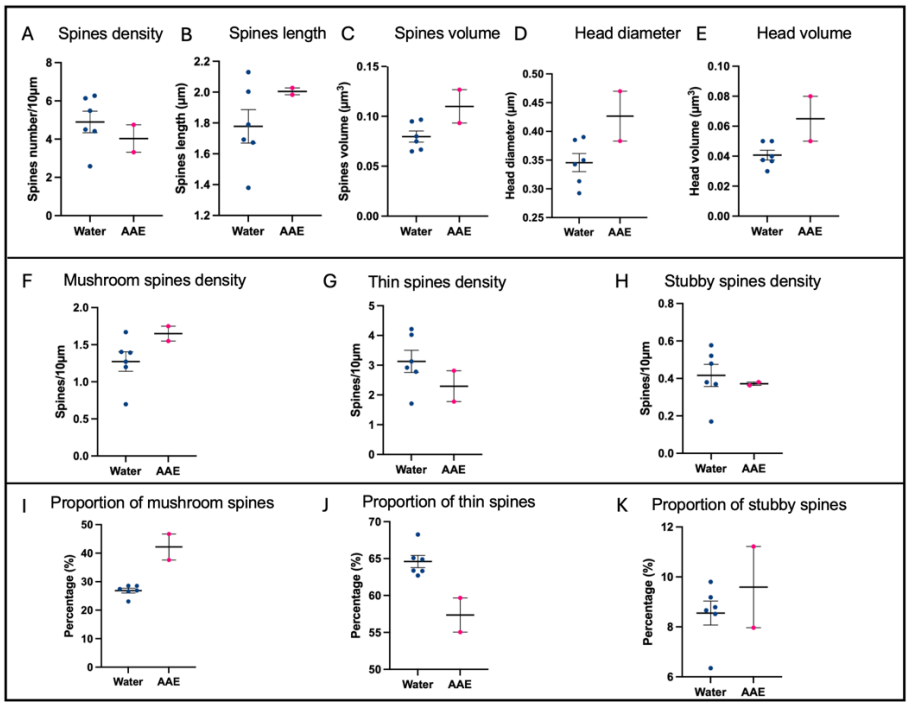

Figure 17: Dendritic spine analysis of prelimbic layer II/III projection neurons at P80 in water- and AAE mice. (A) Spine density defined as the number of spines per 10µm of dendrite. **(B-E)** Average spine length, volume, head max diameter and head volume of water and AAE mice. **(F-H)** Density of mushroom-, thin-, and stubby-type spines. **(I-K)** Percentage of mushroom-, thin- and stubby-type spines. *Preliminary data are presented as mean ± SEM; n=6 water neurons, n=2 AAE neurons; n=2 water mice, n=1 AAE mouse. No statistical analyses were performed due to the limited sample size in the AAE group.*

Sholl analysis also suggested differences in dendritic organization following AAE exposure. In apical dendrites, AAE-exposed neurons appeared to exhibit fewer intersections at intermediate and distal distances from the soma compared with water controls. In basal dendrites, the overall Sholl profiles appeared broadly comparable between groups, although AAE-exposed neurons displayed slightly higher numbers of intersections at distal radii (**Figure 16E**).

4.2.2.2. Dendritic spine analysis

Due to the limited sample size available in the AAE group at P80 (n = two neurons from one mouse), no statistical analyses were performed. Therefore, the observations reported below are descriptive and should be interpreted with caution. Morphological analysis of dendritic spines nevertheless suggested potential differences between water- and AAE animals (**Figure 17**). Overall spine density appeared slightly reduced in the AAE group compared with water controls (**Figure 17A**). In contrast, several morphological parameters of individual spines appeared slightly increased following AAE exposure, including spine length, spine volume, head diameter, and head volume (**Figure 17B-E**).

Analysis of spine subtypes suggested a shift in spine morphology in AAE animals. Specifically, the density of mushroom spines appeared increased, whereas the density of thin spines appeared reduced compared with controls (**Figure 17F-G**). Stubby spine density appeared relatively unchanged between groups (**Figure 17H**). Consistent with these observations, the relative proportion of mushroom spines was higher in the AAE group, while the proportion of thin spines was lower. The proportion of stubby spines did not show marked differences between conditions (**Figure 17K**).

4.2.3. Differential dendritic spine analysis between P43 and P80

Because only one AAE mouse was available at P80 (n = two neurons), statistical comparisons across developmental stages could only be performed for the water group. Consequently, all observations involving AAE-exposed animals at P80 are descriptive and should be interpreted with caution.

Analysis of dendritic spine subtype proportions suggested age-dependent change in spine composition in water-exposed mice (**Figure 18-C**). Indeed, in control animals, the proportion of mature mushroom spines significantly increased between P43 and P80 ($p=0.0174$) (**Figure 18A**), whereas the proportion of stubby spines significantly decreased over the same period ($p=0.0047$) (**Figure 18C**). No significant change was observed in the proportion of thin spines ($p=0.2608$) (**Figure 18B**). Together, these findings indicate that dendritic spine composition continues to evolve between adolescence and adulthood under physiological conditions.

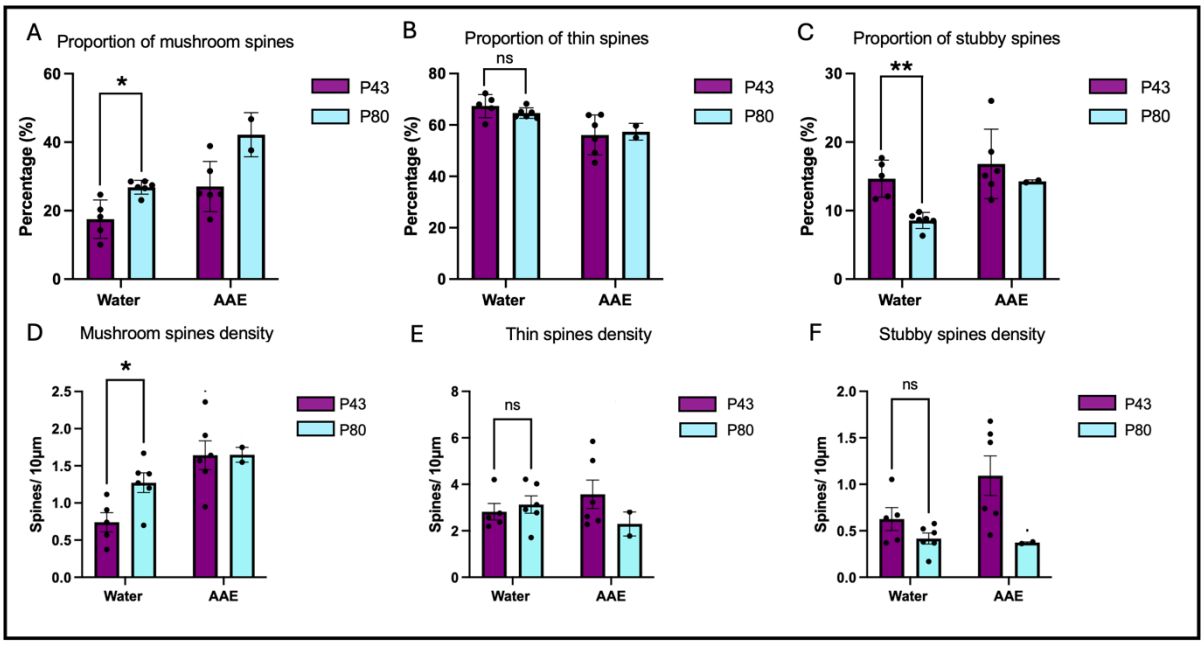

Figure 18: Evolution of dendritic spine morphology between P43 and P80. (A-C) Change in spine subtype proportion between P43 and P80. **(D-F)** Change in spine subtype densities between P43 and P80. Statistical analyses were performed using Welch's t-test. No statistical analyses were performed for the AAE group due to the limited sample size at P80. Preliminary data are presented as mean ± SEM. At P43, n=5 water neurons, n=6 AAE neurons; n=2 water mice, n=4 AAE mice. At P80 n=6 water neurons, n=2 AAE neurons; n=2 water mice, n=1 AAE mouse *p < 0.05, **p < 0.01, ***p < 0.0001.

Descriptive observations suggested that AAE animals already displayed an increased proportion of mushroom spines at P43. Consequently, little additional change was observed between P43 and P80, suggesting a potential alteration of the normal developmental trajectory of spine maturation. In contrast, the relative proportion of thin and stubby spines appeared broadly comparable between the two timepoints.

Analysis of spine subtype densities further revealed age-dependent changes in dendritic spine maturation between P43 and P80 (**Figure 18D-F**). In water controls, mushroom spine density significantly increased from P43 to P80 ($p = 0.0184$) (**Figure 18D**), whereas thin spine ($p = 0.5641$) and stubby spine densities ($p = 0.1758$) remained unchanged between the two timepoints (**Figure 18E-F**). These findings suggest a progressive enrichment of mature mushroom spines during normal post-adolescent maturation of prelimbic layer II/III projection neurons.

In AAE mice, descriptive observations suggested that mushroom spine density remained relatively stable between P43 and P80. In contrast, densities of thin and stubby spines appeared slightly higher at P80 than at P43. Although no statistical analyses could be performed in the AAE group because of the limited sample size available at P80, these observations suggest that AAE may alter the normal developmental trajectory of dendritic spine maturation.

4.3. Impact of AAE on interneurons subpopulation in PFC

We next investigated whether AAE alters interneuron populations in the PFC. More specifically, we quantified parvalbumin-, somatostatin-, calretinin-, and calbindin-expressing interneuron in the infralimbic (IL), prelimbic (PL), and anterior cingulate cortex (ACC) at P43 and P80 in both sexes (**Figure 19**).

4.3.1. P43 mice

4.3.1.1. Expression profile of the different interneuron sub-populations in males

Preliminary data examining interneuron subtype expression in the PL, IL, and ACC revealed selective alterations following AAE (**Figure 20**).

Among the four interneuron populations examined, SST interneurons were the most consistently affected. AAE significantly reduced SST expression in both the PL ($p = 0.0072$) and ACC ($p = 0.0392$), whereas no difference was detected in the IL ($p = 0.4544$) (**Figure 20A-C**).

PV interneuron expression was not altered by AAE in the PL ($p = 0.4431$), IL ($p = 0.0986$), or ACC ($p = 0.5065$) (**Figure 20D-F**)

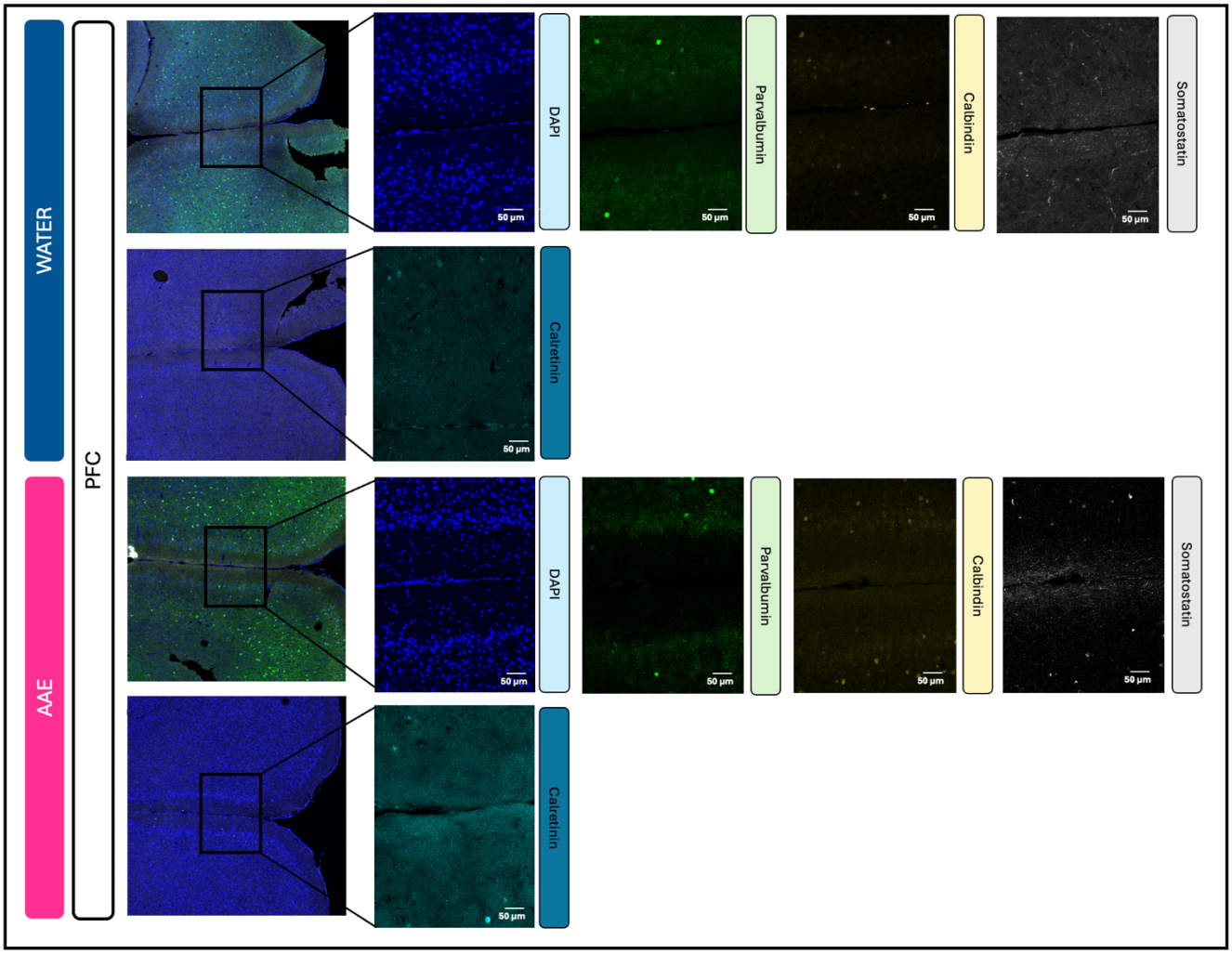

Figure 19: Validation of interneuron immunofluorescence labeling in the prefrontal cortex. Low-magnification images (top) show the localization of the PFC. High-magnification images illustrate immunofluorescence staining in the PFC of AAE and water-exposed (control) mice. Images were acquired using a Leica Stellaris confocal microscope with a 40X objective.

Similarly, CB interneuron expression did not significantly differ between groups in the PL (p = 0.2225), IL (p = 0.2709), and ACC (p =0.1127) (**Figure 20G-I**).

Finally, no significant differences in CR interneuron expression were observed in the PL (p = 0.4248), IL (p =0.1430) and ACC (p = 0.3033) (**Figure 20J-L**).

4.3.1.2. Expression profile of the different interneuron sub-populations in females

Preliminary data examining interneuron subtype expression in the PL, IL and ACC of female mice revealed limited effects of AAE (**Figure 21**).

SST interneuron expression did not significantly differ between AAE mice and water controls in the PL (p = 0.7261), IL (p = 0.3165), or ACC (p = 0.6830) (**Figure 21A-C**).

Similarly, PV interneuron expression did not significantly differ between groups in the PL (p = 0.2797), IL (p = 0.8877) and ACC (p =0.1371) (**Figure 21D-F**).

In contrast, CB interneuron expression was significantly increased in the ACC (p = 0.0405) of AAE mice compared to controls, whereas no significant differences were detected in the PL (p = 0.1948) or IL (p = 0.3394) (**Figure 21G-I**).

Finally, CR interneuron expression did not significantly differ between groups in the PL (p = 0.5138), IL (p = 0.1014) and ACC (p =0.4495) (**Figure 21J-L**).

4.3.2. P80 mice.

4.3.2.1. Expression profile of the different interneuron sub-populations in males

Analysis of interneuron subtype expression in the PL, IL and ACC of male mice at P80 revealed relatively limited long-term effects of AAE (Figure 22). Among the interneuron populations examined, SST interneurons were the only subtype significantly affected by AAE. SST expression was significantly reduced in the PL of AAE mice compared with water controls (p = 0.0222), whereas no significant differences were detected in the IL (p = 0.0569) or ACC (p = 0.5769) (**Figure 22A-C**).

PV interneuron expression did not significantly differ between groups in the PL (p = 0.6153), IL (p = 0.0989) or ACC (p =0.2416) (**Figure 22D-F)**).

Similarly, CB interneuron expression did not significantly differ between groups in the PL (p = 0.2259), IL (p = 0.5590) or ACC (p =0.0559) (**Figure 22G-I**).

Likewise, CR interneuron expression remained unchanged in the PL (p = 0.1561), IL (p = 0.5086) and ACC (p =0.8957) (**Figure 22J-L**).

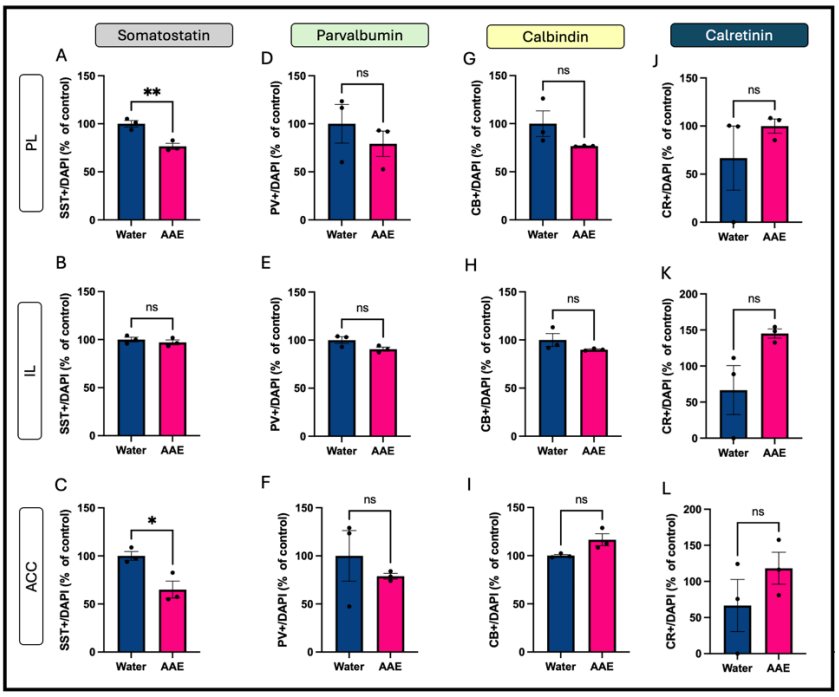

Figure 20: Interneuron subtype expression in PL cortex, IL cortex, and ACC in male mice at P43. (A-C) Expression of somatostatin interneurons in PL cortex, IL cortex and ACC. **(D-F)** Expression of parvalbumin interneurons in PL cortex, IL cortex and ACC. **(G-I)** Expression of calbindin interneuron in PL cortex, IL cortex and ACC. **(J-L)** Expression of calretinin interneuron in PL cortex, IL cortex and ACC. Statistical analyses were performed using Welch's t-test. Preliminary data are presented as mean ± SEM; n=3 water mice, n=3 AAE mouse; *p < 0.05, **p < 0.01, ***p < 0.001.

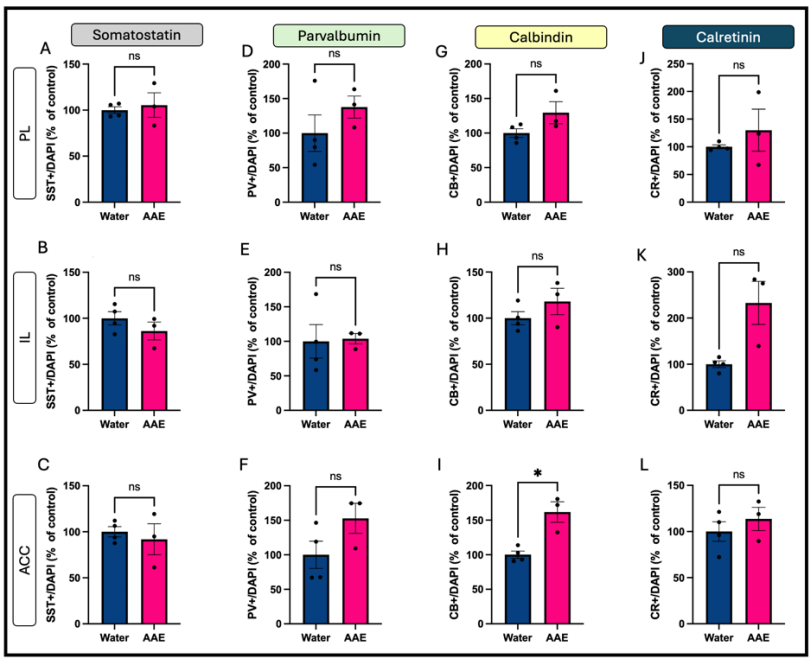

Figure 21: Interneuron subtype expression in PL cortex, IL cortex, and ACC in female mice at P43. (A-C) Expression of somatostatin interneurons in PL cortex, IL cortex and ACC. **(D-F)** Expression of parvalbumin interneurons in PL cortex, IL cortex and ACC. **(G-I)** Expression of calbindin interneuron in PL cortex, IL cortex and ACC. **(J-L)** Expression of calretinin interneuron in PL cortex, IL cortex and ACC. Statistical analyses were performed using Welch's t-test. Preliminary data are presented as mean ± SEM; n=4 water mice, n=3 AAE mouse; *p < 0.05, **p < 0.01, ***p < 0.001.

4.3.2.2. Expression profile of the different interneuron sub-populations in females

Preliminary analysis of interneuron subtype expression in the PL, IL and ACC of female mice at P80 revealed no significant effects of AAE exposure in any of the PFC subregions examined (**Figure 23**).

SST interneuron, expression did not significantly differ between AAE mice and water controls in the PL ($p = 0.6945$), IL ($p = 0.1155$) and ACC ($p = 0.7796$) (**Figure 23A-C**).

Similarly, PV interneuron expression remained unchanged in the PL ($p = 0.5471$), IL ($p = 0.9405$) and ACC $p = 0.3084$). (**Figure 23D-F**).

No significant difference was detected for CB interneuron in the PL ($p = 0.6585$), IL ($p = 0.2308$) and ACC ($p = 0.3164$) (**Figure 23G-I**).

Likewise, CR interneuron expression remained comparable between groups in PL cortex ($p = 0.5285$), IL cortex ($p = 0.6277$) and ACC ($p = 0.2946$) **(Figure 23J-L).**

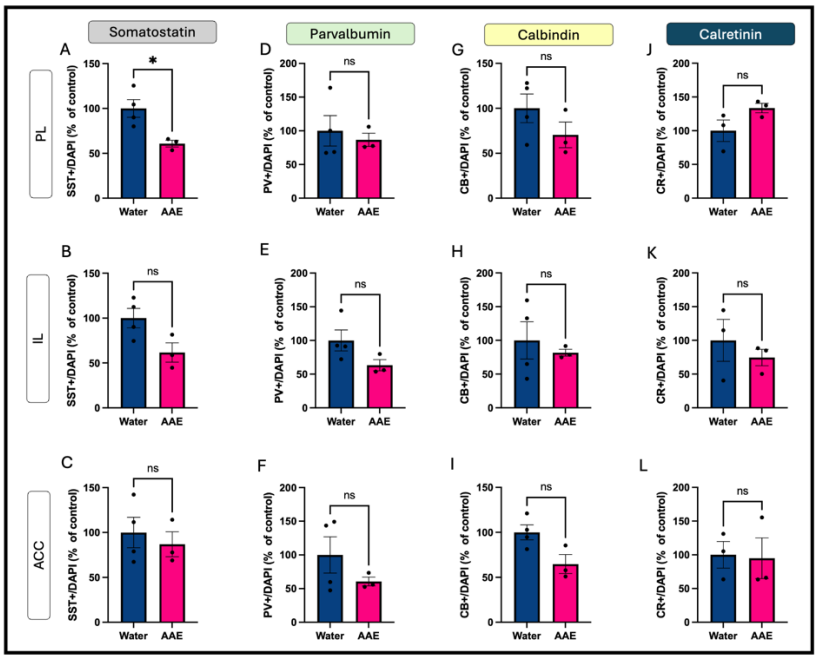

Figure 22: Interneuron subtype expression in PL cortex, IL cortex, and ACC in male mice at P80. (A-C) Expression of somatostatin interneurons in PL cortex, IL cortex and ACC. **(D-F)** Expression of parvalbumin interneurons in PL cortex, IL cortex and ACC. **(G-I)** Expression of calbindin interneurons in PL cortex, IL cortex and ACC. **(J-L)** Expression of calretinin interneurons in PL cortex, IL cortex and ACC. Statistical analyses were performed using Welch's t-test. Preliminary data are presented as mean ± SEM; n=4 water mice, n=3 AAE mouse; *p < 0.05, **p < 0.01, ***p < 0.001.

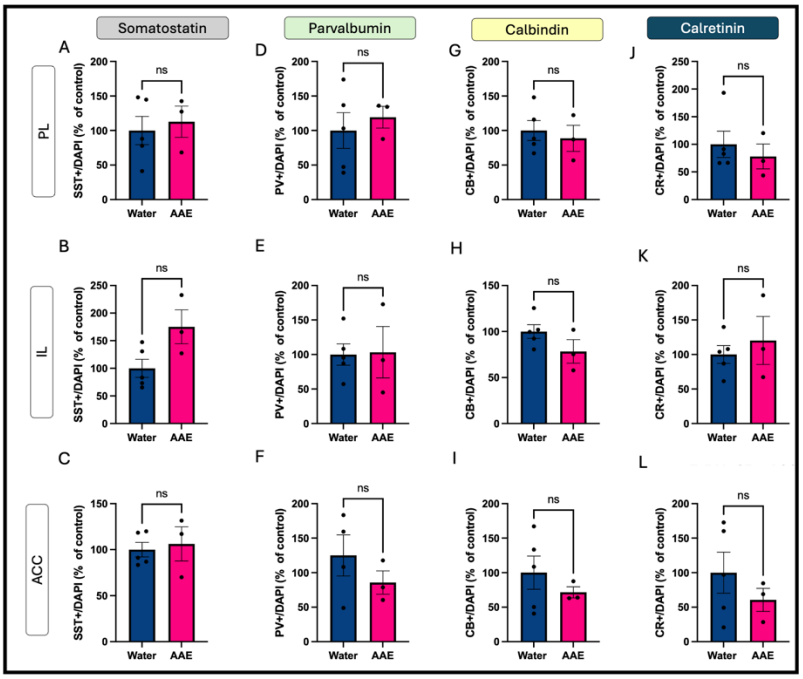

Figure 23: Interneuron subtype expression in PL cortex, IL cortex, and ACC in female mice at P80. (A-C) Expression of somatostatin interneurons in PL cortex, IL cortex and ACC. **(D-F)** Expression of parvalbumin interneurons in PL cortex, IL cortex and ACC. **(G-I)** Expression of calbindin interneurons in PL cortex, IL cortex and ACC. **(J-L)** Expression of calretinin interneurons in PL cortex, IL cortex and ACC. Statistical analyses were performed using Welch's t-test. Preliminary data are presented as mean ± SEM; n=5 water mice, n=3 AAE mouse; *p < 0.05, **p < 0.01, ***p < 0.001.

4.4. Unveiling whether AAE modulates mTORC1 and/or eEF2 activity in the prefrontal cortex

4.4.1. Validation of synaptic fraction

To investigate the effects of AAE on mTORC1 and eEF2 signaling, subcellular fractionation was first validated using established synaptic, cytoplasmic, and nuclear markers (**Figure 24**). PSD95 and synaptotagmin were enriched in the synaptic fraction, whereas CREB and stathmin were enriched in the cytoplasmic fraction. Histone H3 was absent from both fractions, indicating the absence of detectable nuclear contamination. Together, these results validate the quality of the fractionation procedure.

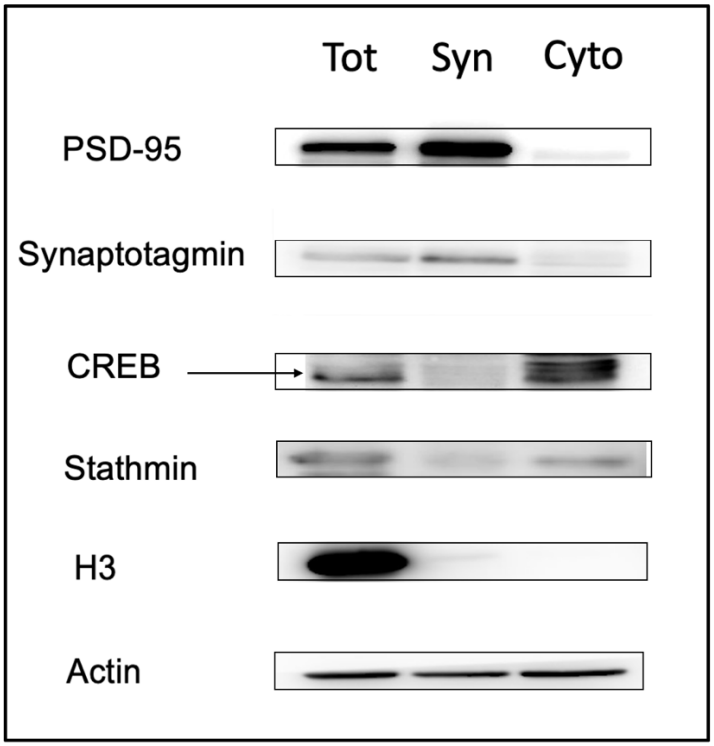

Figure 24: Validation of synaptic fraction in the PFC via Western Blot. Protein expression profiles were compared between total lysate (Tot), synaptic fraction (Syn), and cytosolic fraction (Cyto). PSD-95 and synaptotagmin serve as positive markers to confirm the enrichment of the synaptic fraction. CREB and Stathmin, were enriched in the cytosolic fraction. Histone H3 (H3) is used as a nuclear exclusion marker, demonstrating the absence of nuclear contamination in both the synaptic and cytosolic fractions. Actin levels were monitored to assess overall protein loading across lanes.

4.4.2. Effect of AAE on S6 phosphorylation levels in the PFC at P43

At P43, AAE did not significantly alter pS6/S6 levels in male mice. However, a strong trend toward increased S6 phosphorylation was observed in both the total homogenate ($p = 0.0531$) and the synaptic fraction ($p = 0.0548$), whereas no differences were detected in the cytoplasmic fraction ($p = 0.1800$) (Figure 25).

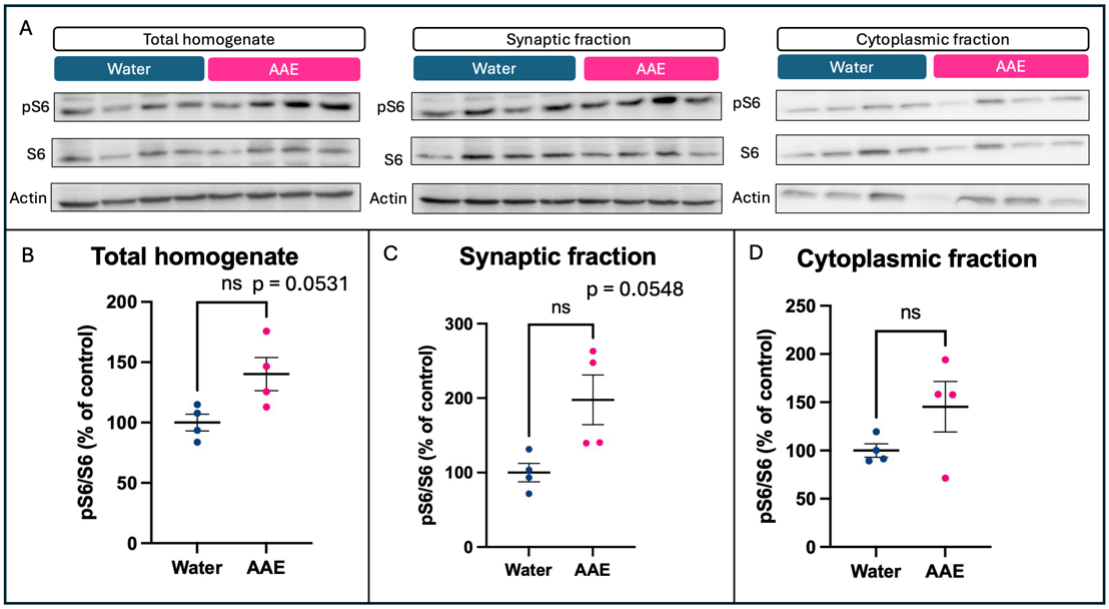

Figure 25: Analysis of the phosphorylation levels of pS6 in the prefrontal cortex of P43 AAE and water male mice by Western Blot analysis. (A) Representative image of S6, phospho-S6 and actin in the total, cytoplasmic and synaptic fractions of PFC of male mice**. (B)** Quantification of pS6 in total homogenate. **(C)** Quantification of pS6 in synaptic fraction. **(D)** Quantification of pS6 in cytoplasmic fraction. Statistical analyses were performed using Welch's t-test. Preliminary data are presented as mean ± SEM; n=4; *p < 0.05, **p < 0.01, ***p < 0.001.

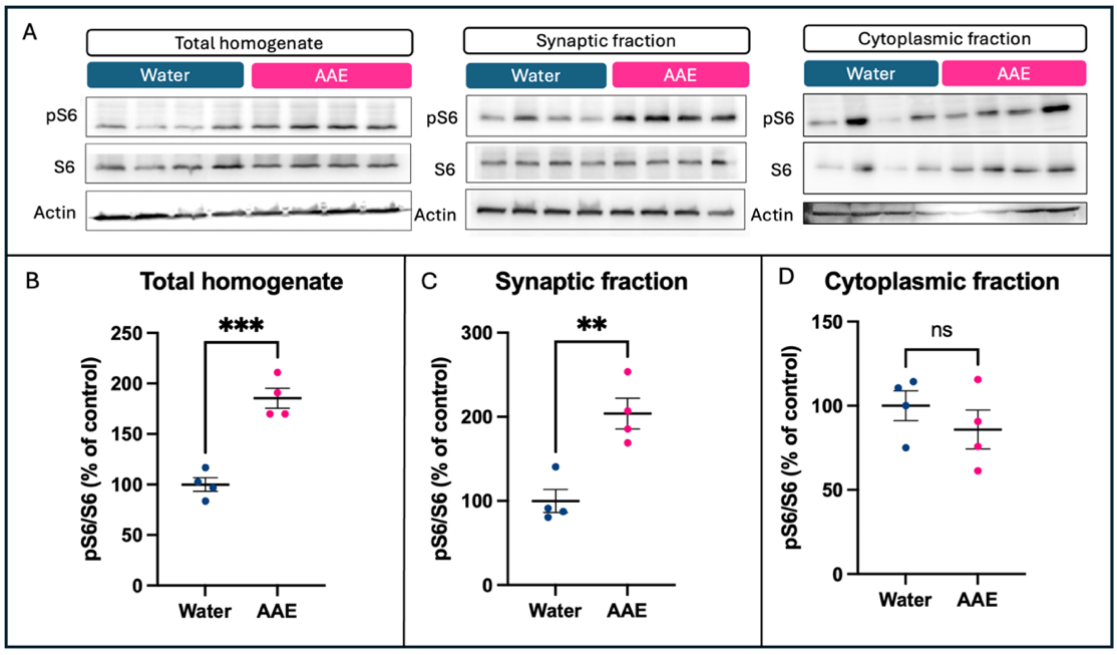

Figure 26: Analysis of the phosphorylation levels of pS6 in the prefrontal cortex of P43 AAE and water female mice by Western Blot analysis. (A) Representative image of S6, phospho-S6 and actin in the total, cytoplasmic and synaptic fractions of PFC of female mice**. (B)** Quantification of pS6 in total homogenate. **(C)** Quantification of pS6 in synaptic fraction. **(D)** Quantification of pS6 in cytoplasmic fraction. Statistical analyses were performed using Welch's t-test. Preliminary data are presented as mean ± SEM; n=4 water mice, n=4 AAE mouse; *p < 0.05, **p < 0.01, ***p < 0.005

In females, at P43, in the total homogenate, the pS6/S6 ratio was significantly higher in the AAE group compared to the water control group ($p = 0.0006$). Similarly, within the synaptic fraction, the pS6/S6 ratio was significantly increased in the AAE mice compared to the control group ($p = 0.0048$). Conversely, within the cytoplasmic fraction, no significant differences were observed between the water and AAE groups ($p = 0.3709$) (**Figure 26**).

4.4.3. Effects of AAE on eEF2 phosphorylation levels in the PFC at P43

4.4.3.1. In male mice

No significant differences in eEF2 phosphorylation levels were detected between AAE and water control mice in either the total homogenate ($p > 0.9999$) or the cytoplasmic fraction ($p = 0.3498$). (**Figure 27B-C**).

Similarly, total eEF2 protein levels did not significantly differ between groups in both fractions (total homogenate: $p = 0.4493$; cytoplasmic: $p = 0.0831$) (**Figure 27D-E**). Data from the synaptic fraction could not be reliably quantified because of technical issues affecting several samples and were therefore not included in the statistical analyses. (**Figure F-G**).

4.4.3.2. In female mice

Data from the synaptic fraction could not be analyzed because of technical issues affecting sample quality and signal quantification. Consequently, only the total homogenate and cytoplasmic fractions are presented.

No significant differences in phosphor-eEF2 levels were observed between water and AAE mice in either the total homogenate ($p = 0.1831$) or cytoplasmic ($p = 0.7453$) fractions (**Figure 28B-C**). In contrast, total eEF2 protein levels were significantly increased following AAE in the total homogenate ($p = 0.0251$), whereas cytoplasmic eEF2 levels remained unchanged ($p = 0.6315$) (**Figure 28D-E**).

Because of technical issues affecting sample quality and signal quantification, data from the synaptic fraction could not be analyzed and are therefore not included in the present study. These experiments will need to be repeated in future investigations.

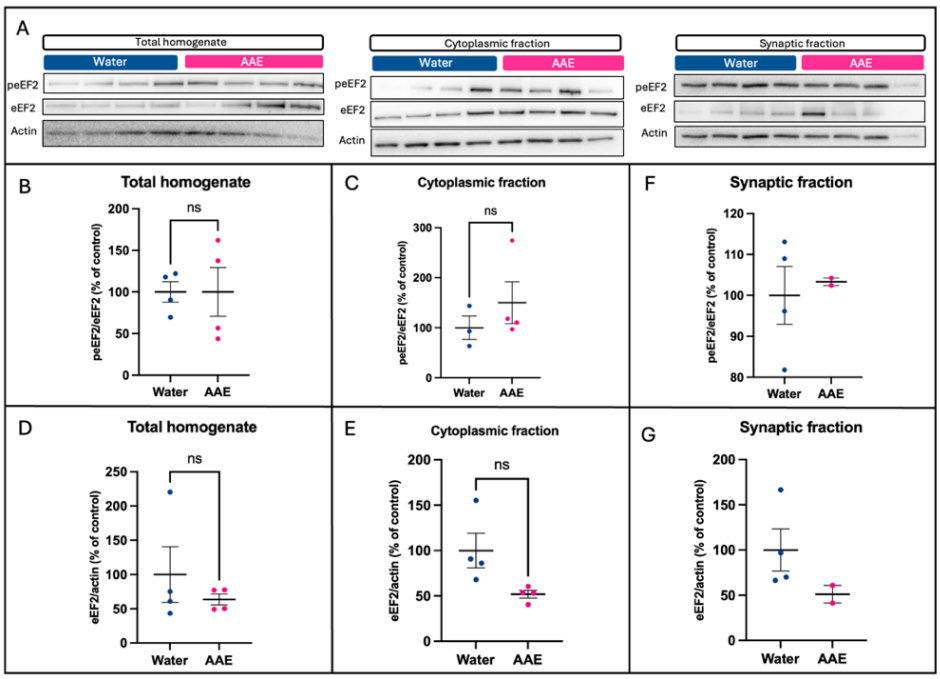

Figure 27: Analysis of the phosphorylation levels of eEF2 in the prefrontal cortex of P43 AAE and water male mice by Western Blot analysis. (A) Representative image of eEF2, phospho-eEF2 and actin in the total, cytoplasmic and synaptic fractions of PFC of male mice. **(B)** Quantification of peEF2 in total homogenate. **(C)** Quantification of peEF2 in cytoplasmic fraction. **(F)** Quantification of peEF2 in synaptic fraction. **(D)** Quantification of eEF2 in total homogenate. **(E)** Quantification of eEF2 in cytoplasmic fraction. **(G)** Quantification of eEF2 in synaptic fraction. Statistical analyses were performed using Welch's t-test. Preliminary data are presented as mean ± SEM; n=3 water mice, n=4 AAE mouse; *p < 0.05, **p < 0.01, ***p < 0.001.

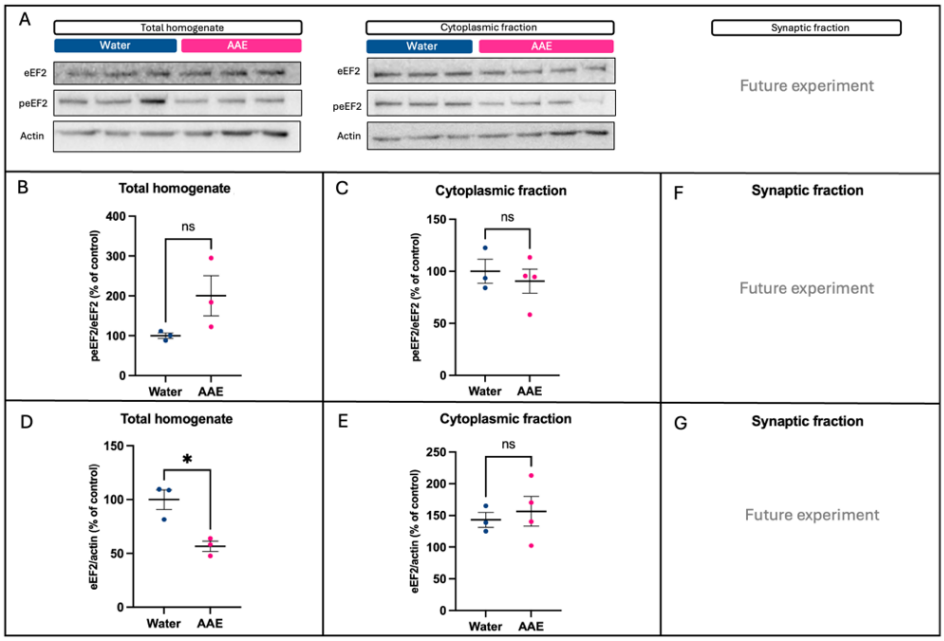

Figure 28: Analysis of the phosphorylation levels of eEF2 in the prefrontal cortex of P43 AAE and water female mice by Western Blot analysis. (A) Representative image of eEF2, phospho-eEF2 and actin in the total, cytoplasmic and synaptic fractions of PFC of female mice. **(B)** Quantification of peEF2 in total homogenate. **(C)** Quantification of peEF2 in cytoplasmic fraction. **(F)** Quantification of peEF2 in synaptic fraction. **(D)** Quantification of eEF2 in total homogenate. **(E)** Quantification of eEF2 in cytoplasmic fraction. **(G)** Quantification of eEF2 in synaptic fraction. Statistical analyses were performed using Welch's t-test. Preliminary data are presented as mean ± SEM; n=3 water mice, n=4 AAE mouse; *p < 0.05, **p < 0.01, ***p < 0.001.

Discussion

5.1. The adolescent DID paradigm as a model of voluntary binge-like alcohol exposure

The present study relied on a modified DID paradigm to model adolescent binge-like alcohol consumption. This voluntary drinking procedure is widely used to investigate the neurobiological consequences of excessive alcohol intake and has previously been validated in our laboratory (Van Hees et al., 2022). In contrast to forced administration procedures such as intraperitoneal injections, oral gavage, or vapor exposure, the DID paradigm allows animals to voluntarily consume alcohol. This feature represents an important advantage, as it more closely mimics the motivational component of human alcohol consumption and avoids potential confounding effects associated with stress induced by forced alcohol administration (Crews et al., 2019; Thiele & Navarro, 2014). Consequently, the DID paradigm provides a more ethologically relevant model for investigating alcohol-induced neuroadaptations.

In the present study, adolescent C57BL/6 mice consumed substantial amounts of alcohol during the 4-hour drinking sessions, reaching average consumptions of 5.602 g/kg/4h in males and 5.804 g/kg/4h in females. As previously reported by Van Hees *et al.*, mice consuming at least 4g/kg/4h reach blood alcohol concentrations above 0.08 g/dl, the threshold commonly used to define binge-drinking in humans (Van Hees et al., 2022). Therefore, alcohol intake achieved in the present study can be considered representative of binge-like alcohol exposure.

Interestingly, no significant differences in overall alcohol consumption were observed between males and females. This contrasts with previous findings, obtained using the same paradigm, which reported higher alcohol intake in female mice (Van Hees et al., 2022). The absence of a significant sex effect in the present study may be explained by the smaller sample size of the current cohort (44 males and 22 females) compared with the larger population analyzed by Van Hees *et al.* (153 males and 162 females). Importantly, this mouse model differs from many commonly used models of alcohol exposure. First, alcohol consumption is entirely voluntary and takes advantage of the natural nocturnal behavior of rodents, which consume most of their food and water during the dark phase (Fritz & Boehm, 2016; Van Hees et al., 2022). Second, unlike forced administration procedures, voluntary drinking minimizes potential confounding factors associated with repeated handling, stress response and alcohol toxicity (Crews et al., 2019; Thiele & Navarro, 2014). Moreover, because animals are neither food- nor water-deprived, alcohol consumption is not artificially driven by physiological needs. Finally, the inclusion of a two-day abstinence period between P33 and P35 allows the model to better

reproduce the intermittent pattern of alcohol consumption typically observed during adolescent binge-drinking episodes and in individuals with AUD (Van Hees et al., 2022).

An additional strength of the present study is the inclusion of both short-term (P43) and long-term (P80) analysis timepoints. Because molecular and cellular analyses were performed following periods of abstinence, the observed alterations are unlikely to reflect acute pharmacological effects of ethanol. Instead, they may represent neuroadaptations induced by AAE that persist beyond the drinking period itself.

Together, these characteristics make the adolescent DID paradigm a relevant experimental model for investigating how binge-like alcohol consumption affects PFC maturation and contributes to long-term neurobiological vulnerability.

5.2. Adolescent C57Bl/6 mice as a model to investigate the impact of AAE on prefrontal cortex maturation

The use of mice for studying PFC development and dysfunction remains a subject of debate. Across evolution, the PFC has undergone substantial phylogenetic changes. In particular, the human PFC contains a well-defined granular layer IV, whereas the rodent PFC is considered agranular and lacks this characteristic feature (Le Merre et al., 2021). In addition, the granular dorsolateral PFC of primates, which is implicated in working memory and executive control, projects extensively to the dorsal striatum, whereas comparable agranular regions in rodent do not display identical connectivity patterns (Carlén, 2017). Consistent with this, evidence indicates that portions of the human caudate nucleus and putamen (i.e., dorsal striatum) exhibit cortical connectivity features that are absent in rodents, highlighting the emergence of species-specific cortical networks during mammalian evolution (Balsters et al., 2020). These anatomical differences represent an important limitation when translating findings obtained in rodents to human AUD.

Nevertheless, despite these structural differences, rodents exhibit a broad range of behaviors that depend on PFC function, including impulse control, behavioral flexibility, attention, novelty seeking, risk-taking, and decision-making (Carlén, 2017). Furthermore, many of the cellular and molecular mechanisms underlying synaptic plasticity, circuit maturation, and cortical development are highly conserved across species. Consequently, although mice cannot fully reproduce the complexity of the human PFC, they remain a valuable model for investigating fundamental mechanisms involved in PFC maturation and vulnerability to environmental insults such as alcohol exposure. Another relevant consideration concerns the developmental period selected to model AAE. In the present study, mice were exposed to ethanol from P29 to P40, a developmental window generally considered to correspond to early-to-mid adolescence in rodents and broadly comparable to human adolescence (Spear, 2000).

Although the precise boundaries of adolescence remain difficult to define, rodent adolescence, from the perspective of brain maturation, is commonly divided into early (P21-34), middle (P34-46), and late (P46-59) stages (Moore et al., 2010). This period is characterized by profound hormonal, behavioral, and neurobiological changes, including the onset of puberty, increased sensation-seeking behavior, heightened social interactions, and continued maturation of neural circuits involved in executive control (Spear, 2000).

Importantly, adolescence is associated with extensive remodeling of the PFC across species. Processes such as synaptic pruning, refinement of excitatory and inhibitory circuits, and maturation of long-range connectivity continue throughout this developmental period (Spear, 2000). Consistent with this, previous studies have demonstrated that structural maturation of the mouse PFC extends well beyond P40, supporting the relevance of this developmental window for investigating factors that may interfere with normal cortical maturation. Furthermore, rodents within this age range display behavioral characteristics typically associated with adolescence, including increased novelty seeking, risk-taking, and peer-oriented social behavior (Spear, 2000). Together, these observations support the validity of the P29-P40 exposure period as a biologically relevant model of AAE. (Spear, 2000).

Another important limitation concerns the use of the C57Bl/6J strain. This strain displays a natural preference for ethanol, and readily consumes alcohol without requiring a habituation phase (Thiele & Navarro, 2014b). While this characteristic facilitates the establishment of reliable binge-drinking paradigms and improves experimental reproducibility, it may also limit direct extrapolation to the heterogeneous trajectories of alcohol initiation observed in humans. Human adolescents typically acquire alcohol-drinking behaviors progressively through social and environmental influence, whereas C57Bl/6J mice possess an inherent predisposition toward ethanol consumption. Therefore, this genetic susceptibility should be considered when interpreting the translational relevance of findings obtained using this model. Altogether, despite recognized species-specific differences and strain-related limitations, adolescent C57Bl/6J mice represent a useful experimental model for investigating how binge-like alcohol exposure affects PFC maturation and contributes to the development of long-lasting neurobiological alterations.

5.2.1. Sex difference in alcohol addiction

Sex differences represent a critical factor in the development and progression of AUD. Although AUD and binge-drinking remain more prevalent among men worldwide, alcohol consumption among women has increased substantially over the past decades, resulting in a progressive narrowing of the historical sex gap (Our World in Data, 2024; White, 2020; World Health Organization, 2024). In contrast, rodent studies consistently report higher levels of voluntary alcohol consumption in adolescent females than in males, including in the DID paradigm used in the present study (Van Hees et al., 2022). Such discrepancies likely reflect the complex social, cultural and environmental factors that contribute to alcohol consumption in humans but are not fully captured in animal models.

Nevertheless, substantial evidence indicates that alcohol affects males and females differently at the neurobiological level. For instance, human neuroimaging studies have shown that adolescent female binge drinkers display increased frontal cortical thickness compared with controls, suggesting delayed cortical maturation, whereas their male counterparts exhibit excessive cortical thinning (Verplaetse et al., 2021). Similarly, in rodents, AAE leads to a more pronounced reduction in myelinated axon density within the medial PFC of males, highlighting sex-specific vulnerability of neural circuits involved in executive control (Flores-Bonilla, 2020). Together, these findings suggest that the mechanisms through which alcohol alters brain maturation may differ between males and females. Consequently, considering sex as a biological variable is important when investigating the neurodevelopmental consequences of AAE.

Due to experimental constraints, a comprehensive sex-specific analysis could not be conducted for all aspects of the present study. Morphological analyses were restricted to male mice, whereas interneuron and translational signaling analyses were conducted in both sexes. Consequently, potential sex-dependent effects of AAE on dendritic morphology remain to be investigated. However, the inclusion of both sexes in the interneuron and molecular analyses allowed us to identify potential sex-specific responses to alcohol exposure, which are discussed in the following sections.

5.3. Structural defect analysis: investigating whether AAE alters the morphology of dendrites and/or dendritic spines in layer II/III projection neurons of the prelimbic PFC

Building on previous findings from our laboratory showing that AAE alters dendritic spine morphology in layer V prelimbic projection neurons during adolescence (P43), the present study investigated whether similar structural alterations could also be detected inn layer II/III projection neurons of the prelimbic PFC.

The prelimbic cortex is a critical component of the medial prefrontal cortex (mPFC). The mPFC functions as a sophisticated neural “control board”, integrating diverse inputs from across the brain and distilling them into updated signals sent to various cortical and subcortical output structures. As a central hub for high-order executive processing, the mPFC is indispensable for managing decision-making, emotional regulation, sociability, and impulse control. By maintaining highly organized projection networks, the mPFC exerts a critical top-down influence, orchestrating the complex interplay between affective states and motivational behaviors (Kolk & Rakic, 2022; Xu et al., 2019).

Layer II/III projection neurons are particularly important because they establish extensive intra and intercortical connections and contribute to information integration across cortical networks. Given the prolonged maturation of these circuits during adolescence, they may be especially vulnerable to alcohol-induced neurodevelopmental perturbations (Gerfen et al., 2018).

5.3.1. AAE alters dendritic spine subtype distribution in layer II/III prelimbic projection neurons of adolescent but not adult mice

The present study revealed that AAE induced a significant shift in dendritic spine subtype distribution in layer II/III prelimbic projection neurons at P43. Specifically, AAE increased the proportion of mushroom spines while reducing the proportion of thin spines. Similar alterations were previously observed in layer V projection neurons following AAE, suggesting that AAE may affect synaptic maturation across multiple cortical layers.

In contrast, morphometric analyses revealed no significant differences in spine length, spine volume, spine head diameter, or spine head volume following AAE. These results suggest that AAE mainly affects spine subtype composition rather than individual spine morphology. Likewise, preliminary data from analyses of dendritic arborization revealed no significant change in total dendritic length, branching complexity, or overall dendritic organization. Together, these findings suggest that AAE does not induce major structural remodeling of layer II/III projection neurons but rather modifies specific features of synaptic organization.

Dendritic spine morphology is closely associated with synaptic function and maturation. Mushroom spines are generally considered more stable and mature structures that support long-lasting synaptic connections, whereas thin spines are highly dynamic and are often regarded as substrates for experience-dependent plasticity (Gipson & Olive, 2017; Pchitskaya & Bezprozvanny, 2020). Consequently, the increase in mushroom spines accompanied by a reduction in thin spines observed following AAE may reflect an alteration of the normal developmental trajectory of synaptic maturation. Because mushroom spines are generally considered more mature and stable structures, these findings raise the possibility that AAE promotes a premature shift toward a more mature spine phenotype during adolescence.

However, caution is required when interpreting these findings, as spine morphology alone does not directly predict synaptic efficacy or neuronal function.

Interestingly, similar alcohol-induced increases in mushroom spine abundance associated with reductions in thin spines have previously been reported in layer II/III prelimbic neurons following chronic alcohol exposure in young adult mice (P66) (Varodayan et al., 2018). The present findings extend these observations by showing that comparable alterations can already be detected during adolescence, shortly after the end of alcohol exposure, suggesting that synaptic remodeling represents an early neuroadaptation induced by AAE.

At P80, morphological analyses were also performed in both control and AAE-exposed animals. However, because only two neurons were available for analysis in the AAE group, no statistical comparisons could be conducted. Consequently, no definitive conclusion can currently be drawn regarding the persistence of these morphological alterations into adulthood. Nevertheless, descriptive observations suggested that the increase in mushroom spine abundance observed in AAE-exposed mice at P43 was no longer clearly apparent at P80, although this interpretation remains highly speculative given the limited sample size. Additional experiments with larger cohorts will therefore be required to determine whether the synaptic changes observed at P43 represent transient developmental effects or long-lasting.

Finally, the functional significance of these structural alterations remains to be determined. Future studies combining morphological analyses with electrophysiological recordings and molecular approaches will therefore be necessary to establish whether the observed changes in spine subtype distribution are associated with alterations in synaptic transmission, synaptic plasticity and cortical circuit function. In addition, considering the well-established sex differences in brain maturation and alcohol sensitivity, it will be important to determine whether similar alterations occur in female mice.

5.4. Sex- and region-specific effects of AAE on PFC interneurons

This master's thesis investigated the impact of AAE on distinct interneuron subpopulations in the PFC, focusing on PV-, SST-, CR- and CB- expressing interneurons within the PL, IL, and ACC. Analyses were conducted at both P43 and P80 in male and female mice in order to evaluate the short- and long-term consequences of AAE. Overall, our findings reveal selective region-specific, and sex-dependent alterations in interneuron populations, with stronger and more persistent effects observed in males than in females. Among all interneuron populations examined, SST interneurons appeared particularly vulnerable to AAE.

At P43, male mice exposed to AAE displayed a significant reduction in SST-immunoreactive cells within the PL cortex and ACC, whereas no changes were detected in the IL.

In contrast, female mice showed no significant differences between water- and AAE-exposed animals in any of the regions examined. Interestingly, alterations in SST expression persisted into adulthood. At P80, a significant reduction remained detectable in the PL of males. Near-significant effects were observed in the IL of male mice. ACC were not significantly affected. These preliminary data suggest that some consequences of AAE persist long after alcohol consumption has ceased, particularly within the PL, a region critically involved in behavioral flexibility, inhibitory control and decision-making. SST interneurons primarily target the distal dendrites of pyramidal neurons and play a key role in regulating cortical excitability and synaptic integration. As a major source of dendritic inhibition in the neocortex, SST interneurons critically contribute to the regulation of excitation/inhibition balance within PFC circuits. Therefore, alterations in SST signaling may impair inhibitory control and disrupt neural processes underlying executive functioning (Urban-Ciecko & Barth, 2016).

Importantly, the reduction of SST-immunoreactive cells observed after AAE does not necessarily indicate a loss of SST interneurons. SST expression is activity-dependent and can be regulated by transcriptional pathways such as CREB signaling. Therefore, the observed decrease may reflect reduced SST peptide expression rather than a reduction in interneuron number. This interpretation is consistent with developmental studies showing that SST expression varies across development despite the persistence of SST-expressing neuronal population (Urban-Ciecko & Barth, 2016). In this context, AAE may alter SST signaling and thereby contribute to long-lasting modifications of inhibitory function within the PFC.

Our findings are consistent with previous studies reporting alcohol-induced alterations of GABAergic interneuron populations, particularly SST interneurons, in cortical and limbic structures. SST interneurons have also been implicated in stress-related behaviors and substance abuse disorders, and recent evidence suggests sex-dependent alterations in their excitability. Furthermore, moderate-to-high doses of alcohol have been shown to strongly inhibit SST interneuron activity *in vivo*, potentially leading to cortical disinhibition. Reduced SST signaling has also been associated with impaired cognitive flexibility and increased anxiety-like behaviors, two behavioral phenotypes commonly reported following AAE (Li et al., 2021).

Future studies will be required to determine whether the reduction in SST-immunoreactive cells reflects altered SST expression, changes in interneuron activity, or genuine alteration in SST interneuron population. Electrophysiological approaches will be particularly valuable for assessing the functional consequences of AAE on SST-mediated inhibition and prefrontal network function.

In contrast, PV interneuron expression was not significantly altered by AAE in either sex at either age. Nevertheless, near-significant effects were observed in the IL of male mice at both P43 and P80, suggesting that this interneuron population may warrant further investigation. PV interneurons are fast-spiking inhibitory neurons that play a central role in cortical oscillations, network synchronization, and maturation of executive circuits (Hu et al., 2014; Ruden et al., 2021). They are highly metabolically demanding, which may increase their susceptibility to stressors such as inflammation or neurotoxic exposure (Ruden et al., 2021). Previous studies have reported alcohol-induced reductions in PV interneuron density associated with long-term cognition and emotional impairment (Rice et al., 2019), although findings remain inconsistent across species and exposure paradigms, as some studies in rats have reported no significant changes in adulthood (De Giorgio et al., 2012). The absence of significant PV alterations in the present study may therefore reflect differences in alcohol exposure protocols, developmental timing, or methodological sensitivity, or simply limited statistical power.

No significant changes in CR interneuron expression were detected in either sex at P43 or P80. However, a non-significant trend was observed in all PFC subregions in males and in the IL of females at P43. CR interneurons are thought to contribute primarily to early developmental regulation of neuronal excitability and circuit assembly (Camp & Wijesinghe, 2009). Because adolescence represents a critical developmental period during which interneuron subtype composition undergoes substantial refinement within the PFC (Caballero et al., 2016), these observations remain of potential interest despite the absence of statistical significance**.** PV interneurons progressively mature during this period and become major contributors to cortical inhibitory control, whereas CR interneurons are thought to play a more prominent role during earlier developmental stages.

One possibility is that AAE could delay**.** Although the present data do not provide sufficient evidence to conclude that AAE alters PV or CR interneuron populations, future studies with larger cohorts will be required to determine whether alcohol exposure interferes with the normal maturation of inhibitory circuits. If confirmed, alterations in CR expression could reflect the persistence of a more immature interneuron profile or compensatory adaptations within developing cortical networks. While these interpretations remain speculative and require further experimental validation, they support the hypothesis that AAE interferes with developmental processes that normally shape inhibitory circuit maturation within the PFC.

CB interneuron expression was largely unaffected in males at both ages. However, in females, CB expression was significantly altered in the ACC at P43 but not at P80.

Given the isolated and transient nature of this effect, it should be interpreted cautiously until replicated in larger cohorts. CB-positive interneurons contribute to calcium buffering and modulation of neuronal excitability, and transient alterations may reflect adaptive responses to alcohol induced neuronal stress rather than persistent circuit dysfunction.

An important finding of this study is the marked sex difference in vulnerability to AAE. Male mice exhibit more robust and persistent alterations, particularly affecting SST interneurons, whereas females showed relatively limited and transient changes. Because formal sex-by-treatment interaction analyses were not performed, these observations should be interpreted cautiously. Nevertheless, these findings align with growing evidence indicating that males and females respond differently to AAE. Differences in sex hormones, developmental trajectories, neuroimmune signaling, and cortical maturation may all contribute to these distinct outcomes (Sharrett-Field et al., 2013). Female mice may exhibit greater compensatory plasticity or resilience mechanisms within inhibitory circuits, although this hypothesis remains to be experimentally tested.

Overall, these findings identify SST interneurons as a particularly vulnerable interneuron population following AAE and suggest that AAE induces selective, region-specific, and potentially sex-dependent alterations of inhibitory circuitry within the PFC.

Several limitations should nevertheless be acknowledged. Sample sizes were relatively small, which limits statistical power and increases the possibility that subtle effects remained undetected. Consequently, the present results should be considered preliminary and require replication in larger cohorts. Future studies combining immunohistochemistry with electrophysiological recordings and functional circuit analyses will be necessary to establish the functional significance of these alterations and to better understand how AAE affects inhibitory network maturation within the PFC.

5.5. Effects of adolescent alcohol exposure on mTORC1 and eEF2 signaling in the PFC.

The aim of this part of Master's thesis was to determine whether AAE modulates the activity of the mTORC1 and eEF2 pathways in the PFC at P43. To address this question, the phosphorylation levels of S6, a downstream target commonly used as a readout of mTORC1 signaling (Laguesse & Ron, 2020), and eEF2, a key regulator of translational elongation (David et al., 2020; Laguesse & Ron, 2020), were analyzed in total homogenate, cytoplasmic, and synaptic fractions of male and female mice.

First, the quality of the synaptic fractionation procedure was validated by WB analysis. The enrichment of synaptic markers such as PSD-95 and synaptotagmin in the synaptic fraction,

together with the absence of the nuclear marker histone H3, confirmed the successful isolation of synaptic proteins and the lack of nuclear contamination. These results support the reliability of the fractionation protocol and provide confidence in the subsequent analyses of subcellular protein distribution.

At P43, AAE led to a significant increase in the pS6/S6 ratio in both the total homogenate and the synaptic fraction of female mice. In contrast, male mice at the same age only exhibit a strong trend toward an increase in these two fractions (total homogenate: $p = 0.0531$; synaptic fraction: $p = 0.0548$), while no differences or trends were detected in the cytoplasmic fraction for either sex. Importantly, previous studies from our laboratory reported increased S6 phosphorylation in the same fractions following AAE, supporting the biological relevance of the present observation. Since S6 phosphorylation is widely used as a downstream indicator of mTORC1 signaling, these preliminary data are consistent with enhanced mTORC1-related signaling following AAE (Laguesse & Ron, 2020). The selective increase observed in the synaptic fraction further suggests that these alterations may occur preferentially at synaptic sites, where mTORC1 plays a critical role in local protein synthesis and synaptic plasticity. Synaptic mTORC1 activation has been implicated in learning, memory formation, and alcohol-induced neuroadaptations (Niu et al., 2018; Ron & Barak, 2016). Therefore, the increased synaptic phosphorylation of S6 observed in female mice may reflect enhanced local translational processes that contribute to long-lasting alterations in PFC function following AAE.

The analysis of eEF2 signaling revealed a different pattern. In male mice, neither peEF2 levels nor total eEF2 expression were significantly altered by AAE in the fractions that could be analyzed. These preliminary data suggest that AAE may not affect eEF2-dependent regulation of translational elongation in the male PFC at P43. However, interpretation of these results is limited by the absence of reliable data from synaptic fraction. Due to technical issues during WB analysis, only two AAE samples could be quantified, preventing meaningful statistical analysis. Since eEF2 is known to regulates local protein synthesis at synapses, the lack of synaptic data represents an important limitation of the present study.

Similarly, no significant differences in eEF2 phosphorylation were observed in female mice in total homogenate and cytoplasmic fraction. Interestingly, total eEF2 protein levels were significantly increased in the total homogenate of AAE-exposed mice. The biological significance of this observation remains uncertain, as eEF2 activity is primarily regulated through phosphorylation rather than changes in total protein abundance (Taha et al., 2013). Consequently, it is currently difficult to determine whether this increase reflects a functionally relevant modification of translational elongation.

Taken together, the present data provide preliminary evidence that AAE alters mTORC1-related signaling within the adolescent PFC, particularly at synaptic sites, whereas evidence supporting alterations of eEF2 signaling remains limited. Because technical issues prevented reliable analysis of synaptic eEF2, additional experiments will be required before conclusions can be drawn regarding the involvement of this pathway in alcohol-induced neuroadaptations.

Interestingly, female mice exposed to AAE exhibited both increased S6 phosphorylation and elevated total eEF2 levels. Since, enhanced S6 phosphorylation is commonly interpreted as evidence of enhanced mTORC1-related signaling and increased translational initiation. Although no changes in eEF2 phosphorylation were detected, the increase in total eEF2 expression could suggest that AAR may also influence components of the translational machinery. However, because eEF2 activity is primarily regulated through phosphorylation rather than protein abundance, the functional significance of this observation remains unclear. Additional studies will therefore be required to determine whether these molecular alterations result in measurable changes in protein synthesis.

One possible explanation for this apparent dissociation between increased S6 phosphorylation and unchanged eEF2 phosphorylation is that mTORC1 activation may not be sufficient to alter eEF2 activity under these conditions. Alternatively, compensatory mechanisms may maintain eEF2 phosphorylation despite increased mTORC1-related signaling. Future studies should therefore investigate eEF2 kinase (eEF2K), the major upstream regulator of eEF2 activity. Since mTORC1 signaling can influence translational elongation through inhibition of eEF2K, assessing eEF2K expression and phosphorylation could provide valuable mechanistic insight into the relationship between mTORC1 activation and protein synthesis following AAE (Heise et al., 2016; Laguesse & Ron, 2020).

Future studies should increase the number of animals to improve statistical power. Repeating the analysis of eEF2 in the synaptic fraction will also be essential to determine whether local translational control is altered by AAE. In addition, investigating other components of the mTORC1 pathway, including p70S6K and 4E-BP, would provide a more comprehensive assessment of translational signaling (Laguesse & Ron, 2020). Finally, examining these pathways at additional timepoints would improve our understanding of their temporal regulation following AAE. Assessing mTORC1- and eEF2-related signaling immediately after the last alcohol exposure, such as at P40, would help distinguish acute alcohol-induced effects from persistent neurobiological adaptations. Extending these analyses to later developmental stages, such as P80, would determine whether the molecular alterations identified at P43 persist into adulthood and potentially contribute to the long-term behavioral consequences of AAE.

Conclusion

The aim of this Master's thesis was to investigate the impact of AAE on PFC maturation using a voluntary binge-drinking mouse model. Overall, the results indicate that alcohol exposure during adolescence induces selective neurobiological alterations affecting synaptic organization, interneuron populations, and molecular pathways involved in protein synthesis.

At the structural level, AAE modified dendritic spine subtype distribution in layer II/III prelimbic projection neurons, suggesting altered synaptic maturation and plasticity without major changes in overall dendritic architecture. At the cellular level, SST interneurons emerged as particularly vulnerable to AAE, with male mice displaying significant reductions in SST immunoreactivity, some of which persisted into adulthood. These findings suggest that AAE may alter inhibitory circuits that are essential for proper PFC function. In contrast, female mice showed fewer and more transient alterations, highlighting important sex-dependent differences in susceptibility to alcohol-induced neuroadaptations.

At the molecular level, AAE increased S6 phosphorylation in female mice, particularly in synaptic fractions, providing preliminary evidence for enhanced mTORC1-related signaling following AAE. However, no major changes were observed in eEF2 phosphorylation, and additional studies will be required to clarify the relationship between alcohol exposure and translational control mechanisms.

Several limitations, including relatively small sample sizes and the preliminary nature of some datasets, warrant cautious interpretation of the results. Future studies combining behavioral, electrophysiological, and molecular approaches will be necessary to determine the functional consequences of the alterations identified in this work.

In conclusion, this study provides further evidence that adolescence represents a critical window of vulnerability during which alcohol exposure can interfere with normal PFC maturation. By identifying structural, cellular, and molecular alterations induced by AAE, this work contributes to a better understanding of the neurobiological mechanisms through which adolescent binge-drinking may alter brain maturation and increase vulnerability to AUD later in life.

Bibliography

Alasmari, F., Goodwani, S., McCullumsmith, R. E., & Sari, Y. (2018). Role of glutamatergic system and mesocorticolimbic circuits in alcohol dependence. *Progress in Neurobiology*, *171*, 32–49. https://doi.org/10.1016/j.pneurobio.2018.10.001

Alfonso-Loeches, S., & Guerri, C. (2011). Molecular and behavioral aspects of the actions of alcohol on the adult and developing brain. *Critical Reviews in Clinical Laboratory Sciences*, *48*(1), 19–47. https://doi.org/10.3109/10408363.2011.580567

Balsters, J. H., Zerbi, V., Sallet, J., Wenderoth, N., & Mars, R. B. (2020). Primate homologs of mouse cortico-striatal circuits. *eLife*, *9*, e53680. https://doi.org/10.7554/eLife.53680

Blakemore, S.-J. (2012). Imaging brain development: The adolescent brain. *NeuroImage*, *61*(2), 397–406. https://doi.org/10.1016/j.neuroimage.2011.11.080

Buffington, S. A., Huang, W., & Costa-Mattioli, M. (2014). Translational Control in Synaptic Plasticity and Cognitive Dysfunction. *Annual Review of Neuroscience*, *37*(1), 17–38. https://doi.org/10.1146/annurev-neuro-071013-014100

Caballero, A., Granberg, R., & Tseng, K. Y. (2016). Mechanisms contributing to prefrontal cortex maturation during adolescence. *Neuroscience & Biobehavioral Reviews*, *70*, 4–12. https://doi.org/10.1016/j.neubiorev.2016.05.013

Caballero, A., Orozco, A., & Tseng, K. Y. (2021). Developmental regulation of excitatory-inhibitory synaptic balance in the prefrontal cortex during adolescence. *Seminars in Cell & Developmental Biology*, *118*, 60–63. https://doi.org/10.1016/j.semcdb.2021.02.008

Camp, A. J., & Wijesinghe, R. (2009). Calretinin: Modulator of neuronal excitability. *The International Journal of Biochemistry & Cell Biology*, *41*(11), 2118–2121. https://doi.org/10.1016/j.biocel.2009.05.007

Carlén, M. (2017). What constitutes the prefrontal cortex? *Science*, *358*(6362), 478–482. https://doi.org/10.1126/science.aan8868

Chesnokova, E., Bal, N., & Kolosov, P. (2017). Kinases of eIF2a Switch Translation of mRNA Subset during Neuronal Plasticity. *International Journal of Molecular Sciences*, *18*(10), 2213. https://doi.org/10.3390/ijms18102213

Crews, F. T., Robinson, D. L., Chandler, L. J., Ehlers, C. L., Mulholland, P. J., Pandey, S. C., Rodd, Z. A., Spear, L. P., Swartzwelder, H. S., & Vetreno, R. P. (2019). Mechanisms of Persistent Neurobiological Changes Following Adolescent Alcohol Exposure: NADIA Consortium Findings. *Alcoholism: Clinical and Experimental Research*, *43*(9), 1806–1822. https://doi.org/10.1111/acer.14154

Cservenka, A., & Brumback, T. (2017). The Burden of Binge and Heavy Drinking on the Brain: Effects on Adolescent and Young Adult Neural Structure and Function. *Frontiers in Psychology*, *8*, 1111. https://doi.org/10.3389/fpsyg.2017.01111

David, O., Barrera, I., Gould, N., Gal-Ben-Ari, S., & Rosenblum, K. (2020). D1 Dopamine Receptor Activation Induces Neuronal eEF2 Pathway-Dependent Protein Synthesis. *Frontiers in Molecular Neuroscience*, *13*, 67. https://doi.org/10.3389/fnmol.2020.00067

De Giorgio, A., Comparini, S. E., Intra, F. S., & Granato, A. (2012). Long-term alterations of striatal parvalbumin interneurons in a rat model of early exposure to alcohol. *Journal of Neurodevelopmental Disorders*, *4*(1), 2. https://doi.org/10.1186/1866-1955-4-18

Farhy-Tselnicker, I., & Allen, N. J. (2018). Astrocytes, neurons, synapses: A tripartite view on cortical circuit development. *Neural Development*, *13*(1), 7. https://doi.org/10.1186/s13064-018-0104-y

Flores-Bonilla, A. (2020). Sex Differences in the Neurobiology of Alcohol Use Disorder. *Alcohol Research: Current Reviews*, *40*(2), 03. https://doi.org/10.35946/arcr.v40.2.04

Fritz, B. M., & Boehm, S. L. (2016). Rodent models and mechanisms of voluntary binge-like ethanol consumption: Examples, opportunities, and strategies for preclinical research. *Progress in Neuro-Psychopharmacology and Biological Psychiatry*, *65*, 297–308. https://doi.org/10.1016/j.pnpbp.2015.05.012

Gerfen, C. R., Economo, M. N., & Chandrashekar, J. (2018). Long distance projections of cortical pyramidal neurons. *Journal of Neuroscience Research*, *96*(9), 1467–1475. https://doi.org/10.1002/jnr.23978

Ghin, F., Beste, C., & Stock, A.-K. (2022). Neurobiological mechanisms of control in alcohol use disorder – Moving towards mechanism-based non-invasive brain stimulation treatments. *Neuroscience & Biobehavioral Reviews*, *133*, 104508. https://doi.org/10.1016/j.neubiorev.2021.12.031

Gilmore, E. C., & Herrup, K. (1997). Cortical development: Layers of complexity. *Current Biology*, *23*(10), 472–477.

Gilmore, J. H., Knickmeyer, R. C., & Gao, W. (2018). Imaging structural and functional brain development in early childhood. *Nature Reviews Neuroscience*, *19*(3), 123–137. https://doi.org/10.1038/nrn.2018.1

Gilpin, N. W. (2008). Neurobiology of Alcohol Dependence. *Neurobiology of Alcohol Dependence*.

Gipson, C. D., & Olive, M. F. (2017a). Structural and functional plasticity of dendritic spines – root or result of behavior? *Genes, Brain and Behavior*, *16*(1), 101–117. https://doi.org/10.1111/gbb.12324

Gipson, C. D., & Olive, M. F. (2017b). Structural and functional plasticity of dendritic spines – root or result of behavior? *Genes, Brain and Behavior*, *16*(1), 101–117. https://doi.org/10.1111/gbb.12324

Glock, C., Biever, A., Tushev, G., Nassim-Assir, B., Kao, A., Bartnik, I., Tom Dieck, S., & Schuman, E. M. (2021). The translatome of neuronal cell bodies, dendrites, and axons. *Proceedings of the National Academy of Sciences*, *118*(43), e2113929118. https://doi.org/10.1073/pnas.2113929118

Glock, C., Heumüller, M., & Schuman, E. M. (2017). mRNA transport & local translation in neurons. *Current Opinion in Neurobiology*, *45*, 169–177. https://doi.org/10.1016/j.conb.2017.05.005

Hasselgård-Rowe, J., Senchyna, A., Broers, B., & Haller, D. M. (2022). Heterogeneity of definitions and measurements of binge drinking in research on adolescents and young adults. *Drug and Alcohol Dependence*, *241*, 109650. https://doi.org/10.1016/j.drugalcdep.2022.109650

Heise, C., Taha, E., Murru, L., Ponzoni, L., Cattaneo, A., Guarnieri, F. C., Montani, C., Mossa, A., Vezzoli, E., Ippolito, G., Zapata, J., Barrera, I., Ryazanov, A. G., Cook, J., Poe, M., Stephen, M. R., Kopanitsa, M., Benfante, R., Rusconi, F., … Sala, C. (2016). eEF2K/eEF2 Pathway Controls the Excitation/Inhibition Balance and Susceptibility to Epileptic Seizures. *Cerebral Cortex*, bhw075. https://doi.org/10.1093/cercor/bhw075

Hiller-Sturmhöfel, S., & Spear, L. P. (2018). *Binge Drinking's Effects on the Developing Brain—Animal Models*.

Holt, C. E., Martin, K. C., & Schuman, E. M. (2019). Local translation in neurons: Visualization and function. *Nature Structural & Molecular Biology*, *26*(7), 557–566. https://doi.org/10.1038/s41594-019-0263-5

Hu, H., Gan, J., & Jonas, P. (2014). Fast-spiking, parvalbumin^{+} GABAergic interneurons: From cellular design to microcircuit function. *Science*, *345*(6196), 1255263. https://doi.org/10.1126/science.1255263

İLhan, M. N., & Yapar, D. (2020). Alcohol consumption and alcohol policy. *TURKISH JOURNAL OF MEDICAL SCIENCES*, *50*(5), 1197–1202. https://doi.org/10.3906/sag-2002-237

Jadhav, K. S., & Boutrel, B. (2019). Prefrontal cortex development and emergence of self-regulatory competence: The two cardinal features of adolescence disrupted in context of alcohol abuse. *European Journal of Neuroscience*, *50*(3), 2274–2281. https://doi.org/10.1111/ejn.14316

Jeanblanc, J. (2015). Comorbidity Between Psychiatric Diseases and Alcohol Use Disorders: Impact of Adolescent Alcohol Consumption. *Current Addiction Reports*, *2*(4), 293–301. https://doi.org/10.1007/s40429-015-0076-5

Kalsi, G., Prescott, C. A., Kendler, K. S., & Riley, B. P. (2009). Unraveling the molecular mechanisms of alcohol dependence. *Trends in Genetics*, *25*(1), 49–55. https://doi.org/10.1016/j.tig.2008.10.005

Kamalova, A., Manoocheri, K., Liu, X., Casello, S. M., Huang, M., Baimel, C., Jang, E. V., Anastasiades, P. G., Collins, D. P., & Carter, A. G. (2024). CCK+ Interneurons Contribute to Thalamus-Evoked Feed-Forward Inhibition in the Prelimbic Prefrontal Cortex. *The Journal of Neuroscience*, *44*(23), e0957232024. https://doi.org/10.1523/JNEUROSCI.0957-23.2024

Kamigaki, T. (2019). Dissecting executive control circuits with neuron types. *Neuroscience Research*, *141*, 13–22. https://doi.org/10.1016/j.neures.2018.07.004

Klein-Flügge, M. C., Bongioanni, A., & Rushworth, M. F. S. (2022). Medial and orbital frontal cortex in decision-making and flexible behavior. *Neuron*, *110*(17), 2743–2770. https://doi.org/10.1016/j.neuron.2022.05.022

Kolk, S. M., & Rakic, P. (2022). Development of prefrontal cortex. *Neuropsychopharmacology*, *47*(1), 41–57. https://doi.org/10.1038/s41386-021-01137-9

Koob, G. F., & Volkow, N. D. (2016). Neurobiology of addiction: A neurocircuitry analysis. *The Lancet Psychiatry*, *3*(8), 760–773. https://doi.org/10.1016/S2215-0366(16)00104-8

Laguesse, S., Morisot, N., Shin, J. H., Liu, F., Adrover, M. F., Sakhai, S. A., Lopez, M. F., Phamluong, K., Griffin, W. C., Becker, H. C., Bender, K. J., Alvarez, V. A., & Ron, D. (2017). Prosapip1-Dependent Synaptic Adaptations in the Nucleus Accumbens Drive Alcohol Intake, Seeking, and Reward. *Neuron*, *96*(1), 145-159.e8. https://doi.org/10.1016/j.neuron.2017.08.037

Laguesse, S., & Ron, D. (2020). Protein Translation and Psychiatric Disorders. *The Neuroscientist*, *26*(1), 21–42. https://doi.org/10.1177/1073858419853236

Le Merre, P., Ährlund-Richter, S., & Carlén, M. (2021). The mouse prefrontal cortex: Unity in diversity. *Neuron*, *109*(12), 1925–1944. https://doi.org/10.1016/j.neuron.2021.03.035

Lee, M.-S., & Lee, H. (2023). Associations between binge drinking experience, depressive mood, and suicidality in adolescents: Based on the 2021 Korea Youth Risk Behavior Web-based Survey. *Journal of Affective Disorders*, *323*, 386–391. https://doi.org/10.1016/j.jad.2022.11.086

Lees, B., Meredith, L. R., Kirkland, A. E., Bryant, B. E., & Squeglia, L. M. (2020). Effect of alcohol use on the adolescent brain and behavior. *Pharmacology Biochemistry and Behavior*, *192*, 172906. https://doi.org/10.1016/j.pbb.2020.172906

Li, M., Cabrera-Garcia, D., Salling, M. C., Au, E., Yang, G., & Harrison, N. L. (2021). Alcohol reduces the activity of somatostatin interneurons in the mouse prefrontal cortex: A neural basis for its disinhibitory effect? *Neuropharmacology*, *188*, 108501. https://doi.org/10.1016/j.neuropharm.2021.108501

Li, W., Ali, T., Zheng, C., Liu, Z., He, K., Shah, F. A., Ren, Q., Rahman, S. U., Li, N., Yu, Z.-J., & Li, S. (2021). Fluoxetine regulates eEF2 activity (phosphorylation) via HDAC1 inhibitory mechanism in an LPS-induced mouse model of depression. *Journal of Neuroinflammation*, *18*(1), 38. https://doi.org/10.1186/s12974-021-02091-5

Lodato, S., & Arlotta, P. (2015). Generating Neuronal Diversity in the Mammalian Cerebral Cortex. *Annual Review of Cell and Developmental Biology*, *31*(1), 699–720. https://doi.org/10.1146/annurev-cellbio-100814-125353

Marshall, E. J. (2014). Adolescent Alcohol Use: Risks and Consequences. *Alcohol and Alcoholism*, *49*(2), 160–164. https://doi.org/10.1093/alcalc/agt180

McKlveen, J. M., Myers, B., & Herman, J. P. (2015). The Medial Prefrontal Cortex: Coordinator of Autonomic, Neuroendocrine and Behavioural Responses to Stress. *Journal of Neuroendocrinology*, *27*(6), 446–456. https://doi.org/10.1111/jne.12272

Mills, K. L., Goddings, A.-L., Herting, M. M., Meuwese, R., Blakemore, S.-J., Crone, E. A., Dahl, R. E., Güroğlu, B., Raznahan, A., Sowell, E. R., & Tamnes, C. K. (2016). Structural brain development between childhood and adulthood: Convergence across four longitudinal samples. *NeuroImage*, *141*, 273–281. https://doi.org/10.1016/j.neuroimage.2016.07.044

Moore, E. M., Mariani, J. N., Linsenbardt, D. N., Melón, L. C., & Boehm, S. L. (2010). Adolescent C57BL/6J (but not DBA/2J) Mice Consume Greater Amounts of Limited-Access Ethanol Compared to Adults and Display Continued Elevated Ethanol Intake into Adulthood. *Alcoholism: Clinical and Experimental Research*, *34*(4), 734–742. https://doi.org/10.1111/j.1530-0277.2009.01143.x

Nishimura, Y. V., Shinoda, T., Inaguma, Y., Ito, H., & Nagata, K. (2012). Application of in utero electroporation and live imaging in the analyses of neuronal migration during mouse brain development. *Medical Molecular Morphology*, *45*(1), 1–6. https://doi.org/10.1007/s00795-011-0557-0

Niu, B., Liu, P., Shen, M., Liu, C., Wang, L., Wang, F., & Ma, L. (2018). GRK5 Regulates Social Behavior Via Suppression of mTORC1 Signaling in Medial Prefrontal Cortex. *Cerebral Cortex*, *28*(2), 421–432. https://doi.org/10.1093/cercor/bhw364

Oliveira, M. M., & Klann, E. (2021). A deep dive into local mRNA translation in neurons. *Proceedings of the National Academy of Sciences*, *118*(45), e2117116118. https://doi.org/10.1073/pnas.2117116118

Our World in Data. (2024). *Alcohol Consumption*. https://ourworldindata.org/alcohol-consumption?utm_source=www.moneyfittmorning.com&utm_medium=referral&utm_campaign=down-that-heineken

Pascale, A., Stephenson, M., Barr, P., Latvala, A., Aaltonen, S., Piirtola, M., Viken, R., Rose, R. J., Kaprio, J., Maes, H., Dick, D. M., & Salvatore, J. E. (2022). Exploring the relationships between adolescent alcohol misuse and later life health outcomes. *Alcoholism: Clinical and Experimental Research*, *46*(9), 1753–1765. https://doi.org/10.1111/acer.14917

Paulin, J. J. W., Haslehurst, P., Fellows, A. D., Liu, W., Jackson, J. D., Joel, Z., Cummings, D. M., & Edwards, F. A. (2016). Large and Small Dendritic Spines Serve Different Interacting Functions in Hippocampal Synaptic Plasticity and Homeostasis. *Neural Plasticity*, *2016*, 1–11. https://doi.org/10.1155/2016/6170509

Pchitskaya, E., & Bezprozvanny, I. (2020). Dendritic Spines Shape Analysis—Classification or Clusterization? Perspective. *Frontiers in Synaptic Neuroscience*, *12*, 31. https://doi.org/10.3389/fnsyn.2020.00031

Rice, J., Coutellier, L., Weiner, J. L., & Gu, C. (2019). Region-specific interneuron demyelination and heightened anxiety-like behavior induced by adolescent binge alcohol treatment. *Acta Neuropathologica Communications*, *7*(1), 173. https://doi.org/10.1186/s40478-019-0829-9

Risher, W. C., Ustunkaya, T., Singh Alvarado, J., & Eroglu, C. (2014). Rapid Golgi Analysis Method for Efficient and Unbiased Classification of Dendritic Spines. *PLoS ONE*, *9*(9), e107591. https://doi.org/10.1371/journal.pone.0107591

Ron, D., & Barak, S. (2016). Molecular mechanisms underlying alcohol-drinking behaviours. *Nature Reviews Neuroscience*, *17*(9), 576–591. https://doi.org/10.1038/nrn.2016.85

Ruden, J. B., Dugan, L. L., & Konradi, C. (2021). Parvalbumin interneuron vulnerability and brain disorders. *Neuropsychopharmacology*, *46*(2), 279–287. https://doi.org/10.1038/s41386-020-0778-9

Rudy, B., Fishell, G., Lee, S., & Hjerling-Leffler, J. (2011). Three groups of interneurons account for nearly 100% of neocortical GABAergic neurons. *Developmental Neurobiology*, *71*(1), 45–61. https://doi.org/10.1002/dneu.20853

Sancho, L., Contreras, M., & Allen, N. J. (2021). Glia as sculptors of synaptic plasticity. *Neuroscience Research*, *167*, 17–29. https://doi.org/10.1016/j.neures.2020.11.005

Selemon, L. D. (2013). A role for synaptic plasticity in the adolescent development of executive function. *Translational Psychiatry*, *3*(3), e238–e238. https://doi.org/10.1038/tp.2013.7

Sharrett-Field, L., Butler, T. R., Reynolds, A. R., Berry, J. N., & Prendergast, M. A. (2013). Sex differences in neuroadaptation to alcohol and withdrawal neurotoxicity. *Pflügers Archiv - European Journal of Physiology*, *465*(5), 643–654. https://doi.org/10.1007/s00424-013-1266-4

Sicher, A. R., Starnes, W. D., Griffith, K. R., Dao, N. C., Smith, G. C., Brockway, D. F., & Crowley, N. A. (2023). Adolescent binge drinking leads to long-lasting changes in cortical microcircuits in mice. *Neuropharmacology*, *234*, 109561. https://doi.org/10.1016/j.neuropharm.2023.109561

Spear, L. P. (2000). The adolescent brain and age-related behavioral manifestations. *Neuroscience & Biobehavioral Reviews*, *24*(4), 417–463. https://doi.org/10.1016/S0149-7634(00)00014-2

Spear, L. P. (2016). Alcohol Consumption in Adolescence: A Translational Perspective. *Current Addiction Reports*, *3*(1), 50–61. https://doi.org/10.1007/s40429-016-0088-9

Squeglia, L. M., & Gray, K. M. (2016). Alcohol and Drug Use and the Developing Brain. *Current Psychiatry Reports*, *18*(5), 46. https://doi.org/10.1007/s11920-016-0689-y

Steinberg, L. (2008). A social neuroscience perspective on adolescent risk-taking. *Developmental Review*, *28*(1), 78–106. https://doi.org/10.1016/j.dr.2007.08.002

Stiles, J., & Jernigan, T. L. (2010). The Basics of Brain Development. *Neuropsychology Review*, *20*(4), 327–348. https://doi.org/10.1007/s11065-010-9148-4

Taha, E., Gildish, I., Gal-Ben-Ari, S., & Rosenblum, K. (2013). The role of eEF2 pathway in learning and synaptic plasticity. *Neurobiology of Learning and Memory*, *105*, 100–106. https://doi.org/10.1016/j.nlm.2013.04.015

Thiele, T. E., & Navarro, M. (2014). “Drinking in the dark” (DID) procedures: A model of binge-like ethanol drinking in non-dependent mice. *Alcohol*, *48*(3), 235–241. https://doi.org/10.1016/j.alcohol.2013.08.005

Trinh, M. A., & Klann, E. (2013). Translational control by eIF2α kinases in long-lasting synaptic plasticity and long-term memory. *Neurobiology of Learning and Memory*, *105*, 93–99. https://doi.org/10.1016/j.nlm.2013.04.013

Urban-Ciecko, J., & Barth, A. L. (2016). Somatostatin-expressing neurons in cortical networks. *Nature Reviews Neuroscience*, *17*(7), 401–409. https://doi.org/10.1038/nrn.2016.53

Van Driesche, S. J., & Martin, K. C. (2018). New frontiers in RNA transport and local translation in neurons. *Developmental Neurobiology*, *78*(3), 331–339. https://doi.org/10.1002/dneu.22574

Van Hees, L., Didone, V., Charlet-Briart, M., Van Ingelgom, T., Quertemont, E., Nguyen, L., & Laguesse, S. (2022). Voluntary alcohol binge-drinking in adolescent C57Bl6 mice induces delayed appearance of behavioural defects in both males and females. *Addiction Biology*, *27*(1), e13102. https://doi.org/10.1111/adb.13102

Varodayan, F. P., Sidhu, H., Kreifeldt, M., Roberto, M., & Contet, C. (2018). Morphological and functional evidence of increased excitatory signaling in the prelimbic cortex during ethanol withdrawal. *Neuropharmacology*, *133*, 470–480. https://doi.org/10.1016/j.neuropharm.2018.02.014

Verplaetse, T. L., Cosgrove, K. P., Tanabe, J., & McKee, S. A. (2021). Sex/gender differences in brain function and structure in alcohol use: A narrative review of neuroimaging findings over the last 10 years. *Journal of Neuroscience Research*, *99*(1), 309–323. https://doi.org/10.1002/jnr.24625

Vetreno, R. P., & Crews, F. T. (2015). Binge ethanol exposure during adolescence leads to a persistent loss of neurogenesis in the dorsal and ventral hippocampus that is associated with impaired adult cognitive functioning. *Frontiers in Neuroscience*, *9*. https://doi.org/10.3389/fnins.2015.00035

Vijayakumar, N., Op De Macks, Z., Shirtcliff, E. A., & Pfeifer, J. H. (2018). Puberty and the human brain: Insights into adolescent development. *Neuroscience & Biobehavioral Reviews*, *92*, 417–436. https://doi.org/10.1016/j.neubiorev.2018.06.004

Volkow, N. D., Michaelides, M., & Baler, R. (2019). The Neuroscience of Drug Reward and Addiction. *Physiological Reviews*, *99*(4), 2115–2140. https://doi.org/10.1152/physrev.00014.2018

White, A. (2020). Gender Differences in the Epidemiology of Alcohol Use and Related Harms in the United States. *Alcohol Research: Current Reviews*, *40*(2), 01. https://doi.org/10.35946/arcr.v40.2.01

World Health Organization. (2024). *Alcohol*. https://www.who.int/news-room/fact-sheets/detail/alcohol

Xu, P., Chen, A., Li, Y., Xing, X., & Lu, H. (2019). Medial prefrontal cortex in neurological diseases. *Physiological Genomics*, *51*(9), 432–442. https://doi.org/10.1152/physiolgenomics.00006.2019

Yan, Z., & Rein, B. (2022). Mechanisms of synaptic transmission dysregulation in the prefrontal cortex: Pathophysiological implications. *Molecular Psychiatry*, *27*(1), 445–465. https://doi.org/10.1038/s41380-021-01092-3

Yang, W., Singla, R., Maheshwari, O., Fontaine, C. J., & Gil-Mohapel, J. (2022). Alcohol Use Disorder: Neurobiology and Therapeutics. *Biomedicines*, *10*(5), 1192. https://doi.org/10.3390/biomedicines10051192

Annexes

Tables of alcohol consumption data of adolescent mice in group 1 to 7 used for my master's thesis analysis. Amount of alcohol consumed for each session and the average consumption per mouse in g/kg/4h.

WT mice			Alcohol consumption (g/kg/4h)										Mean (g/kg/4h)
Group	Sex	ID	Sessions										
			1	2	3	4	5	6	7	8	9	10	
Group 1 (LO19)	♂	753	4,56	4,72	2,77	3,33	5,38	5,79	8,18	4,34	5,17	3,86	4,81
	♂	755	7,57	3,91	1,39	3,94	4,16	7,09	8,84	5,56	4,23	5,74	5,24
	♂	756	4,16	4,92	4,24	4,64	5,18	6,46	9,76	3,39	3,67	9,63	5,5
	♂	758	4,27	3,2	1,6	3,92	3,12	5,06	7,4	1,62	4,44	4,93	3,96
	♂	760	4,27	3,45	2,95	2,39	3,37	6,26	6,19	2,18	4,96	4,88	4,09
	♂	761	5,2	4,48	3,74	6,25	5,6	6,09	9,76	3,62	7,5	8	6,02
	♂	762	7	5,17	5,2	1,44	2,83	4,28	6,16	3	5,17	4,74	4,5
Group 2 (LO20)	♂	726	9,32	4,46	8,29	7,54	7,38	7,69	8,9	6,53	6,73	8,75	7,56
	♂	727	6,67	2,76	7,53	2,88	4,79	4,18	4,35	4,63	11,02	4,13	5,29
	♂	728	7,88	3,24	6,57	4,53	4,69	6,81	6,44	5,44	11,7	4,83	6,21
	♂	729	7,95	5,88	8,74	5,01	7,56	9,03	5,74	7,6	4,18	5,42	6,71
	♂	730	9,05	5,69	11,22	3,31	4,48	5,43	4,7	3,93	5,44	5,91	5,92
	♂	731	5,99	4,91	8,93	5,06	7,7	10,23	6,43	8,5	8,98	4,28	7,1
	♂	732	9,11	6	8,35	4,19	7,7	7,38	5,47	4,64	6,17	4,07	6,31
	♂	733	8,8	6,24	11,21	6,32	6,23	9,96	10,9	10,25	7,91	7,27	8,51
Group 3 (LO21)	♂	740	1,08	3,55	4,9	4,04	1,69	9,91	4,84	4,14	3,9	2,07	4,01
	♂	741	4,17	4,11	7,31	4,58	4	7,21	6,5	9,15	9,25	6,67	6,3
	♂	742	3,16	8	10,28	5,19	2,65	5,02	5,39	7,37	5,75	6,05	5,89
	♂	743	7,48	4,21	7,65	3,76	3,25	9,92	9,7	9,02	8,52	8,37	7,19
	♂	744	7,35	6,88	10,73	4,2	5,75	8,32	6,9	4,22	6,81	7,13	6,83
Group 4 (LO22)	♀	776	8,85	7,43	9,82	7,84	9,99	7,29	9,35	8,02	6,28	10,27	8,51
	♀	777	6,52	6,31	7,43	9,05	7,74	5,34	4,84	4,08	3,52	6,48	6,13
	♀	778	5,01	6,44	8,16	1,34	4,93	4,83	6,07	4,97	6,98	7,48	5,62
	♀	779	7,26	7,46	6,7	5,56	6,74	7,78	5,82	4,74	2,49	4,77	5,93
	♀	780	0,63	4,09	6,42	5,38	9,42	3,92	5,72	7,72	6,23	11,57	6,11
	♀	781	5,34	2,96	9,75	6,49	12,08	7,82	8,65	2,99	10,48	8,45	7,5
	♀	782	5,88	7,65	9,18	6,58	7,23	7,66	7,04	6,75	8,38	9,69	7,6
	♂	784	7,47	8,24	7,63	8,31	9,00	7,09	6,03	7,65	8,88	8,07	7,84
	♂	785	3,15	5,61	6,32	5,76	10,05	2,15	4,48	5,98	4,27	7,45	5,53
	♂	787	9,89	5,13	6,84	8,73	10,17	8,27	8,28	7,41	10,65	10,96	8,63
	♂	788	4,34	5,08	7,41	5,77	8,19	4,86	7,13	6,37	5,78	9,32	6,42
	♂	790	4,96	3,99	7,16	4,78	5,97	4,95	5,33	5,11	4,37	6,06	5,27
	♂	791	5,31	3,27	7,22	5,95	6,48	5,69	8,36	5,07	7,97	11,80	6,71
Group 5 (LO23)	♀	712	8,67	9,86	-9,44	8,35	6,24	6,24	3,81	7,46	6,46	4,36	5,2
	♀	715	11,95	3,34	2,54	5,43	5,31	2,57	6,82	6,23	6,19	7,73	5,81
	♀	717	28,37	7,41	3,48	3,88	2,93	5,97	8,76	7,68	7,61	8,09	8,42
	♀	445	12,40	7,42	8,30	2,02	7,78	9,99	11,77	9,58	11,06	10,01	9,04
	♀	446	9,78	8,67	7,15	9,09	7,22	8,61	8,65	10,25	9,09	6,13	8,47
	♂	714	11,62	9,95	6,59	8,20	6,04	7,26	8,89	4,12	7,70	8,13	7,85
	♂	701	9,15	8,15	6,98	9,48	5,78	9,03	8,72	7,20	8,65	5,38	7,85
	♂	702	5,97	7,22	4,76	9,85	1,61	2,21	4,95	5,44	6,84	5,15	5,4
	♂	703	9,53	8,45	4,28	6,46	3,28	6,84	10,11	7,27	8,83	6,32	7,14
	♂	704	14,18	7,92	8,41	9,01	6,13	8,00	7,84	6,93	7,68	3,56	7,97
	♂	705	9,42	5,66	5,48	8,29	6,56	3,87	6,02	8,27	8,19	8,19	6,99
	♂	706	7,47	5,35	5,35	7,14	6,11	6,14	9,06	6,07	6,09	4,27	6,30
	♂	441	7,30	7,74	6,71	7,21	5,87	5,96	6,51	7,59	7,04	4,21	6,61
	♂	442	8,76	5,87	6,15	6,48	4,63	4,11	4,77	4,62	5,20	3,06	5,37
Group 6 (LO24)	♀	SB1	5,31	8,12	5,25	6,50	11,06	4,24	6,24	8,51	8,51	4,11	6,79
	♀	457	6,59	6,83	4,95	6,48	8,57	7,87	8,99	2,05	2,05	8,45	6,28
	♀	SB4	5,39	3,75	5,17	6,40	9,94	6,64	6,88	6,01	6,01	5,15	6,13
	♀	458	8,48	2,25	3,06	4,59	5,65	5,13	5,15	6,89	6,89	6,40	5,45
	♂	451	6,09	6,87	4,99	4,76	7,48	7,55	5,41	6,34	6,34	4,88	6,07
	♂	SB6	6,13	6,13	4,38	4,26	7,76	4,01	7,19	5,01	5,01	2,76	5,26
	♂	453	6,53	8,13	2,16	1,44	6,49	4,52	5,01	7,01	7,01	3,52	5,18
	♂	454	6,45	7,94	7,94	5,40	6,95	11,20	5,17	6,40	6,40	3,91	6,78
	♂	SB2	4,19	6,03	5,96	8,48	6,65	4,06	7,09	6,01	6,01	3,82	5,83
	♂	SB4	7,23	6,90	6,72	6,72	12,54	1,25	6,67	4,19	4,19	3,41	5,98
Group 7 (IS1)	♀	SB1	10,78	0,84	5,74	2,90	5,81	6,88	9,34	5,56	6,96	9,94	6,48
	♀	796	5,85	0,42	7,33	1,33	4,37	6,98	9,03	7,71	8,80	8,80	6,06
	♀	SB2	9,40	0,35	9,57	-0,13	6,95	6,01	8,19	6,62	11,24	6,58	6,48
	♀	797	6,25	0,43	6,13	3,33	2,77	9,02	6,82	6,72	12,07	7,24	6,08
	♀	SB3	5,50	0,70	7,93	3,75	6,68	6,79	10,67	6,70	9,66	9,16	6,75
	♀	798	6,49	0,59	10,26	-0,49	8,04	9,46	12,65	9,97	11,11	0,00	6,81
	♂	792	25,51	1,06	10,10	2,90	8,76	9,71	10,28	5,41	9,57	7,60	9,09
	♂	793	12,75	0,40	7,30	1,33	8,61	7,07	2,44	3,60	7,41	7,22	5,81
	♂	794	9,82	1,01	9,52	-0,13	8,43	9,08	8,84	6,70	10,11	6,99	7,04

Table 1: Adolescent alcohol consumption of WT mice.